BIOSYNTHESIS OF LEAD SELENIDE (PbSe) SEMICONDUCTOR QUANTUM PARTICLES IN MARINE FUNGUS

Thesis

Submitted in partial fulfillment of the requirements for the degree of

DOCTOR OF PHILOSOPHY

in

CHEMICAL ENGINEERING

by

Ms. Jaya Mary Jacob

Register. No. 123016CH12F05

DEPARTMENT OF CHEMICAL ENGINEERING
NATIONAL INSTITUTE OF TECHNOLOGY KARNATAKA,
SURATHKAL, MANGALORE - 575 025
December, 2015

D E C L A R A T I O N

I hereby declare that the Research Thesis entitled "Biosynthesis of Lead Selenide (PbSe) Quantum Particles in Marine Fungus" which is being submitted to the **National Institute of Technology Karnataka, Surathkal** in partial fulfillment of the requirements for the award of the Degree of **Doctor of Philosophy** in Chemical Engineering is a *bonafide report of the research work carried out by me*. The material contained in this thesis has not been submitted to any University or Institution for the award of any degree.

Jaya Mary Jacob

123016CH12F05

Department of Chemical Engineering
National Institute of Technology Karnataka
Surathkal- 575 025

Place: NITK-Surathkal

Date:

C E R T I F I C A T E

This is to *certify* that the Research Thesis entitled "Biosynthesis of Lead Selenide (PbSe) Quantum Particles in Marine Fungus" submitted by Ms. Jaya Mary Jacob (Register No. 123016CH12F05) as the record of the research work carried out by her, is *accepted as the Thesis submission* in partial fulfillment of the requirements for the award of degree of **Doctor of Philosophy**.

Signature of the Research Supervisor:
Name of the Research Supervisor : Dr. Raj Mohan B
Date :

Signature of the Chairman- DRPC :
Date :

Dedicated to Mummy and Daddy

"For giving my dreams.. the wings to fly"

ACKNOWLEDGEMENT

Every accomplishment begins with a decision to try. The decision to pursue my doctoral research in NITK and the subsequent years of hard work was backed by numerous valuable contributors; who assured me that the challenges were worth taking and those who lend a helping hand to reach the destination. It is my pleasure to convey my heartfelt gratitude to all of them for their priceless contribution in this journey.

Firstly, I would like to express my sincere gratitude to my research supervisor Dr. Raj Mohan B, Associate Professor and Head, Department of Chemical Engineering, NITK Surathkal. It takes a big heart to shape little minds and Raj Mohan Sir has been kind enough to provide me with the right mix of guidance, encouragement and genuine care in each and every stage of my research. His support and faith in me during the past three years has enabled me to aim high and achieve success. Thank You Sir!

It is my privilege to thank the members of my research progress assessment committee; Dr. Manu Basvaraju, Dr. Keyur Raval and Dr. Noyel Victoria for their valuable inputs and advices that ushered me to widen my research from various perspectives. I would also like to express my thanks to the respected Director, NITK Surathkal for giving me an opportunity to be a part of this renowned institution and for providing me the necessary facilities, funding and support during the phase of this project work. I wish to thank Dr. Vidya Shetty (former HOD Chemical), Dr. Gopal Mugeraya, Dr. G. Srinikethan, Dr. DVR Murthy, Dr. Prasanna BD, Dr. Hari Mahalingam and other faculty members of the Department of Chemical Engineering for their support in assorted ways towards my research work in NITK.

My sincere thanks also goes to Dr. Udaya Bhat K, Dr. Anadhan S and Dr. RajendraUdupa, Department of Materials Science and Metallurgical Engineering, NITK Surathkal; for extending the TEM, XRD, FTIR and SEM characterization facilities. Special

thanks to the respective HODs of the Department of Physics and Chemistry for extending the necessary support for my research work.

I wish to express my earnest gratitude to Dr. Aravindakumar, Dean, Faculty of Environmental and Atmospheric Sciences, MG University, Kottayam and Dr. Selvaraju, Department of Chemistry, Karunya University for the analysis of my samples. The support by SAIF, IISc, Bangalore; ARI, Pune; Innovation Center, MIT, Manipal, CSIR IHBT, Palampur and the Department of Chemistry, Mangalore University is highly appreciated.

The timely help and cooperation of the non-teaching staff of the Department of Chemical Engineering need special mention. Their help in multifarious manner, from the maintenance of the equipment to the supply of drinking water; was inevitable for the smooth conduct of my research work. I express my sincere thanks to Mr. Sadashiva, Mrs. Trithila, Mrs. Shashikala, Mrs. Prema, Mr. Ananda, Mr. Mahadeva, Mr. Harish, Mr. Suresh, Ms. Sandhya, Mrs. Sheela and others.

The assistance by the operators and research scholars of the sophisticated instruments in the Department of Materials and Metallurgical Engineering, Chemistry and Physics was priceless. In spite of their busy schedule, my friends were kind enough to spare time for the analysis of my samples and have always welcomed me unconditionally. I take this opportunity to thank Ms. Rashmi, Mr. Prashanth, Mr. Arun Augustin, Mr. Arun (Mangalore University), Mr.Vinayak, Mr. Srijesh, Mr. Nimith, Mr. Dickson, Dr. Ahipa, Mr. Goutham, Mr. Sreejith, Mr. GnanaPrakasham, Mr. Suresh, Ms. Neethu (Karunya University) and Ms. Manju Mathew (MG University).

The best part during my doctoral research was the Summer School at Technion, Israel Institute of Technology. I am highly indebted to the Technion faculty for providing me the lifetime opportunity. I am also thankful to Department of Science and Technology for

providing the travel assistance and Dr. Arun M Isloor, Department of Chemistry, NITK Surathkal for re-assuring me with his valuable experiences in Israel.

Coming to the folks who made the imperfections endurable- my friends!! From the ones who made my days brighter to those who conveyed lessons worth a lifetime- I thank all of you for knowing me, being with me and gifting me unforgettable memories. I am grateful to Mr. Gopinath and Ms. Priyanka for being great friends whom I could always count on to. Special thanks to Mr. Sumit, Mr. Akshay, Mr. Chinnapandi R, Ms. Anushka, Ms. Soumya Raj, Ms. Viashnavi, Dr. Dilna, Ms. Deepika, Ms. Sindhu, Ms. Teena and Co., and my other dear friends in M Tech and B Tech courses. I am also thankful to Ms. Smitha, Dr. Sogra Fathima, Mrs. Shruthee, Mr. Kunal, Mr. Abhinav, Dr. Prajna, Mr. Harsha, Mr. Vishnu, Mr. Ajuy, and other fellow research scholars. Thanks to Anitha Madam and Co., for adding flavor to my hostel days.

This acknowledgment would lose its value if I fail to thank the great minds who inspired me to carry forward my quest for learning; heartfelt thanks to all my teachers! I would also like to thank my sister and family and my fiancé for their encouragement and prayers towards the completion of my doctoral research.

Lastly, I would like to thank my parents, for their love, prayers, constant support and encouragement. Whether it is the way they comforted me when I was disheartened or the way they magically wiped out my frowns, they were there day after day to make sure that my life turned out this way. Thank you mummy and daddy!!

Above all, I would like to thank my loving God for giving me the strength, wisdom and faith that led me each second. I could not ask for more; for his loving care has been the greatest gift of all!!

Jaya Mary Jacob

ABSTRACT

Lead selenide (PbSe) quantum particles (QPs), a typical semiconductor material of the IV–VI group are capturing the attention of material scientists for their shape controlled synthesis to utilize their excellent size tunable optical properties in diverse sectors. In order to address the disadvantages of the traditional chemical approach for PbSe QP synthesis, biosynthesis of these technologically relevant nano-fabrications was initiated in Pb and Se tolerant marine *Aspergillus terreus*. The formation of PbSe QPs were confirmed using TEM and SEM images that revealed the formation of rod like structures having an average diameter of 59 nm with an aspect ratio between 10 and 70. Detailed characterization to reveal the other structural and optical properties of the colloidal PbSe QPs were also carried out. The cyclic voltammogram of the biosynthesized PbSe QPs were characterized with five reaction peaks corresponding to the oxidation of PbSe, Se_2O_3 and $Pb(OH)_2$ and the reduction of PbO_2 and $Pb(OH)_2$. Further, the statistical optimization of the process parameters during the biosynthesis of PbSe QPs for an enhanced fluorescence was carried out. It was observed that parameter optimization results in a florescence blue shift and a reduction in PbSe QP's size to dimensions comparable to its excitonic Bohr radius (21nm). The fluorescence amenability of the biosynthesized PbSe QPs was utilized for the development of in-situ cadmium (II) sensing array. Initial experimental observations revealed sensitive and detectable quenching in fluorescence of the biogenic colloidal PbSe QPs in the presence of cadmium (II) ions in comparison to other tested metal ions. Subsequently advanced chromatographic and spectroscopic analyses confirmed the involvement of metal binding peptides namely metallothioneins, phytochelatins and superoxide dismutase that play a prominent role in the microbial metal detoxification system for the biosynthesis of PbSe QDs.

Key Words: *Aspergillus terreus*, Biosynthesis, Bio sensing, Characterization, Fluorescence, Lead Selenide, Quantum Particles

TABLE OF CONTENTS

LIST OF FIGURES

LIST OF TABLES

LIST OF ABBREVIATIONS

Title	Abbreviation
Atomic Absorption Spectrometer	AAS
Analysis of Variance	ANOVA
Box Behnken Design	BBD
Cyclic voltammetry	CV
Elemental Determination using X-rays	EDX
Endoplasmic Reticulum	ER
Förster Resonance Energy Transfer	FRET
Fourier Transform Infra-Red Spectroscopy	FTIR
Tri-isopropyl phosphine	i-TPP
Internal Transcribed Sequence	ITS
Linear combination of atomic orbitals	LCAO
Matrix assisted laser desorption ionization time of flight mass spectroscopy	MALDI-ToF
Metallothionein	MT
Nanocrystals	NCs
Nanoparticles	NPs
Plackett-Burman Design	PB
Potato Dextrose Agar	PDA
Potato Dextrose Broth	PDB

Photoluminescence spectrum	PL
Phytochelatin Synthase	PS
Quantum Dots	QDs
Quantum Particles	QPs
Quantum Rods	QRs
Response Surface Methodology	RSM
Scanning Electron Microscopy	SEM
Super oxide dismutase	SOD
Tri-butyl phosphine	TBP
Tetra-decylphosphonic acid	TDPA
Transmission Electron Microscopy	TEM
Tri-octyl phosphine	TOP
Tri-octyl phosphine oxide	TOPO
UV-Vis Spectroscopy	UV-Vis
X-ray Diffraction	XRD

1. INTRODUCTION

1.1 BACKGROUND

The past few decades have evinced an unrivaled impact of science and technology on global economy, development and growth. Of the various disciplines in scientific research, the innovations at the nanoscale was found to have implications in diverse sectors like healthcare (Raffa et al. 2010), global sustainability (Maclurcan and Radywyl 2011) and energy (Serrano et al. 2009). Some of the noteworthy contributions of nanotechnology include high resolution displays, multitudes of nano sized sensor assemblies for environmental pollution detection, high throughput opto-electronic devices, nano-engineered solar cells and a host of disease targeting fluorescent labels (Uldrich and Newberry 2003).

By definition, nanotechnology deals with various structures of matter having dimensions of the order of a billionth (1×10^{-9}) of a meter. While the word nanotechnology is relatively new, the knowledge on the existence of nano structures were evident since the birth of our mother earth (Jr and Owens 2003). However, a dramatic surge in fundamental and applied interest in this field has been observed only in the recent past. This could be attributed to the increasing recognition of nanostructured materials in numerous applications, including catalysis (Jin 2012), magneto- and opto-electronics, photonics(Ventra et al. 2004), cosmetics (Mihranyan et al. 2012) and medicine (Emerich and Thanos 2003).

Over the years, material scientists have initiated the nano scale synthesis of various compounds of organic and inorganic elemental combinations that exhibit prospective opto-electronic and dimensional attributes superior to their bulk counterparts (Sanvicens and Marco 2008). Organic nanoparticles (NPs) include carbon in the form of fullerenes, liposomes, dendrimers and polymeric micelles and the inorganic NPs consist of magnetic, noble metal (like gold and silver), and semiconductor NPs (like $TiO_2$and CdS) (Fuente and Grazu 2012). Irrespective of their type, all nanoparticles are characterized by high surface to

volume ratio and offer prospects to modulate their properties, thus capacitating them as multifunctional technical tools (Rotello 2012).

The aforementioned functionalities of nanomaterials have paved way towards the advent of a nano-revolution focused on exploring newer nano scale materials with improved practical utilities. One important class of nanostructured materials that have drawn wide research attention comprise of chalcogenide semiconductors; known as quantum particles (QPs) that are composed of II–VI or III–V group elements (Liu et al. 2010). These NPs are characterized by unique electronic and optical properties due to quantum confinement effects (Peng et al. 1997; Jiang 2012) that results in shifted emission spectra, that are distinct from the bulk equivalents (Herz et al. 2003). This in turn emanates in enhanced fluorescence emissions from these nanofabrications (Biju et al. 2008).

The benefits of size tunable fluorescence quantization effects are especially noteworthy in quantum dots (QDs) of IV-VI materials, particularly PbSe that offer a unique possibility of strong quantum confinement leading to absorptive and dispersive non-linearities that are theoretically predicted to be 1000 times larger than other chalcogenide QPs (Baek et al. 2008).The superior quantum confinement in PbSe QPs bestows size and composition tunable emission spectra and a high quantum yield that enable their use as significant fluorescent entities (Lifshitz et al. 2003). Further, PbSe QPs are also resistant to photo-bleaching and exhibit significant resistance to photo chemical and thermal degradation (Wujcik et al. 2015), and hence are attaining interest as superior agents for various applications (Ellingson et al. 2005). Some of the major domains where the properties of PbSe nanocrystallites (NCs) have been effectively harnessed include the solar energy sector where in these materials have been used as photo effective solar cell coatings (Kamat 2008), biosensors (Gu et al. 2013)and biological labels for targeted drug delivery (Marc Achermann 2004; Schaller and Klimov 2004).

The early phase in nanotechnology evinced numerous chemical means for synthesis of PbSe semiconductor nano crystals with precision in terms of size, shape and properties (Lifshitz et al. 2003; Schaller and Klimov 2004; Yong et al. 2006a; Baek et al. 2008). However developments were often hazed by the concerns raised due to the use of toxic chemicals and stringent reaction conditions followed by the harmful effects caused by the reaction byproducts to the environment (Sengül and Theis 2009). The situation demanded the development of an eco-friendly and green approach towards synthesizing these nano clusters (Parikh et al. 2011; Ramanathan et al. 2011; Syed and Ahmad 2013). Seeking lessons from nature's tools in assembling miniature functional materials in biological systems in elegant and ingenious ways, material scientists have turned their focus to harness these potent sources as biological factories to synthesize nano materials. The knowledge gained from the biological world has led to relentless attempts by the scientists in material science to utilize the potential of the single cells for initiating laboratory-based biomimetic synthesis of QDs (Bao et al. 2010a, 2010b; Prasad and Jha 2010a; Mi et al. 2011; Pandian et al. 2011). In this regard, numerous prokaryotic bacteria and eukaryotic systems like fungus, yeast and earthworm have been employed as biogenic factories for QD synthesis. However, in spite of the prospective advantages of working with PbSe QPs, the deliberate biosynthesis of the same is relatively new and largely unfathomed.

1.2 SCOPE OF THE STUDY

Lead Selenide (PbSe) semiconductor nano crystals possess excellent quantum confinement effects in their nano scale. However, the chemical syntheses of these semiconductor nano composites involve stringent reaction conditions that increase the overall cost of the process and leads to environmental problems. Hence it is important to explore the competency of microbial sources for the green synthesis of PbSe QPs. The present study was aimed at utilizing heavy metal tolerant fungal species as potential eco-friendly biological alternative for PbSe QP synthesis. Developing and optimizing such protocols would unveil the potential applications of these quantum particles in environmental and energy sectors.

1.3 OBJECTIVES OF THE STUDY

The overall goal of the present study was the development of eco-friendly and rapid means of synthesis of PbSe quantum particles in marine fungus and to explore its utility for the efficient fluorescence based bio-sensing of heavy metals in water.

The specific objectives include:

1. Isolation, screening, identification and medium optimization of lead and selenium tolerant fungal species from marine ecosystem
2. Biosynthesis of lead selenide quantum particles by the marine fungal species
3. Characterization of the structural, morphological, optical and electrochemical properties of the biosynthesized lead selenide quantum particles
4. Optimization of the parameters that influences the fluorescence of the nanocrystallites
5. Development of an efficient fluorescence based sensor system for the selective detection of heavy metals in aqueous phase using lead selenide quantum particles
6. To elucidate the fungal mechanism involved in the biosynthesis of PbSe quantum particles

1.4 ORGANIZATION OF THE THESIS

This research study is presented in five chapters. Chapter I introduces the background of the investigation highlighting the active role of nanotechnology as a scientific discipline and the importance of nanomaterials in diverse sectors of human application. Further, the concepts of quantum particles as significant nanostructured materials have been presented.

Chapter 2 is an extensive archive of the literature related to quantum particles which comprehensively covers various aspects regarding their properties, traditional chemical synthesis means, archives on microbial factories for the green synthesis of QPs, and some illustrations on the microbial mechanisms that can initiate biosynthesis of QPs. The diverse applications of QPs in various sectors are also briefly discussed.

Chapter 3 describes the materials and methodology used in this research work. Description regarding the experimental protocols used for the different objectives is enumerated and details of the statistical modeling of the various optimization techniques are elaborated. Chapter 1, 2 and 3 are common for all the subsequent chapters.

Chapter 4 is a compilation of the results of the experimental work and the discussion of the critical findings. Initially the isolation of the marine fungus and the results on their tolerance and growth are reported. Further, experimental evidences on the biosynthesis of PbSe QPs have been reported. The detailed elaboration on the morphological, optical and electrochemical properties and the application of the biosynthesized PbSe QPs for heavy metal sensing in aqueous phase are further described. The critical findings are discussed in the light of previous literature.

Chapter 5 provides a summary of the entire study and the implications of the findings for theory and practice, recommendations for further research and conclusions.

2. REVIEW OF LITERATURE

The pace of advancement for any new technology is driven in part by its very newness. This notion along with the handiness of ample resources and creativity has been accounting for the rapid evolution in the study of nanoscopic systems using quantum dots (Ling 2005). The scientifically sound background on QD science provided by various researchers has intrigued significant research outcomes towards practically integrating these entities in day to day life. However, the increasing thrust on environmental friendly technological approaches has opened a new research arena focused on exploring green sources for QD synthesis (Narayanan and Sakthivel 2011). The present chapter details the relevant literature in relation to chalcogenide QDs viz. their properties and the various synthesis methodologies. Further the biosynthesis of QDs, the microbial mechanisms that initiate biosynthesis and the process control for an effective size dependent quantization are elaborated.

2.1 Quantum particles

Quantum Particles are essentially low dimensional semiconductors, recognized as accomplished nano scale building blocks demonstrating functional attributes intermediate to that of a macroscopic semiconductor and that of an atomic or molecular system(Smith and Nie 2010). The interest towards quantum particles can be traced back to the early 1980's, when the oil crisis in the late 1970`s stemmed in the development of these semiconductor nanocrystals (NCs) with enhanced surface chemistry as important solar energy harvesting systems and dye sensitized solar cells (Konstantatos and Sargent 2013). Further research efforts in this arena were triggered by the discovery of quantum size effects in the optical spectra of nanometer-sized semiconductors (Bawendi et al. 1990; Ekimov et al. 1993). Thereafter, various efforts directed towards mastering the production of quantum particles in

the form of uniform, size tunable NCs, with adaptable physical and chemical properties were evinced (Peng et al. 1997; Lifshitz et al. 2003; Yong et al. 2006a; Gu et al. 2013).

Regardless of their chemical composition, all QPs are considered as an intermediate species between atoms or molecules on one hand and bulk materials on the other hand. According to the LCAO (linear combination of atomic orbitals) approach, every molecule consists of the atoms that combine to form molecular orbitals (Parak et al. 2003). The molecular orbitals with energy lower than that of the atomic orbitals are termed as bonding orbitals and those with energy higher than the atomic orbitals are called the anti-bonding orbitals. The molecular orbitals further combine to form bands viz. the valence band formed by bonding orbitals and the conduction band by the anti-bonding orbitals (Rogach 2008). The spacing between the valence and the conduction bands is termed as the energy band gap (Fig.2.1).

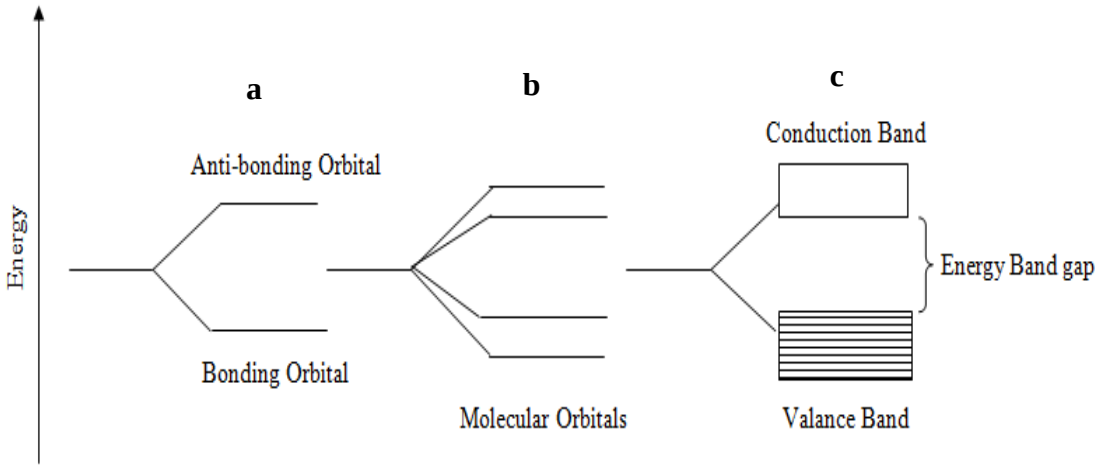

Fig. 2.1 The concept of LCAO; (a) When the orbitals of two atoms overlap, one bonding orbital and one antibonding orbital of significantly different energies are formed; (b) When the orbitals of four atoms overlap, four molecular orbitals are formed; (c) When the orbitals of N atoms overlap where N is a large number, N orbitals are formed. With so many orbitals, the orbital energies differ from each other and form continuous bands

According to the concept of energy bands, a semiconductor contains a completely filled valence band and a completely empty conduction band separated by the band gap. For an electron to jump from the valence band to the conduction band, it absorbs a photon and acquires energy to cross the band gap. As the valence electron jumps across the band gap, it leaves behind a positively charged "hole". The raised electron and the hole can then be considered as an "exciton". The average physical separation between the electron and the hole is referred to as exciton Bohr radius (Mathieu et al. 1992). However, the valence electrons stay in the conduction band only temporarily before falling back to their corresponding valence position. This recombination event is associated with the simultaneous release of an electromagnetic radiation having a wavelength different from that of the stimulus required to raise the electron to the conduction band (Sze and Ng 2006).

The band gap of a bulk material is constant and hence the energy transmitted during the electron-hole recombination is also fixed leading to fixed emission frequencies. Nevertheless, the reduction in dimensions of the semiconductor to its exciton Bohr radius seizes its resemblance to the bulk counterpart resulting in the formation of discrete energy levels (Sze and Ng 2006). The concept of discrete energy levels separated by a finite distance in a quantum particle as opposed to the typical continuous bands in a bulk semiconductor is called quantum confinement (Herz 2001).

Quantum confinement can be best described by the particle in a box analogy. In this analogy, the energy of a particle of mass "m" (m_e for electron) confined by a one dimensional box of dimension l of infinite potential is given by the equation (1):

$$E_n = \frac{n^2 h^2}{8 m_e l^2} \quad (1)$$

Where E_n is the energy of the particle, m_e mass of an electron, n is the quantum number, h is Plank`s Constant

Equation 1 implies that on decreasing the dimension "l" of the box, the electron-hole pairs are constrained within the reduced dimensions which in turn cause a change in the density of the electronic states resulting in discrete energy levels separated by an altered energy band gap. This in turn leads to an increase in the energy of the photon released as a consequence of the recombination event (Zheng et al. 2007).

According to Konstantatos and Sargent (2013), the large degree of confinement within a quantum particle ensue an enhancement in Coulomb interaction within the exciton which brings forth a shift in the emission spectra. In the presence of more excitons, exciton-exciton interactions can yield multi excitonic quasi particles with additional shifts in the energy spectrum and an intense fluorescence as a result. In essence, quantum confinement leads to altered emission lifetimes as well as altered luminescence quantum efficiency in quantum particles (Overney and Sills 2001). Additionally, quantum confined structures exhibit a shifted band edge that allows for the production of varied emission peak wavelengths as dictated by the size of the confinement (i.e. the size of the quantum dot) (Fig.2.2). Based on the spatial confinement of the exciton into the volume of the nanocrystal, quantum particles are categorized into quantum wells; wherein the exciton is confined only in one dimension, quantum rods (QRs) having confinement in two dimensions and quantum dots (QDs) characterized by confinement in all three dimensions of the semiconductor (Lifshitz et al. 2003).

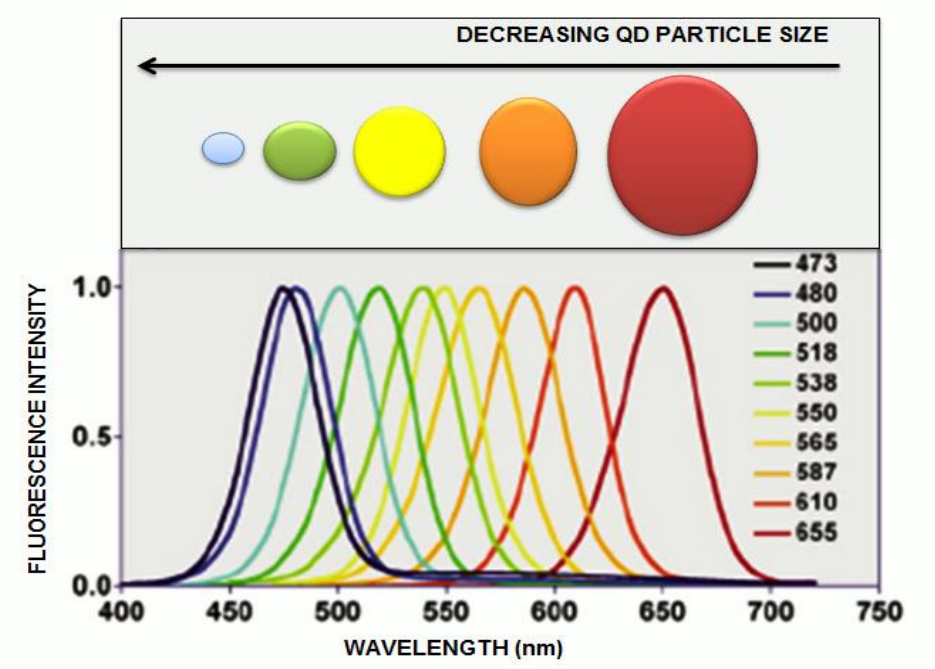

Fig. 2.2 Size tunable fluorescence spectra of QDs (Torchynska and Vorobiev 2011)

2.2 Candidate quantum particle materials

Quantum particles are usually compound semiconductors (e.g., CdSe, PbTe, ZnS, InAs) made up of elements of group II and VI, IV and VI, or III and V (Alivisatos 1996). An essential property inherent to an ideal candidate for a QP fabrication is that, the material should be a semiconductor with a high dielectric constant. The effective masses of the electron and the hole also play an important role in the choice of a suitable material for making a quantum particle. Furthermore the material should preferably be a direct band gap semiconductor for which quantum confinement effects on size tuning are achievable (Machol et al. 1994). Until the mid-1990's, a major challenge in QP research was to master the production of quantum particles in the form of uniform, well-dispersed, size-tunable and isolable NCs. But, the hot-injection method introduced by Murray et al (2001) proved to be an effective technique that enabled the synthesis of highly mono-disperse cadmium chalcogenide NCs. Thereafter various synthesis protocols based on the modification of hot injection method and other vapor phase-liquid phase deposition and the colloidal synthesis

for mono-disperse NCs of II-VI (CdSe, CdTe, CdS) (Herz 2001; Peng and Peng 2001; Huang et al. 2008a), III-V (InP- InAs) (Micic et al. 1995)and IV-VI (PbS, PbSe, PbTe) (Allan and Delerue 2004; Yong et al. 2006b; He et al. 2009) with precision in terms of size and emission properties have been reported.

Table 2.1 Characteristics of typical QD materials

QD Material	Dielectric Constant (ε)	Exciton Bohr Radius (nm)	Electron Bohr Radius (nm)	Hole Bohr Radius (nm)
II-VI: CdSe	6.23	3	3	<1
II-VI: CdS	5.23	2	2	<1
III-V: InP	10.60	9	7	2
IV-VI: PbSe	**25.00**	**47**	**23**	**24**

Table. 2.1 enumerate some of the important theoretical characteristics of typical QD materials. It can be observed that the electron and Bohr radii in case of II-VI and III-V semiconductors exhibit a larger difference in comparison to the IV-VI semiconductors. According to Murray et al (1993), the difference the in the electron and Bohr radii in II-VI and III-V semiconductors inhibit the realization of strong confinement effects in these QP fabrications. In contrast the similar electron and Bohr radii in IV-VI semiconductors, and in particular the lead-salt compounds, allow easy access to the strong confinement regime due to the congruent nature of their electron and Bohr radii. A typical example is PbSe, IV-VI semiconductor with crystalline rock-salt structure that possesses a narrow band gap of 0.27eV at ambient temperature. The conduction and valance bands of PbSe QDs are formed from the p-orbital chains of Pb and Se, respectively and the Bohr radius of an exciton in PbSe is as large as 47 nm. The optical transition from the valance band to the conduction band is almost

symmetrical. PbSe is also known for its strong dielectric screening (Vayssieres 2010). The above mentioned characteristics result in prominent quantum confinement effects in PbSe QDs. In brief, QDs of IV-VI materials have properties reflecting all the benefits of strong quantum confinement i.e., for the same level of confinement as QDs of II-VI or III-V materials, the surface-to-volume ratio can be quite low in IV-VI materials and hence strong confinement can then be achieved in relatively large QDs (Jiang 2012).

Further, the properties of Pb chalcogenide QDs are then far less likely to be influenced by surfaces effects like surface traps and defects. Additionally, their similarly small electron and hole masses lead to a large and nearly equal partitioning of the confinement energy between the charge carriers. Ultimately, these attributes result in sparse electron and hole states and a simple intense energy spectra (Wise 2000). Studies of extremely confined IV-VI QDs have revealed that these materials having unique vibration modes (Murray et al. 2001) can exhibit extremely weak electron-phonon coupling (Kang and Wise 1997)with negligible exchange and Coulomb energies (Andreev and Lipovskii 1999), and can have a temperature independent band-gap (Allan and Delerue 2004). Moreover, it is reported that lead-salt quantum dots are among the few materials that can provide size-quantized electronic transitions at technologically-important infrared wavelength (Schaller and Klimov 2004). These structures may find use in optoelectronic applications as well as in biophysical applications such as fluorescence microscopy.

2.3 Synthesis of lead chalcogenide QDs- traditional approaches

Despite the potential advantages of working with QDs in the extremely strong confinement limit, IV-VI QDs have received relatively little attention. This is partially due to the difficulty of synthesizing uniformly sized colloidal quantum dots with a narrow size distribution and a well-passivated surface (Allan and Delerue 2004). In general, QDs can be

synthesized through two major routes: hydrothermal, or colloidal synthesis (Fig.2.3) (Street et al. 2014).

In vapor-phase synthesis, quantum dots are grown through epitaxial self-assembly by depositing them on the surface of a semiconductor layer that has a lattice structure compatible with the candidate QD semiconductor material (Pelucchi et al. 2007). In colloidal synthesis, precursors of the QD material are separately dissolved in organophosphorus solvents such as tri-octyl phosphine (TOP), tri-butyl phosphine (TBP), or tri-isopropyl phosphine (i-TPP) and injected into a solution of the heated solvent such as tri-octyl phosphine oxide (TOPO) or a corresponding solvent mixture. This reaction mixture acts as a medium for the growth of the QDs through Ostwald ripening (i.e., small particles are absorbed by bigger ones) (Rosenthal et al. 2007). The addition of stabilizing mixtures like tetra-decylphosphonic acid (TDPA), Tri-octyl phosphine oxide etc. are also known so as to slow down the nanocrystal growth to result in good crystallinity and to improve the size distribution (Mekis et al. 2003). For instance, morphological control of quantum dots leading to the synthesis of rod- or tetrapod- shapes that show better performance for specific applications was achieved by the addition of phosphonic acids (Peng and Peng 2001). The TOPO has been reported to act as a surfactant and capping agent to ensure the solubility of quantum dots in non-polar solvents (Street et al. 2014).

While several modifications over the traditional synthesis methodologies for QD production have been reported over time, quite a lot of them indicate the ineptness of these processes from the environmental point of view. According to literature, one of the main disadvantages of chemical syntheses is their relatively low stability that requires the use of organic stabilizers which further complicates the structure and properties of the whole system. Sengül and Theis (2009) studied the environmental impacts associated with the chemical synthesis of CdSe quantum dots and have concluded that majority of environmental

impacts are associated with the solvents that are used as stabilizers in the QD chemical syntheses. According to literature, the need to search for alternative solvents also stems from the cost of organo-phosphorus solvents which accounts to 90 percent of the total production cost (Peng and Peng 2001). Another concern raised by chemical routes is the difficulty in controlling the QD yield. For example, the ethers formed due to the reaction between the methyl radicals and the oxygen in TOPO (solvent) are known to complex with the selenium in the reaction mixture to significantly vary the yield from 25% to 97%in case of chemical synthesis of QDs (Collins 2005). Further, it is also stated that the energy consumption during chemical synthesis is high (Sengül and Theis 2009).

2.4 Microbial QD synthesis mechanisms

Numerous biological resources have been exploited for the bio-production of QPs, including bacteria, fungi, plant extracts and earthworm. However, the microbial structures, such as the S-layer, flagella, and spores are regarded as potent nano-factories for the production of NPs with exquisite size and shapes (Narayanan and Sakthivel 2011). Nevertheless, the inherent biotransformation and metal bioaccumulation ability in fungi and bacteria draw special focus for the biological generation of semiconductor nanoparticles (Sastry et al. 2003). Among these microorganisms, fungi are reported to be extremely efficient secretors of extracellular enzymes that facilitate the large-scale production of QPs. The other advantages of using fungal-mediated green approaches for synthesis of nanoparticles include economic viability and ease in biomass handling (Ahmad et al. 2002).

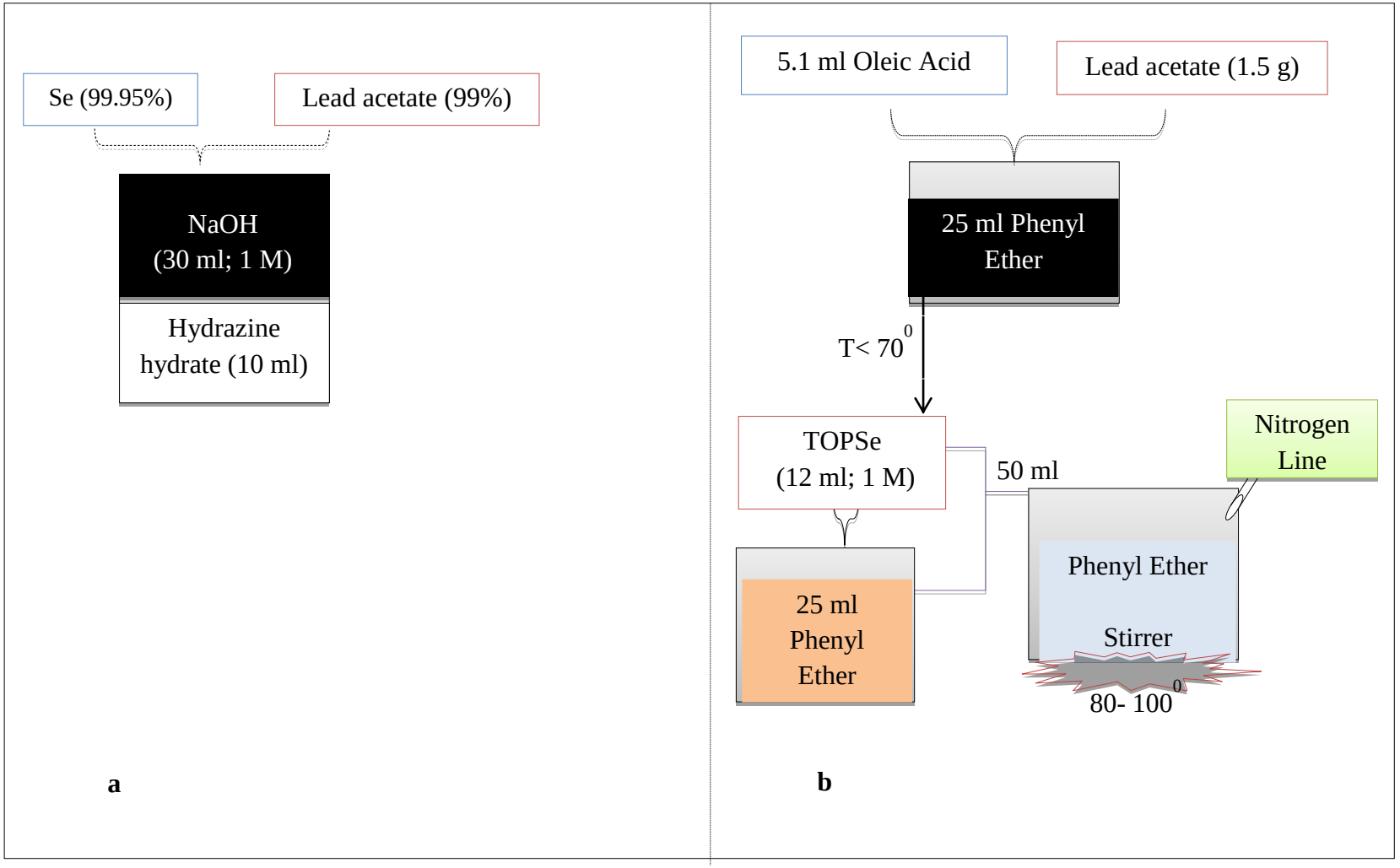

Fig.2.3 Chemical means of synthesis of PbSe quantum particles: (a) Hydrothermal synthesis; (b) Colloidal synthesis

While fungi offer a distinct advantage in nanoparticle synthesis owing to the ease in their scale-up, bacterial mediated synthesis in cell suspensions was also been reported for chalcogenide semiconductor nanoparticles. Moreover, bacterial mediated nanoparticle synthesis confers advantages of directed evolution and genetic manipulation for the over-expression of specific enzymes identified in the synthesis of nanoparticles. In this context, the economic viability and non-toxic nature of the green routes for QD synthesis need to be highlighted, as these circumvent high temperature, pressure, energy or hazardous chemicals and sophisticated operational requirements (Singh et al. 2010). For instance, while biosynthesis of CdSe QDs occur at conditions akin to room temperature (Holmes et al. 1997), the chemical syntheses routes require higher process requirements, temperatures as high as 300^{o}C and the presence of toxic agents like TOPO (Sengül and Theis 2009). As a result, the operational costs during scale up of chemical mediated processes would increase and the downstream pollutant load on the environment is expected to be high.

2.4.1 Intracellular biosynthesis

Biosynthesis of semiconductor nanocrystals was pioneered as early as 1989 when Dameron et al (1989a, 1989b) reported the biosynthesis of quantum crystallites in the yeasts *Candida glabrata* and *Schizosaccharomyces pombe*, cultured in the presence of cadmium salts. Short chelating peptides with the general structure (γ-Glu-Cys)$_n$-Gly were found to control the nucleation and growth of CdS crystallites to peptide-capped intracellular particles of 20 Å diameter. The mechanistic insights into the biosynthesis of CdS affirm the findings that the yeast, upon exposure to cadmium salts, synthesize metal chelating peptides (phytochelatin analogues) (Dameron et al. 1989b).Further, the formation of a Cd-γ-glutamyl complex accompanied by an increase in the intracellular sulphide levels is reported to take place. These sulphides were observed to form a complex with cadmium to result inCdS nanocrystallites that accumulates in the vacuoles of the organism. Subsequent work

(Dameron and Winge 1990) further explained the involvement of a peptide mediated intracellular mechanism in the fungus for the synthesis of semiconductor NCs. Later, Kowshik et al. (2002a, 2002b) initiated the intracellular biosynthesis of CdS and PbS nanoparticles in *S. pombe* and *Torulopsis* strains, respectively. Although descriptive mechanistic insights to these biosynthesis processes are not reported, it is stated that the yeast initiated intracellular biosynthesis in the mid log phase of their growth. According to Dameron et al. (1989a), the intracellular synthesis of CdS in yeast occur by a process involving the sequestration of the Cd^{2+} ions by glutathione-related peptides followed by the consequent production of CdS within the yeast cells.

A major shortcoming of the above discussed studies was that the QDs were synthesized "intracellularly". When the site of nanoparticle synthesis is intracellular, additional downstream processing procedures for the recovery of QDs become vital. The QD recovery and purification procedures in a typical intracellular biosynthesis include cell lysis, centrifugation, freeze thawing and high resolution chromatography respectively (Mi et al. 2011; Pandian et al. 2011; Mousavi et al. 2012). These supplementary processing steps in intracellular biosynthesis protocols often defeat the purpose of developing a simple and cheap process (Kowshik et al. 2002a) and necessitate the need to explore alternate green pathways that can surpass these treatments and provide scalable routes for the large scale synthesis of QDs.

2.4.2 Extracellular biosynthesis

The downstream processing steps of intracellular means of QD biosynthesis has been effectively overcome by the development of the one-step scalable extracellular biosynthesis of semiconductor nano crystallites in microorganisms. The pioneering communication in this regard was reported by Ahmad et al. (2002) who reported the extracellular biosynthesis of CdS NPs using the fungus *Fusarium oxysporum* in a facile enzymatic process. According to

(Bao et al. 2010b) the enzymatic process that aid extracellular biosynthesis of QDs involve the release of specific enzymes such as reductases secreted by the microbe as a part of its defence mechanism. This mechanistic highlight opened up the exciting possibility of designing a rational biosynthesis strategy for nanomaterials of different chemical compositions. Further, the extracellular synthesis process was claimed to be reportedly rapid, and scalable.

A detailed mechanism for the extracellular biosynthesis of CdTe QDs by yeast was given by Bao et al. (2010a). Authors have speculated that the formation of protein-capped CdTe QDs with uniform size involve extracellular growth mechanism comprising of nucleation of metal ions with the yeast secreted proteins followed by Ostwald ripening, wherein small crystals or particles dissolve, and redeposit onto energetically stable larger crystals or particles. The active role of the microorganism in biosynthesis of CdTe QDs were further affirmed by the finding that the absence of yeast cells in precursor mixture led to the formation of an amorphous Te^{2-} colloid and not the CdTe QD.

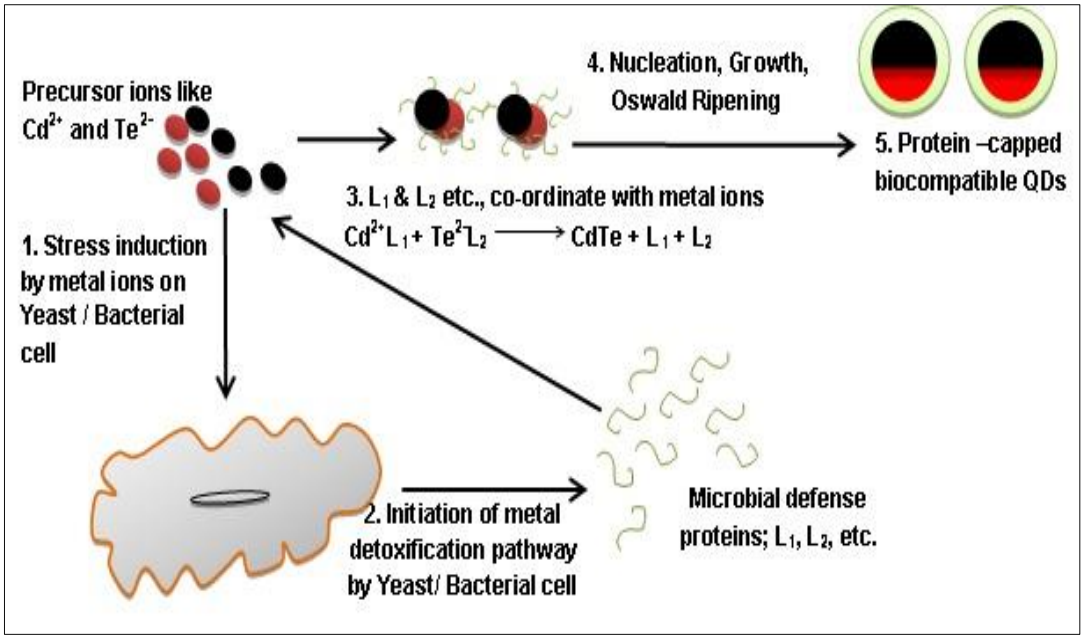

Fig.2.4 Microbial mechanism for the formation of biocompatible QDs

Fig. 2.4 provides a schematic of the microbial mechanism involved in the extracellular biosynthesis of CdTe QDs as proposed by Bao et al. (2010a). According to the authors the Cd^{2+} and Te^{2-} ions in the reaction mixture induce a specific defense mechanism in the yeast cells. This defense mechanism prompts the yeast cells to secrete proteins that can coordinate with the ions to detoxify them. The peptide coordinated ions form clusters (nuclei) that subsequently grow in the medium followed by an early ceasing of the Ostwald ripening process to result in protein capped CdTe QDs (Bao et al. 2010b) with tailored size and excellent crystallinity (Bao et al. 2010a). According to the authors (Bao et al. 2010a), the microbial protein caps on the QDs improve their biocompatibility and enhances their fluorescence. It is also reported that the protein cap confinement leads to a uniform size distribution and good degree of dispersion without any aggregation (Kang et al. 2008; Cui et al. 2009).

Another noteworthy approach for the extracellular biosynthesis of CdS nanoparticles in *Saccharomyces cereviciae* was initiated by Prasad and Jha (2010). It is reported that fungal enzymes like oxido-reductase; phytochelatin synthases etc. were activated by the yeast to quell the metal stress in solution. Collateral stress generated response had earlier been suggested in *Candida glabarata* cells exposed to Cd^{2+} ions in the form of secretion of the enzyme phytochelatin synthase and a protein HMT-1 to effectively reject the CdS NCs into the cytosol. The CdS in the cytosol was found to trigger the oxidation/oxygenation of oxygenases harboured in the endoplasmic reticulum (ER) to initiate specific cellular level detoxification surge. A comparison of the efficiency of bacteria and fungi as candidate systems for biosynthesis of NCs has also been drawn. Based on their findings, authors concluded that better size quantization effects were observable in yeast in comparison to bacterial cells for the production of CdS nanoparticles (Prasad and Jha, 2010).

Bick et al. (2000) detailed the involvement of 5'-adenylylsulfate reductases in sulfate-assimilating bacteria that could efficiently detoxify cadmium ions by the formation of extracellular CdS particles. Drawing inferences from the metal detoxification mechanisms in microorganisms, Malarkodi et al.(2014) proposed a comprehensive mechanistic insight into the biosynthesis of CdS quantum particles in *K. pneumonia*. According to the authors, initially the sulphate ions are taken up by the microbe from the nutrient broth (extracellular environment) and are converted into adenosine phosphosulphate (APS) with the support of the enzyme ATP sulfurylase. The adenosine phosphosulphate would further be phosphorylated to form 3' phosphor adenosine phosphosulphate which undergoes subsequent reduction to sulphite using the enzyme phosphor adenosine phosphosulphate reductases (Malarkodi et al. 2014). These sulphite ions would later be reduced to sulphide ions using sulphite reductases secreted as a part of the microbial metal detoxification system. The sulphide ions later couple with the inorganic metal ions like cadmium in the extracellular environment to result in the formation of cadmium sulphide nanoparticles.

Similar observations were made by Li et al.(2007b) on the involvement of a 30 kDa protein in the extract of *Capsicum annuum* that could effectively reduce selenium ions to selenide ions through an enzymatic reaction. In another study, Luo et al. (2014) observed an increase in the glucan content of the yeast cell walls during the synthesis of CdSe QDs. Further, Kang et al. (2008)genetically engineered *E-coli* strains using plasmids containing phytochelatin synthase from *Schizosaccharomyces pombe* and γ-glutamyl cysteine synthetase that capacitated the bacteria as effective bio-factories for the synthesis of CdS QDs. The important role of phytochelatin synthase in the synthesis of semiconductor QPs has also been elaborated by Liu et al.(2010). The authors utilized histidine tagged phytochelatin synthase (PS) gene expressing *E-coli* cell lysates, the PS from which was selectively immobilized on nickel resins. The immobilized PS enzyme was found to convert the glutathione into the

metal binding peptide phytochelatin thus mediating the synthesis of phytochelatin capped CdS nanocrystals.

Taking into consideration the prospective advantages of utilizing microbial sources for QD synthesis, a more comprehensive understanding regarding the mechanisms that initiate biosynthesis, hold enormous significance. According to Ramezani et al. (2010), the metabolic complexities of viable microorganisms complicate the identification of active microbial species in the nucleation and growth of NPs. Further studies on the biochemical and molecular mechanisms that mediate QD biosynthesis can improve our understanding of such processes to achieve the production of smaller and mono-dispersed QDs using microorganisms.

2.5 Biosynthesis of QDs

The aforementioned metal detoxification mechanisms in microbes have paved way towards the active utilization of these micro-factories as efficient sources for QD synthesis. Although the constraints in the cultivation of microorganisms and the shape and size control of the microbiologically generated NPs have been reported as significant drawbacks of bio-mediated processes (Gericke and Pinches 2006), several authors have overcome these limitations through the regulation of process parameters such as the pH, incubation time, temperature, metal salt concentration and the amount of biological inoculum together with a variety of physical factors.

Table 2.2 summarizes the efforts of various researchers for biosynthesis of cadmium and lead based chalcogenide semiconductor quantum particles. Both eukaryotic and prokaryotic organisms have been used in the biosynthesis of quantum particles. It is noteworthy that all the biosynthesis procedures follow a similar trend wherein (Fig. 2.4), the respective microorganisms are incubated with the metal salts for a given period of time to

initiate a metal detoxification process leading to the formation of the respective quantum particle.

2.6 Influence of various parameters on synthesis and fluorescence of quantum particles

2.6.1 Growth phase of the organism:

Experimental efforts to optimize and enhance the synthesis of semiconductor nanoparticles have been reported by several authors. Pandian et al. (2011) studied the effect of growth phase of biomass on the synthesis of CdS nanoparticles. It was observed that during stationary phase, the organism produced a relatively high amount of nanoparticles when compared with the biomass obtained from other phases. Sweeney et al. (2004) demonstrated intracellular dense packing of CdS nanoparticles in *E-coli* at the stationery phase of the bacterial growth. According to literature, the metal tolerance of the fungus is enhanced during stationary phase due to the release of enzymes and other chemical metabolites that quell the metal stress. Furthermore, the metal tolerance capacity is reported to vary with the type of microbe and the metal under consideration. For instance, the presence of nickel in the growth medium is testified to result in an extended mid log phase in *Aspergillus* sp. However, the presence of chromium in the medium was reported to protract stationary phase for the same organism (Shankar 2007). Nevertheless, majority of the literature suggest the preferential use of microbes in their stationery phase for nanoparticle synthesis.

2.6.2 pH and precursor concentration

The molar ratios of reactants have also been reported as important parameters that influence the QD size in chemical synthesis protocols. It is generally accepted that the concentration of reactants can directly affect the products in a chemical synthesis. Yong et al. (2006a) demonstrated that the shape of PbSe nanocrystals can be controlled systematically by varying the precursor concentration. According to the authors, Pb:Se ratio of 1:1 (mol %)

yielded T-shaped and L-shaped quantum rods. However, T-, cube-, and dot-shaped particles were reported for 2:1, 3:1 or 1:2 of Pb:Se respectively. Although a definite trend between the precursor concentrations and the shape of the nanocrystal is not interpreted, it could be noted that precursors at a higher molar ratio have a significant effect on the shape of the nano particles.

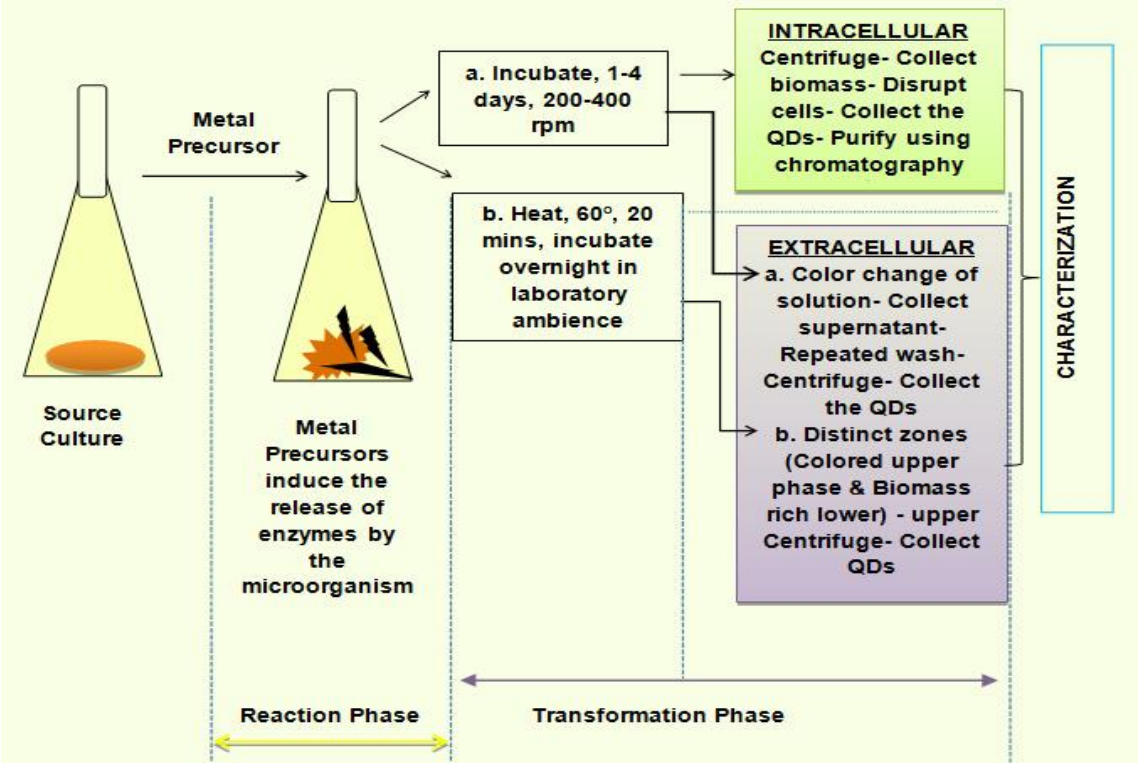

Fig. 2.5 General scheme followed for biosynthesis of quantum particles by microorganisms

Table 2.2 Biosynthesis of cadmium and lead based chalcogenide quantum particles

Semiconductor NC	Organism	Site of Biosynthesis	Size and Shape	Spectral Properties	Other Characteristics	Ref
Cadmium Telluride (CdTe)	*Escherichia coli*	Extracellular	2-3 nm, QDs	Fluorescence emission: 488 to 551 nm	Folic acid functionalized QDs used for bio imaging cervical cancer cell lines.	(Bao et al. 2010b)
	Saccharomyces cervisiae	Extracellular	2-3.6 nm, QDs	Fluorescence emission: 492 nm	Fluorescent, Biocompatible QDs used in bio imaging	(Bao et al. 2010a)
	Fusarium oxysporum	Extracellular	15-20 nm, QDs	Fluorescence emission: 475 nm	Thermally stable with antibacterial properties	(Syed and Ahmad 2013)
	Lumbricus rubellus earthworm	Intracellular	2.33+0.59 nm, QDs	Fluorescence emission: 460, 520 nm	Crystalline water soluble luminescent nanoparticle; Native and PEG capped QDs used in cellular imaging.	(Stürzenbaum et al. 2012)
Cadmium Sulphide (CdS)	*Candida glabrata* and *Schizosaccharomyces pombe*	Intracellular	20 Å, QDs	-	Peptide-capped particles, Short chelating peptides (γ-Glu-Cys)n-Gly control the nucleation and growth	(Dameron et al. 1989a, 1989b; Dameron and Winge 1990)
	Klebsiella pneumonia	Extracellular	> 5 nm	Absorbance maximum: 381, 424 nm	Band gap: 2.9 eV, cysteine desulfhydrase aided synthesis	(Holmes et al. 1997)

Schizosaccharoyes pombe	Intracellular	1–1.5 nm, QDs	Absorbance maximum: 305 nm	Wurtzite ($Cd_{16}S_{20}$)-type hexagonal lattice structure.	(Kowshik et al. 2002a)
Escherichia coli	Intracellular	2–5 nm, QDs	-	Bacteria in stationary phase release thiol compounds to assist NC formation.	(Sweeney et al. 2004)
Fusarium oxysporum	Extracellular	5-20 nm, QDs	Absorption maximum: 450 nm	Sulfate reducing enzyme-based process	(Ahmad et al. 2002)
Rhodopsueodomonas palustris	Extracellular	8 nm, QDs	Absorption maximum: 425 nm	Face centered cubic lattice crystallinity, Cytoplasmic cysteine desulfhydrase enzyme	(Bai et al. 2009)
Coriolus versicolor	Extracellular	100-200 nm, Spherical	Fluorescence peak: 450 nm	Cd bioremediation and CdS synthesis in a continuous column mode	(Sanghi and Verma 2009)
Brevibacterium casei	Intracellular	10-30 nm, QDs	Fluorescence peak: 430 nm	PHB encapsulated NCs with enhanced stability, reduced toxicity, used for bio imaging	(Pandian et al. 2011)
Escherichia coli	Intracellular	6 nm, QDs	Fluorescence emission: 445-510 nm.	Genetically engineered to introduce CdS binding peptide; water soluble biocompatible	(Mi et al. 2011)

	Lactobacillus sp.	Extracellular	4.93 nm, QDs	Maximum absorbance: 393 nm	Band gap energy: 2.52 eV; biosynthesis initiated by membrane bound oxido-reductases	(Prasad and Jha 2010a)
	Saccharomyces cerevisiae	Extracellular	3.57 nm, QDs	Maximum absorbance: 369 nm	Band gap energy: 2.607 eV.	
	Enterobacteriaceae	Intracellular	5-200 nm, QDs	Maximum absorbance: 450 nm	Optimized conditions: pH: 9, Temperature: 30^{o}, Growth Phase: stationary	(Mousavi et al. 2012)
	Serrantia nematodiphila	Extracellular	12 nm, QDs	Maximum absorbance: 420 nm	Stable particles with antibacterial activity	(Malarkodi et al. 2014)
	Klebsiella pneumonia	Extracellular	10-25 nm, QDs	Maximum absorbance: 420 nm	QDs with antimicrobial activity	(Bick et al. 2000)
Lead Sulphide (PbS)	*Torulopsis* yeast	Intracellular	2–5 nm, QDs	Absorption maximum: 330 nm	Band gap of 3.75 eV	(Kowshik et al. 2002b)
Cadmium Selenide (CdSe)	*Fusarium oxysporum*	Extracellular	2-7 nm, QDs			(Kumar et al. 2007)

Pandian et al. (2011) for the biosynthesis of CdS nano particles in *Brevibacterium* have reported an enhanced luminescence by the bacteria during biosynthesis reactions at higher concentrations of the precursor molecules. However, Mi et al. (2011) accounted that the fluorescence emission exhibited an obvious red-shift with the increase of the concentration of reactant within the range of 0.5–10 mM. According to the authors, the increase of reactant concentrations would have weakened the control over CdS nanocrystals' nucleation by foreign proteins in the bacterial cells, which resulted in the increase of average particle size and the consequent red shift in emission wavelength. Pendyala and Rao (2009) prepared PbS samples with Pb:S molar ratios 5:1 and 1:5, such that the excess of Pb or S results in the surfaces terminated either with Pb or S respectively. The Pb terminated samples with Pb:S at 5:1 were reported to exhibit very high signal in the blank sample itself with no observable changes in the PL spectrum in the presence of various metallic ions including silver and mercury. This negative result was attributed to the Pb cover on the QD surface. In their previous report, the authors have shown that surplus Pb resulted in the formation of bigger particles with a wide size distribution (Pendyala and Rao 2008).

The pH of the solution is also stated to have a profound effect on the reduction reaction of the metallic ions. Pandian et al. (2011) analyzed the effect of various pH conditions on the synthesis of CdS nano crystallites by *Brevibacterium* sp. The pH of the incubation mixtures was adjusted using 1M HCl and 1M NaOH solutions. It was observed that synthesis of nanoparticles and fluorescence intensity of the particles varied vastly with pH and at pH 9 an enhanced fluorescence by the nanoparticles was observed. The alkaline environment has previously been found to aid the synthesis of various nanoparticles in association with the protein molecules (Gurunathan et al. 2009). Kowshik et al. (2002b) checked the pH stability of the biosynthesized

PbS nanocrystallites by adjusting the pH of sample aliquots to the desired value in the range 5-11 and recording the fluorescence spectra. It was observed that acidification of the nanocrystallites from pH 7 to 6 led to attenuation of λ_{max} with a very small blue shift. However, at pH values below 6 the nanocrystallites were found to precipitate out of solution. Damerone and Winge (1990) showed that acidification of microbially produced CdS particles from pH 5 to 4 resulted in attenuation of λ_{max} albeit with a red shift as opposed to the blue shift obtained for the PbS nano crystallites (Kowshik et al. 2002b). Further, it was observed that under alkaline conditions, PbS nanocrystallites exhibited an enhancement of the λ_{max} and a minimal red shift of λ_{max}.

2.6.3 Temperature and reaction duration (growth and incubation time):

Lifshitz et al. (2003) described the chemical synthesis and characterization of PbSe quantum wires, multipods, quantum rods, and cubes and analyzed the effect of metal precursors in the presence of various surfactants and the resultant morphology of nanocrystallites formed under different conditions of temperature and reaction duration. It was observed that, while lower temperatures (~10 ^{o}C) resulted in the formation of quantum wires, the quantum dots and cubes where formed at 60 ^{o}C and 117 ^{o}C respectively. Although temperature was found to have an edge in the morphology of the nano crystals, the influence of growth time variation was not significant. Growth time variations from 10 min to one hour yielded QWs and multi pods. Their investigation revealed that there is a delicate balance, which determines the morphology of the NCs, controlled by the solvent, temperature, and reaction duration. Baek et al. (2008) in their study on synthesis of PbSe Quantum Dots by hot solution method examined the effect of growth and nucleation temperatures on the size and absorbance. It was shown that the size of the PbSe QDs decreases with increase in nucleation and growth temperature leading to the shift in λ_{max} to lower wavelengths.

Although chemical syntheses report better size control at temperatures as high as 100 ^{o}C, the studies on size tunability of biosynthesized semiconductor nanocrystallites under wide temperature ranges and incubation times are limited. Bao et al. (2010a) analyzed the effect of incubation period and temperature on the biosynthesis of CdTe QDs in yeast. Although the yeast cells can grow in a temperature range from 5 to 35°C, the QDs has been reported to show better growth at a relatively high temperature. UV–Vis spectroscopic studies indicated that when the reaction time was increased from 1 day to 8 days, the absorption edge of the CdTe samples showed a much larger red-shift (70 nm) at 35°C than that (20 nm) observed at 25 °C. This suggested that the growth of the CdTe QDs is much slower at 25 °C, and that the size can be easily tuned by choosing the appropriate reaction time at a relatively high temperature (35 °C). Mi et al. (2011) reported that the intracellular formation of CdS QDs in genetically engineered *E-coli* vary dramatically with the parameters, such as reaction time, temperature and incubation period. Increase in incubation time beyond 12 h had led to a drastic decrease in the intensity of fluorescence and absorbance.

2.7 Applications of QDs

The exceptional optoelectronic properties of QDs have enabled their application in diverse sectors. An important property of the QDs that make them ideal nanomaterials for ultrasensitive optical sensing and therapeutic applications is their fluorescence response. A typical sensing event by a QD is based on fluorescence transduction. In principle, the chemical or physical interactions occurring on the surface of the QDs change the efficiency of their radiative recombination, either leading to photoluminescence activation or quenching (Frasco and Chaniotakis 2009). Following this approach, the changes induced by the direct interaction between the analytes and the QDs' surface (unmodified or functionalized with a given ligand)

have supported the selective detection of a multitude of compounds (Pendyala and Rao 2009; Wu et al. 2010; Kim et al. 2012).

The growing ability to functionalize the QD surface with stimuli selective receptors along with the progressive knowledge on their functional attributes like toxicity etc. have enabled their applications in in-vivo labeling, imaging and biomedicine (Jamieson et al. 2007a; Medintz et al. 2008). There are ongoing efforts to extend their in vivo suitability by developing QDs of higher biocompatibility. Efforts are also underway to utilize QDs that possess near-infrared emission frequencies so as to take advantage of the improved tissue penetration and reduced background fluorescence. Further, QDs have been tagged to multiple biomolecules to provide information on disease-related molecular events essential for diagnosis and treatment (Medintz et al. 2008Kairdolf et al. 2013; Prokopovich 2015).

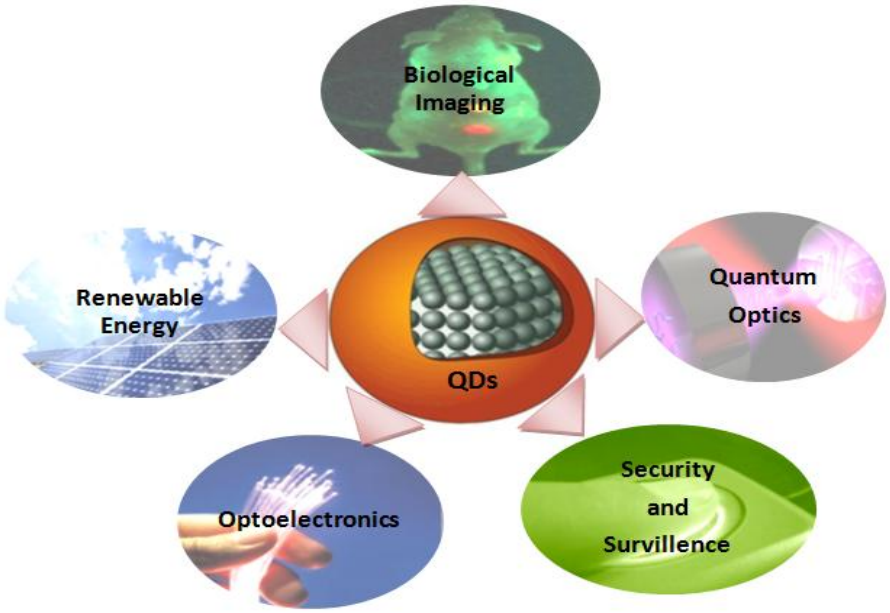

Fig. 2.6 Applications of QDs

Pollutant/analyte sensing have also taken advantage of the new functional platform provided by QDs, as demonstrated by numerous works summarized in the literature (Altavilla and Ciliberto 2010). Many of the designed sensing assemblies are based on energy flow such as transfer of electronic excitation energy between the components of such nano assemblies. This can occur when light energy absorbed by QDs (donor) is transferred to a nearby acceptor species, such as an organic fluorophore/ the bound analyte (acceptor) in a process called Förster Resonance Energy Transfer (FRET) (Clapp et al. 2006). The rate of energy transfer depends on the distance between the donor and the acceptor, their relative orientations, and the spectral overlap. Therefore, the energy flow at the nano scale can be altered, initiated or disrupted, by small perturbations such as specific interactions due to molecular binding events. Due to the small size and high surface area-to-volume ratio of the nanoparticles, the photoluminescence of QDs is very sensitive to modifications on the surface configurations. Changes on QD's surface charge or ligands can affect the efficiency of electron–hole recombination (Leatherdale et al. 2000) yielding in consequence a significant alteration on the magnitude of the fluorescence emission either in a quenching or in an enhancing effect (Jin et al. 2005). Since the first study demonstrating the energy transfer from QDs to organic chromophores (Willard et al. 2006), the usage of QDs scaffold for FRET assays by many researchers have been reported.

For instance, CdTe quantum dots synthesized by *Saccharomyces cerevisiae* were used as *in-situ* bio-labels in yeast cells (Bao et al. 2010b). In another study, surface passivated luminescent CdTe QDs synthesized in *Lumbricus rubellus* earthworms were utilized for the fluorescence based cell imaging of ovarian cancer cell lines (Stürzenbaum et al. 2013). Of late, chemically synthesized QDs have been applied in fluorescence assays for the quantification of distinct analytes (Huang et al. 2008b; Malik et al. 2014) including metals (Xie et al. 2004;

Fernández-Argüelles et al. 2005; Li et al. 2007a; Zhang et al. 2008; Koneswaran and Narayanaswamy 2009). Recently, synthesis of graphene QDs via chemical route was employed for the efficient Cu^{2+} ions in solution (Wang et al. 2014). However, the possibilities for tapping the fluorescence potential of biosynthesized chalcogenide QDs as sensors for the detection of environmental pollutants and heavy metals are largely unfathomed. Thus it is pointed out that the gap between the analytes to be sensed and the availability of efficient, non-toxic and user friendly sensors is large (Basabe-Desmonts et al. 2007). In summary, despite the advancements in the biosynthesis of chalcogenide QDs, the prospects of these nanofabrications, in particular PbSe, in analyte sensing and other environmental applications is largely unexplored.

3. MATERIALS AND METHODS

This chapter describes the materials used and the experimental methodologies adopted to achieve the stated objectives. Descriptions the statistical modeling of the various optimization techniques are also elaborated. All the experiments were carried out using laboratory grade chemicals with purity levels ≥ 99% and all the solutions were prepared using distilled water. The catalog for the laboratory chemicals used in the experiments is provided in Appendix-I. The results were represented as the mean value with the standard deviation of triplicate sets of experimental runs.

3.1 Collection of samples, isolation, screening, and identification of lead and selenium tolerant fungal species from marine ecosystem

3.1.1 Collection of samples

Sea water and sediment samples were collected in clean sampling containers from coastline near industrial environs in Mangalore, Karnataka, India (Fig.3.1). These samples were brought to laboratory and stored at 4 ^{o}C for further processing.

3.1.2 Lead and selenium analysis in samples

Water and sediment samples were analyzed for their total content of lead and selenium. The sediment samples were oven dried at 105 °C. A sample of 1 g was digested with 5 ml HNO_3 and 10 ml HCl. Digestion was carried out on a hot plate until dense fumes evolved and a clear solution was obtained. The clear solution was filtered through a Millipore filter (0.45 μm) and diluted to 50 ml with distilled water prior to analysis. However, 50 ml of sea water was directly used for lead and selenium analysis. A double beam GBC932 plus Atomic Absorption Spectrometer (AAS) with selenium and lead lamps was used for the respective metal content

analysis. Stock Solutions of lead and selenium for AAS were purchased from Hi-Media Laboratories Pvt Ltd, Mumbai, India. Working standard solutions of lead and selenium were made by the appropriate dilution of the respective 1000 mg/L standard stock solutions.

Fig. 3.1 Localisation of Sampling Sites

3.1.3 Isolation of fungus from collected samples

The sample with the highest concentration of lead and selenium was enumerated for micro-organisms employing a serial dilution technique using Potato Dextrose Agar (PDA) (Hi-Media, Mumbai, India) containing 20 mg/L each of lead and selenium. Initially, 1000 mg/L

stock solutions of lead and selenium were prepared in double distilled water using lead nitrate ($PbNO_3$) and freshly prepared sodium selenosulphate (Na_2SeSO_3) respectively. The stock solutions of the heavy metals were autoclaved separately, diluted to 20 mg/L using double distilled water and were added to sterile PDA medium under sterile conditions. Sea water samples were serially diluted up to 10^{-8} and 1 mL of diluted sample (10^{-8}) was added in sterilized lead and selenium amended PDA plates and incubated for least 3 days at 25°C. Developed colonies were randomly picked and purified isolates were cultured by streaking the colonies repeatedly in PDA medium. Pure cultures of isolated micro-organisms were identified using the standard keys (Dugan 2006).

3.1.4 Tolerance studies on the isolated marine fungi

The tolerance of the isolated fungi to lead and selenium was further quantified by comparing their tolerance indices. A mycilial disc (5 mm) of the respective fungus was cultured on PDA medium containing 20 mg/L of lead and selenium for a period of 7 days at room temperature. Fungal isolates grown on PDA medium sans the metal/metalloid under similar conditions served as control. The index of tolerance, defined as the ratio of the extension radius of the treated colony to that of the untreated colony in the selected fungi was estimated by measuring the radius of the colony extension (mm) in presence of 20 mg/L of metal against the control (medium without metal) after at least 7 days of incubation. The fungal strain with maximum tolerance index was chosen for further studies.

3.1.5 Morphological and molecular identification of the lead and selenium tolerant fungus

The marine fungus that exhibited the highest tolerance to lead and selenium on PDA was examined every day to study the macroscopic morphology and was identified using conventional staining of the fungal spores using lacto-phenol cotton blue stain. A drop of lacto-phenol cotton

blue stain was placed at the centre of a clean glass slide. A small fragment of the fungal colony was removed using a sterile needle and placed on the drop of the stain and teased gently. Cover slip was placed over it and the mount was observed under low and high magnification microscope equipped with a camera (MOTIC BA200). Further, the lead and selenium tolerant fungal strain was subjected to molecular identification (ITS Sequencing of 500-700 base pairs and BLAST search) at the National Fungal Culture Collection of India, Agharkar Research Institute, Pune, India.

3.2 Growth studies on *Aspergillus terreus*

The growth characteristic of heavy metal tolerant *Aspergillus* sp (Brown) was further screened using typical shake flask experiments in Potato Dextrose Broth (PDB). Owing to the remarkably high tolerance index of the fungus, the fungal spores in the form of 2 x 5 mm mycelial discs were seeded on 100 mL PDB medium and observations on growth of fungal isolate were made by measuring the weight of biomass every day after an initial 72 h of incubation for 10 consecutive days.

3.3 Media optimization for *Aspergillus terreus*

3.3.1 Screening of Medium Component for Biomass production Using Plackett-Burman Design

A Plackett-Burman (PB) design was used to select the critical components for maximizing the biomass yield by *Aspergillus terreus*. A total of 11 process parameter including Sucrose (A), Peptone (B), $MgSO_4.7H_2O$ (C), KH_2PO_4 (D), $NaNO_3$(E), KCl (F), $FeSO_4.7H_2O$ (G), pH (H), RPM (I), Temperature (J) and Inoculum concentration (K) were considered in the design, of which pH, Temperature, RPM, and Inoculum concentration were taken as dummy variables. The medium components were added at two levels: low (-1) and high (+1); such as

Sucrose (30 and 40 g/L), Peptone (5 and 10 g/L), $MgSO_4$ (0.4 and 0.8 g/L), KH_2PO_4 (1 and 0.5 g/L), $FeSO_4.7H_2O$ (0.01 and 0.04 g/L), KCl (0.4 and 0.8 g/L) and $NaNO_3$ (5 and 10 g/L). This is a fraction of a two level factorial design and allows the investigation of 'n-1' variables with at least n experiments. The selected factors were screened in twelve combinations to provide an adequate estimate of the error. This design requires that the frequency of each level of a variable should be equal and that in each test the number of high and low variable should be equal. Further, the design characterizes a model that identifies the significant variables when no interaction among the factor is expected. The design matrix created using Design Expert Software (version 8.0.7.1) is represented in Table 3.1. The PB Experimental Design is based on the first order model (equation 2).

$$Y = \beta_0 + \Sigma \beta_i X_i \quad (2)$$

Where Y is the response (Dry weight of Biomass) in g/L, β_0 is the model intercept and β_i is the variable estimate.

3.3.2 Determination of optimal concentration of medium component using Response surface method: Box – Behnken Design (BBD)

The levels of the significant parameters and the interaction effects between various variables that influenced the fungal biomass production were analysed and optimized by Box – Behnken (BBD) methodology. In this study, the experiment consisted of 17 trials and the independent variables were studied at three different levels, low (-1), medium (0) and high (+1), such as Peptone (5, 10, 15 g/L), KH_2PO_4 (0.75, 1, 1.25 g/L) and $FeSO_4.7H_2O$ (0.03, 0.06, 0.09 g/L). The experimental design used for the study is shown in Table 3.2. All the experiments were done in triplicate and the average biomass production obtained was taken as the dependent variable or response (Y). The effect of a particular component on the response was considered significant only if p value ≤ 0.05 was obtained.

3.3.3 Data analysis

The second order polynomial coefficients were calculated and analysed using the 'Design Expert' software (Version 8.0.7.1, Stat-Ease Inc., Minneapolis, USA) statistical package. The general form of the second degree polynomial equation is

$$Y_i = \beta_0 + \Sigma\beta_i X_i + \Sigma\beta_{ii} X_i^2 + \Sigma\beta_{ij} X_i X_j \quad (3)$$

Where Y_i is the predicted response, $X_iX_j$are input variables which influence the response variable Y; β_o is the offset term; β_i is the influence of the i^{th} linear coefficient; β_{ii} is the i^{th} quadratic coefficient and $\beta_{ij}$is the ij^{th} interaction coefficient.

Table 3.1 Placket Burman Design of Experiments for Eleven Variables

Run	A	B	C	D	E	F	G	H	I	J	K
1	1	-1	-1	-1	1	-1	1	1	-1	1	1
2	1	-1	1	1	-1	1	1	1	-1	-1	-1
3	1	1	-1	-1	-1	1	-1	1	1	-1	1
4	-1	-1	-1	1	-1	1	1	-1	1	1	1
5	1	1	-1	1	1	1	-1	-1	-1	1	-1
6	-1	1	1	1	-1	-1	-1	1	-1	1	1
7	-1	-1	-1	-1	-1	-1	-1	-1	-1	-1	-1
8	1	-1	1	1	1	-1	-1	-1	1	-1	1
9	-1	-1	1	-1	1	1	-1	1	1	1	-1
10	-1	1	-1	1	1	-1	1	1	1	-1	-1
11	-1	1	1	-1	1	1	1	-1	-1	-1	1
12	1	1	1	-1	-1	-1	1	-1	1	1	-1

Sucrose (A), Peptone (B), $MgSO_4.7H_2O$ (C), KH_2PO_4 (D), $NaNO_3$(E), KCl (F), $FeSO_4.7H_2O$ (G), Ph (H), RPM (I), Temperature (J) and Inoculum concentration (K)

Table 3.2 BBD Experimental Design

Run	Peptone	KH_2PO_4	$FeSO_4.7H_20$
1	0	-1	-1
2	0	-1	-1
3	-1	0	-1
4	0	0	0
5	1	1	0
6	0	0	0
7	-1	1	0
8	1	0	-1
9	0	0	0
10	0	0	0
11	1	-1	0
12	0	1	-1
13	-1	-1	0
14	-1	0	1
15	0	1	1
16	1	0	1
17	0	0	0

Statistical analysis of the model was performed to evaluate the analysis of variance (ANOVA). This analysis included Fisher's F- test (overall model significance), it's associated probability p(F), correlation coefficient R, determination coefficient R^2 which measure the goodness of fit of regression model. For each variable, the quadratic models were represented as contour plots (3D) and response surface curves were generated using Design Expert software.

3.4 Biosynthesis of lead selenide (PbSe) nanocrystallites in *Aspergillus terreus*

The lead and selenium tolerant fungal species isolated from sea water was cultured in the optimized medium for 96 hours and was treated as source culture for the synthesis of PbSe. Biosynthesis was initiated using the modified protocol by Prasad and Jha(2010a). 10 mL of 0.25M $PbNO_3$ and freshly prepared 10 mL of 0.25 M Na_2SeSO_3 was added to the fungal culture and heated to 60 ^oC for 20 min. The reaction mixture was then allowed to cool and further incubated overnight under room temperature. On the subsequent day, the resulting solution was filtered using Whatmann No.1 filter paper. The filtrate was collected, centrifuged twice at 15,000 rpm for 15 min and the resulting solution was further characterized for the formation of PbSe quantum particles.

3.5 Characterization

3.5.1 Morphological Characterization

The supernatant was morphologically characterized for nano crystallites using Scanning Electron Microscopy (SEM) with Elemental Determination using X-rays (EDAX) and Transmission Electron Microscopy (TEM). The samples for SEM analysis were initially freeze dried to remove the water content. The pretreated specimens were then sputtered with gold particles using a sputter coater under vaccum and then observed under a scanning electron microscope (JSM 6380; JEOL, Tokyo) at an accelerating voltage of 12 kV to capture the images.

The elemental composition of the scanned surface was analyzed using EDAX measurements at 20 kV.

For the TEM analysis, 100 µL of the colloidal PbSe nanoparticle solution was placed on a carbon coated copper grids and dried at room temperature. Thereafter, the grid was visualized under the TEM facility (JSM 2100, JEOL, Tokyo) operated at 200 kV to analyze the particle morphology and the selected area electron diffraction (SAED) patterns. Further, the size distribution of the resulting nanoparticles was analyzed using ImageJ software. The crystallinity of the biosynthesized PbSe nanoparticles were confirmed using X-ray Diffraction (XRD) studies. The XRD equipment was operated at a voltage of 30 kV and a current of 20 mA with Cu Kα radiation ($\lambda = 1.5405$ Å), and the diffracted intensities were recorded from 15° to 100° 2θ angles. The diffraction angles obtained for the sample were compared using 'X' pert high score software with search and match facility and compared with the data by the Joint Committee on Powder Diffraction Standards (JCPDS).

3.5.2 Optical Characterization

The presence of biological capping on the nanocrystallites was affirmed using Fourier transform Infra- Red (FTIR) spectroscopy (Thermo Nicolet 6700, USA). The transmission spectra of the freeze dired samples were recorded from 4000–400 cm^{-1} wavenumbers using KBr pellet method. The absorbance characteristics of the nanoparticle solution were analyzed using UV-Vis absorbance (UV-2550 Shimadzu, Japan) and the fluorescence of the nanoparticle solution was estimated using photoluminescence spectroscopy (RF-6000 Shimadzu, Japan). The detailed optical properties of lead selenide (PbSe) quantum rods biosynthesized in marine

Aspergillus terreus were apprehended theoretically using *ab initio* calculations based on the experimental absorption spectrum.

3.5.3 Electrochemical Property Measurement

The electrochemical property of the PbSe QPs was studied by the potential scan voltammetry on an electrochemical system (CHI660D Electrochemistry Workstation, Austin, USA). The schematic of the electrochemical system setup used in the present study is demonstrated in Fig.3.2.

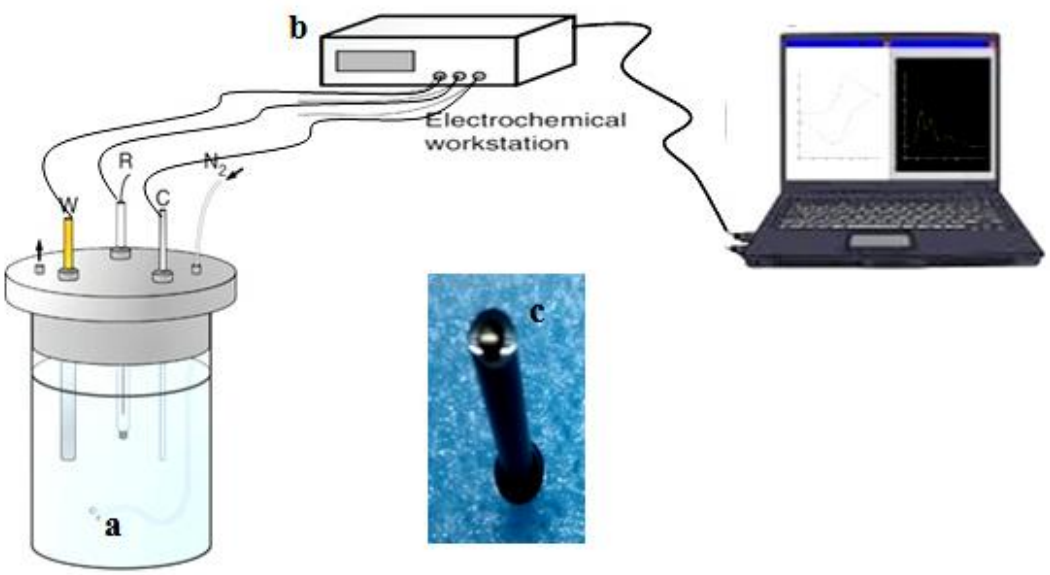

Fig. 3.2 Schematic of the experimental set-up for electrochemical property measurement- (a) The three electrode system (inset); W: Working electrode, R Reference electrode, C: Counter electrode; (b) Electrochemical Workstation (c) The glassy carbon electrode with the drop cast PbSe biogenic quantum particles (inset)

The electrochemical cell was made up of a given electrolyte solution and a three electrode system: the platinum wire counter electrode, a saturated calomel reference electrode against which all potentials were recorded and a working electrode that was prepared as follows:

a little PbSe colloidal quantum particle solution was drop cast of the surface of a glassy carbon electrode and dried at ambient temperature. The electrolyte solution (0.1 mol/L KNO_3) was degassed with ultrapure N_2 prior to the experiment. The potential scan was carried out from -1 V to 1 V with a sweep rate of 0.05 V/s for all the electrochemical experiments. Control experiments with the glassy carbon electrode under similar conditions were also carried out.

3.6 Optimization of the PbSe QP fluorescence by response surface methodology

Biosynthesis of lead selenide (PbSe) nanoparticles was initiated by the green methodology mentioned in section 3.4 using marine *Aspergillus terreus*. The factors influencing the fluorescence of the biogenic PbSe nanoparticles were investigated using the Box-Benhen Design (BBD) of response surface methodology (RSM). A 3 level 3 factors BBD was investigated to select the appropriate independent variables such as reaction temperature (A) ranging from 20 °C to 70 °C, the pH of the reaction mixture (B) from 6 to 12 and the duration of heating (C):10 min to 60 min based on its effect on the fluorescent yield of the QD solution (dependent variable) in as presented in Table 4.2. After the reaction in the aforementioned conditions, the culture flasks were allowed to a sudden temperature quenching at 4 ^{0}C and a subsequent overnight incubation in the laboratory ambience.

The experimental data were fitted to a second-order polynomial model as given in equation 4 where, Where Y_i is the predicted response, X_i, X_j are input variables which influence the response variable Y; β_o is the offset term; β_I is the influence of the ith linear coefficient; β_{ii} is the ith quadratic coefficient and β_{ij} is the ijth interaction coefficient

$$Y_i = \beta_0 + \Sigma\beta_i X_i + \Sigma\beta_{ii} X_i^2 + \Sigma\beta_{ij} X_i X_j \quad (4)$$

3.6.1 Statistical analysis for BBD

The statistical software package Design Expert (Version 8.0.7.1, Stat-Ease Inc., Minneapolis, USA) statistical package was used to analyze the experimental data. The optimal values of the critical variables were obtained by analyzing the contour plots and the statistical analysis in the form of analysis of variance (ANOVA). All the experiments were conducted in triplicates and the effect of a particular component on the response was considered significant only if p value ≤ 0.05 was obtained.

3.6.2 Verification of model

Optimal synthesis conditions for an enhanced fluorescence response were obtained using the predictive equations generated by RSM. Verification experiment was done by carrying out the synthesis at the optimized conditions in duplicates. The experimental values and model predicted values were compared to examine the validity of the model. Further, the QD morphology obtained under the optimum biosynthesis conditions were verified using Transmission electron microscopic (TEM) (JEOL-JSM-6380-LA, Japan) and Atomic Force Microscopic (AFM) (PARK XE-15, Korea) images.

3.7 Applications of biosynthesized PbSe QPs

3.7.1 Antibacterial Properties

The antibacterial activity of the crude nanoparticle solution against various gram positive and gram negative human pathogenic bacteria like *Staphylococcus aureus, Bacillus cereus, Bacillus endophyticus, Salmonella typhi, Escherichia coli, Klebsiella pneumonia, Vibrio cholera and Vibrio parahaemolyticus* was carried out by filter paper bioassay (Bauer et al. 1966). For antibacterial activity, bacterial culture were inoculated in nutrient broth and incubated at 37 ^{o}C for 24 h. From the actively growing bacterial culture broth, 0.1 mL of the suspension (105

CFU/mL) was mixed with half strength nutrient broth (0.9 mL) and was immediately overlaid on the surface of the sterile nutrient agar plates (90 mm diameter). Sterile filter paper discs (Whatman No. 3: 10 mm square) were placed on these agar plates and then loaded with 50 µL suspension of the crude nanoparticles. These plates were incubated for 24 h and visually monitored for the zone of inhibition. Filter paper disc on nutrient agar plate with suspension containing standard antibiotic chloramphenicol (500 µg/mL) was used as positive control. After incubation, the zone of inhibition was measured in millimeter across the filter paper.

3.7.2 Procedures for detection of Cd^{2+} ions

Stock standard solutions 0.1 M Cd (II) were prepared by dissolving an appropriate amount of $CdCl_2 \cdot 2H_2O$ in water and adjusting the volume to 5.0 mL in a volumetric flask. It was further diluted to the working volumes using distilled water. A fixed concentration of PbSe QDs was transferred to a fluorescent cuvette. The fluorescent intensity of the solution was recorded from 340 to 620 nm with excitation wavelength fixed at 320 nm. After appropriate amount of Cd^{2+} ions was titrated, the fluorescent intensity of the solution was again recorded. Similar procedure was performed for various pre-determined concentrations of Cd^{2+} ions and other metal ions. For the sake of comparison, the volume of PbSe QDs solution was fixed to be 2 mL before the addition of Cd^{2+}. All measurements were made at room temperature.

3.7.3 Principles of fluorescence quenching

The Stern-Volmer equation was used to comprehend the mechanism involved in the fluorescence quenching of the PbSe QD solution in the presence and absence of Cd^{2+} ions. While the linear nature of the plot indicates dynamic quenching mechanisms, static quenching is characterized by a non-linear Stern-Volmer plot described by equation 5

$$\frac{F_0}{F} = 1 + K_{SV}\tau_0[Q] \quad (5)$$

Where F_0 and F are the fluorescence intensities before and after the addition of the quencher, respectively; K_{SV} is the rate constant of dynamic (collision) quenching; [Q] is the quencher concentration in solution.

3.8 Studies on mechanism of PbSe QD biosynthesis

To determine the PbSe QD biosynthesis mechanism employed by the fungus, dried fungal biomass and the reaction mixture comprising of the culture supernatant before and after the reaction were analyzed using various sophisticated techniques namely, Scanning Electron Microscopy (SEM) with Energy Dispersive X-ray Analysis (EDAX), Fourier Transform Infra-Red spectroscopic Analysis (FTIR), Liquid Chromatography coupled with Mass Spectrometry (LC-MS) and various assays to confirm the presence of fungal stress proteins were carried out.

3.8.1 Scanning Electron Microscopy (SEM) with Energy Dispersive X-ray Analysis (EDAX)

SEM and EDAX analyses were carried out in order to understand the role of microbial cell surface activity in the presence of Lead and selenium salts. The fungal biomass pre and post treatement with the precursors for PbSe QD synthesis, were harvested by filtration, oven dried at 60 ^{o}C (Rotek, India). The pretreated specimens were then sputtered with gold particles using a sputter coater under vaccum and then observed under a scanning electron microscope (JSM_6380; JEOL, Tokyo) at an accelerating voltage of 12 kV to capture the images. The elemental composition of the scanned surface was analyzed using EDAX measurements at 20 kV.

3.8.2 Fourier Transform Infra-red Spectroscopic Analysis (FTIR)

The fungal biomass before and after the series of reactions for the biosynthesis of PbSe QDs were collected by filteration, washed with distilled water and oven dried at 60 ^{o}C (Rotek, India). The dried biomass was then powdered and analyzed by Thermo Nicolet 6700, FTIR spectrometer to identify the functional groups and bonds present in them in response to heavy metal stress.

3.8.3 Analysis of stress factors using LC-MS

The supernatant after the completion of the biosynthesis reaction was characterized using a liquid chromatographic column equipped with Acela pump and Acela auto-sampler (Thermo Fisher scientific, San Jose, CA, USA). Separation of analytes was conducted on a Luna PFP(2) analytical column (100 mm X 2.0 mm, 3μm). The LC mobile phases were (a) Ammonium formate 0.75 mM adjusted to pH 3.5 with formic acid and (b) methanol. Separation was performed under isocratic conditions with 99% mobile phase A at flow rate of 200 μL/min and a coulmn temperature of 35 ^{o}C. total run time per sample was 10 min and all injection volumes were 10 μL. Mass spectrometric analysis was performed using a TSQ quantum access (Thermo Fisher Scientific, san Jose, CA, USA) triple quarapole mass spectrometer coupled with electron spay ionization (ESI) operated in multiple rections monitoring (MRM) in positive mode. Data acquisition and analysis were performed with Xcalibur software, version 2.0 (Thermo Fisher Scientific, san Jose, CA, USA).

3.8.4 Analysis of the Proteins Involved in Biosynthesis of PbSe QPs

3.8.5 Bradford assay for estimation of total protein content

The crude filtered supernatant before and after the biosynthesis reaction were initially centrifuged to remove the particulate and cellular debris and then analyzed for its total protein content using Bradford assay (Kruger 1994) Different concentrations of Bovine Serum Albumin (BSA) (Hi-Media) was used as the standard protein for plotting the caliberaton curve. The total protein content in the samples were estimated based on their absorbance at 595 nm using a UV-Vıs spectrophotometer (LAMBDA 40, Perkin Elmer, USA) and the linear fit equation of the calibration plot.

3.8.6 Metallothionein assay

Metallothioneins (MTs) are low molecular weight proteins characterized by a high cysteine content and give rise to metal-thiolate clusters (Murthy 2011). In the present study, the metallothionein content the crude filtered supernatant before and after the biosynthesis reaction was initially analyzed using the protocol by Linde and Gracia-vazquez (Linde and Garcia-Vazquez 2006). A standard curve with glutathione (GSH) was used as a standard reference for a correct quantification of MT in the samples. GSH contains one cysteine per molecule; thus, it is a standard for quantifying cysteines in protein analyses. Solutions containing different concentrations of GSH were prepared and their absorbance was measured at 412 nm. The amounts of metallothionein in the samples were estimated using the GSH standard, assuming that 1 mol of MT contains 20 mol of cysteine.

3.8.7 Super Oxide Dismutase assay

Super oxide dismutases (SOD) have been recognized as an important class of anti-oxidant enzymes that combat the oxidative stress in the organisms in the presence of heavy metal/foreign pathogen intrusion (Tsekova and Todorova 2002). The SOD assay is based on the inhibition of the formation of NADH-phenazine methosulphate-nitrobluetetrazolium formazon. The color formed at the end of the reaction can be extracted into butanol and measured at 560 nm. The experimental protocol by Beauchamp and Fridovich (1971) was used to measure the enzyme activity in the the crude filtered supernatant before and after the biosynthesis reaction. One unit of enzyme activity is defined as the amount of enzyme that gave 50% inhibition of NBT reduction in one minute.

3.8.8 MALDI-TOF spectrometry for mass characterization of purified protein sample.

3.8.8.1 Protein purification using acetone precipitation

Absolute acetone chilled at -20 ^{o}C was added to the supernatant collected after PbSe QD biosynthesis process. The concentration of acetone in the reaction mixture was increased step-wise from 40%-80%. After the addition of organic solvent, the supernatant-solvent mix was incubated for 30-60 min under chilled condition and centrifuged at 14000 rpm for 15 min at 1^{o}C. The protein pellets were collected and re-suspended in 5mM tris-HCl, 1mM EDTA at pH-7. The mass of the purified protein collected after acetone precipitation method was characterized at the MALDI-ToF Spectrometric facility available at CSIR-IHBT, Palampur, India.

3.8.8.2 Procedure for mass characterization using MALDI-TOF:

3.8.8.3 In-sol protein digestion

The protein was lyophilized at -80 °C and incubated overnight at 37 °C.For each digest, protein samples were added with 0.5 μL of α-Cyano-4-hydroxycinnamic acid (10 mg/mL) in 30% (v/v) acetonitrile and dried at room temperature.

3.8.8.3 Mass spectrometry

The extracted peptides were subjected to MS using MALDI-ToF/ToF-Proteomics Analyzer (UltrafleXtremeTM mass spectrometer; BrukerDaltonics Inc. Germany). A mass standard starter kit (BrukerDaltonics Inc. Germany) and a standard tryptic BSA digest (BrukerDaltonicsInc, Germany) were used for MS and MS/MS calibrations of the system. A combined MS and LIFT-MS/MS were performed using BioTools 3.0 software (BrukerDaltonics Inc. Germany). The ToF spectra were recorded in positive ion reflector mode with a mass range from 700 to 3500 Da. Five hundred shots were accumulated for each spectra. Two most abundant peptide ions were then subjected to fragmentation analysis to determine the peptide sequence. Database search was performed using MASCOT search engine (Version 2.1, Matrix Science, London, U.K) and Swiss Prot database (Release date, 5th May, 2013; version 121; 540052 sequences). All peptide masses were assumed monoisotopic and $[M+H]^+$. The parameters used for search were as follows: taxonomy, Fungi (65404960 sequences; 23431186099 residues); enzyme, trypsin; the fixed modification; carbamidomethyl (C); the variable modification, Glu->pyro-Glu (N-term Q) and oxidation (M); parent ion mass tolerance at 50 ppm and MS/MS mass tolerance of 0.7dalton; one missed cleavage allowed. The identified proteins had to meet three criteria: (1) be among the top hits on the search report; (2) individual

ions scores > 44 indicate identity or extensive homology ($p<0.05$) as used by various workers (Zhang et al. 2013). Only proteins matched by a minimum of two peptide sequences were included in the results list. Also, to evaluate protein identification, the percentage of sequence coverage was considered. The confidence in the peptide mass fingerprinting matches was based on the score level and confirmed by the accurate overlapping of the matched peptides with the major peaks of the mass spectrum.

4. RESULTS AND DISCUSSIONS

The preceding sections enumerate the findings of the methodologies detailed in Chapter 3 and critically examine the descriptive results in view of the previous state of the subject as outlined in the literature review. Initially, outcomes concerning the isolation of tolerant fungal strains from marine sources followed by the identification and growth optimization of the Pb and Se tolerant fungal species are presented. Further, the results on the biosynthesis of PbSe QPs using the Pb and Se tolerant fungus are briefed. Subsequently, the morphological, structural, optical and electrochemical characteristics of the PbSe QPs are detailed. The statistical optimization of the fluorescence in the biosynthesized PbSe and its application for heavy metal sensing in aqueous solutions are discussed. The antibacterial properties of the biosynthesized PbSe are also described. Finally the results on the fungal protein cadre involved in the biosynthesis of PbSe QDs are elaborated. The results obtained are discussed in light of relevant literature and the data are presented as mean values of triplicate experimental results.

4.1 Sediment and water analysis

With increasing focus on industrial emissions and discharge as prime factors in global pollution generation, efforts are underway to apportion these point sources to specific pollutants. One such study has identified that the common sources of lead and selenium in water bodies include discharge from industries such as electroplating, plastics manufacturing, fertilizer plants and mining and metallurgical process wastes (Zouboulis et al. 2004). In the present study, water and sludge samples were collected from the coastline near industrial environs. The Pb and Se contents in the collected water and sludge samples were analyzed and are listed in Table 4.1.

Results indicate high concentrations of Pb as well as Se in samples that are within 6 km radius from industrial area. The high concentration of Pb and Se in the sea water samples can undergo bio-magnification via the aquatic fauna to eventually affect the consumers in the food chain. According to literature, Pb and Se exposures even below the current EPA (2011) and World Health Organization upper limits of 15 and 10 μg/L respectively are associated with adverse health risks in vertebrates. The high Pb and Se load in sea water also result in numerous modifications in the metabolic activities of the microbial communities therein (Hiraki 1994; Jansen et al. 1994). Hence, the sample S1 characterized by higher Pb and Se content was utilized for the isolation of the metal/metalloid tolerant fungi.

Table 4.1 Pb and Se analysis in water and sediment samples

Marine Sampling sites, Distance in km from the shore	**Water Content**		**Sediment Content**	
	Metals Content (mg/L)			
	mg/L		**mg/kg**	
	Pb	**Se**	**Pb**	**Se**
S1 (6)	1.144	1.191	0.774	2.537
S2 (8)	0.469	0.721	0.762	2.133
S3 (12)	0.408	0.581	0.614	1.414

4.2 Isolation of heavy metal tolerant fungi

The inherent heavy metal tolerance in fungi and yeast biomasses are well documented in literature (Gavrilescu 2004). In the present study, four fungal strains tolerant to Pb and Se were isolated from sea water sample (S1) contaminated with Pb and Se. Based on the keys of Dugan (2006) the fungi isolated were identified as *Aspergillus* sp (Black), *Aspergillus* sp

(Brown),*Penicillium* sp, and *Fusarium* sp (Fig.4.1). The isolates could tolerate 20 mg/L each of Pb and Se in typical plate studies. Earlier, the isolation of fungi from natural sources with tolerance limits up to 25 mg/L has been reported. However, the fungi isolated in the current study are of relevance as the source of isolation is relatively less polluted compared to the sources reported in prior studies (Joshi et al. 2011).

4.3 Tolerance studies on the isolated marine fungi

To compare the tolerance levels of the isolates, the tolerance indices of the metal tolerant strains for Pb and Se were calculated. The index of tolerance showed significant difference between isolates from the same source. The present results are in agreement with the findings by Iramet al.(2012) who confirmed that the response of isolates to heavy metals depended on the metal tested its concentration in the medium and on the isolate under consideration. In the present study, *Aspergillus* sp. (Brown) exhibited significant tolerance index to Pb and Se when compared to the other isolates from the same source (Fig 4.2). While the index of tolerance varied from 0.46-1.11 in other marine fungi and *Aspergillus* sp. (brown) exhibited a significantly high tolerance index of 1.235. These observations affirm prior findings that highlight *Aspergillus* sp isolated from industrial waste water as promising biological entities with metal tolerance (Zafar et al. 2007).

Results of the present study also attest the statement that the level of metal tolerance in microbes depended on the isolate tested, as well as the site of its isolation. The variation in the metal tolerance may be due to the presence of one or more strategies of tolerance or resistance mechanisms exhibited by fungi like the production of organic chelators, acids and anti-oxidants during its growth (Sintuprapa et al. 2000).

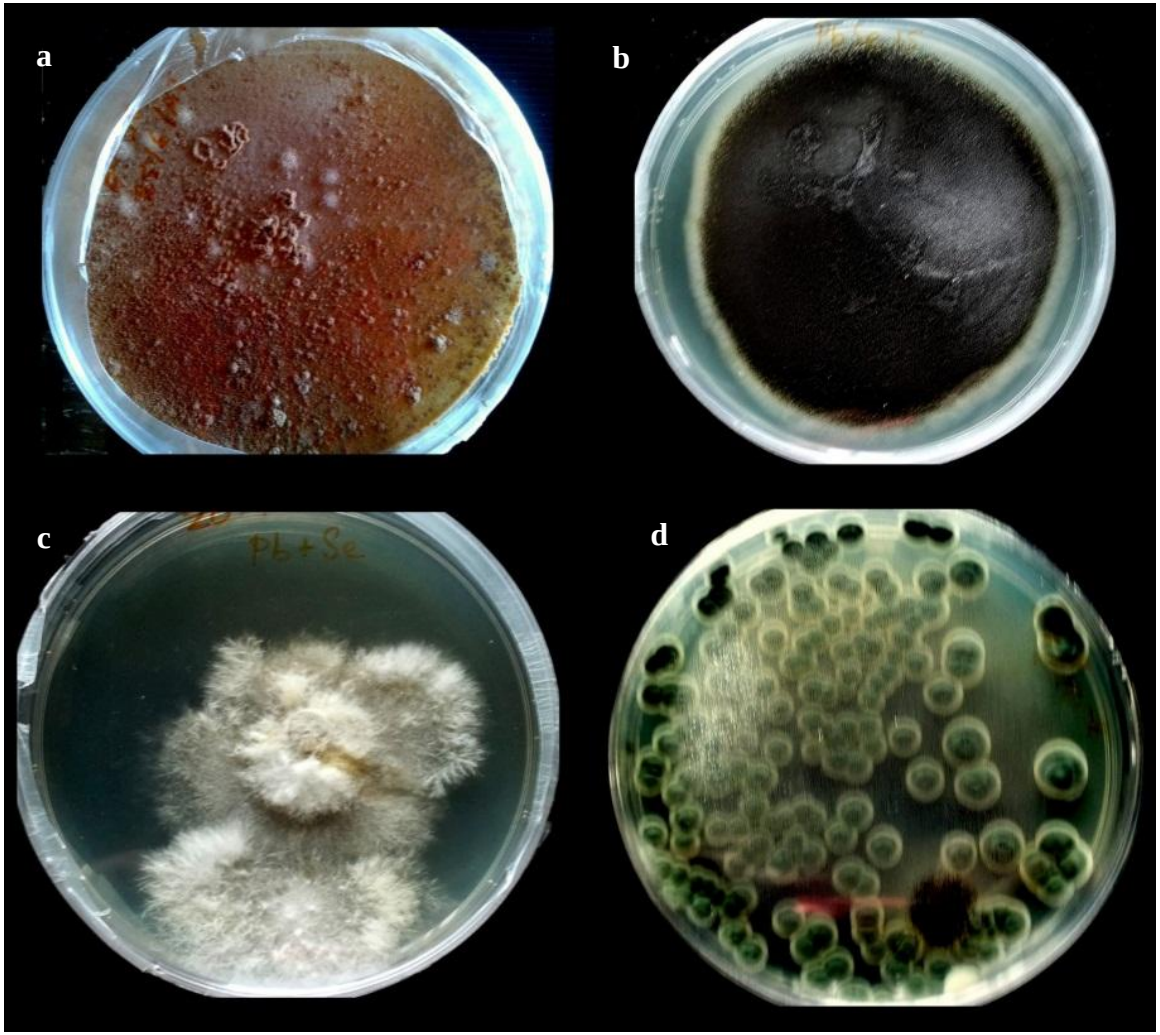

Fig.4.1 Isolated marine fungal species on PDA plates with 20 mg/L of Pb and Se: (a) *Aspergillus* sp. (brown); (b) *Aspergillus* sp. (black); (c) *Fusarium* sp.; (d) *Penicillium* sp.

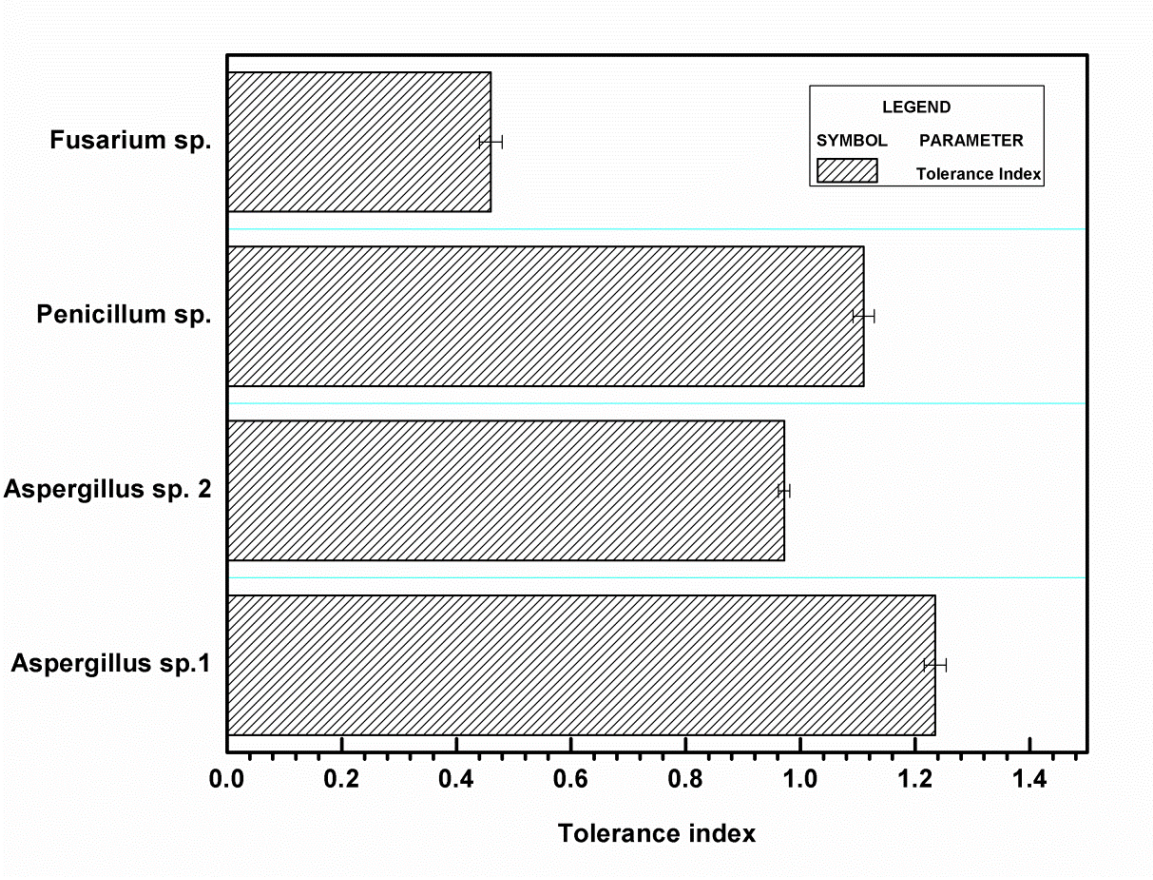

Fig.4.2 Tolerance indices of the marine fungi

4.4 Morphological and molecular identification of the Pb and Se tolerant fungus

The noteworthy Pb and Se tolerance exhibited by *Aspergillus* sp (Brown) was considered as the criterion to direct all future studies using this particular fungus. As a first step the morphological and molecular features of this fungal strain was studied to confirm its species and genus. Macroscopic analysis of the metal/metalloid tolerant fungus demonstrated a typical suede like and cinnamon-buff to sand brown color with a yellow to deep dirty brown reverse on PDA (Fig 4.3). The cellular morphology of the Pb and Se tolerant *Aspergillus* sp. (brown) were further studied by low and high magnification microscopic examinations that revealed compact,

columnar and biseriate conidial heads with globose to ellipsoidal conidia. Based on these observations, the fungus was preliminarily identified as belonging to the genus *Aspergillus* (Nyongesa et al. 2015).

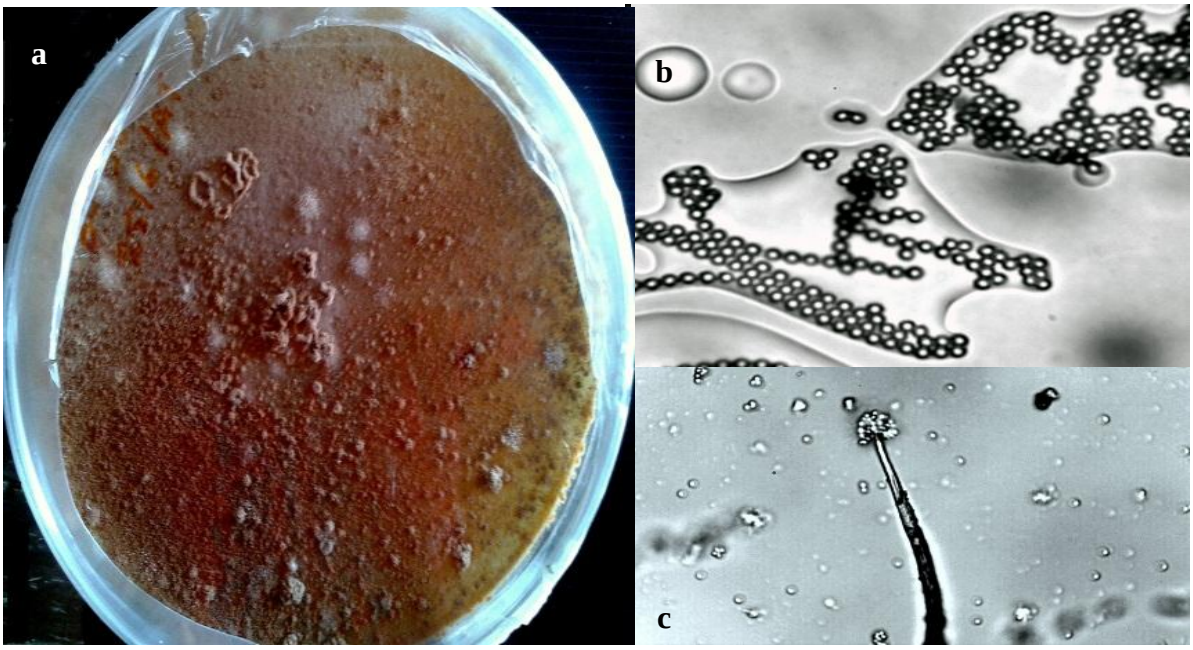

Fig.4.3 Morphological features of marine *Aspergillus* sp. (brown): (a) Colony on PDA; Microscopic features exhibiting (b) spores and (c) conidia

The molecular characterization of this fungus was further carried out to characterize the fungus to the species level. According to literature, the internal transcribed spacer (ITS) region, a stretch of DNA that lays between the 16S RNA and 23S rRNA subunit genes, has proven to show a high degree of variability in both sequence and size at the genus and species level and has henceforth allowed efficient identification of species within a genus (Tang and Stratton2013). In the present study, the ITS of 500-700 base pairs of the DNA isolated from pure cultures of the fungus was carried out in Agharkar Research Institute, Pune, India. The query sequence (Fig.4.4) was further aligned using a Basic Local Alignment Search Tool (BLAST) and the Pb and Se

tolerant fungus isolated from marine sources was found to have 99% similarity with *Aspergillus terreus* with NCBI accession number AB647191.1.

Fig.4.4 ITS of 500-700 base pairs of marine *Aspergillus*sp (brown)

4.5 Growth studies on marine *Aspergillus terreus*

The growth of the Pb and Se tolerant *Aspergillus terreus* was studied for a period of 10 days in order to characterize the various phases of the fungal growth (Fig.4.5). Results indicated that the metal/metalloid tolerant fungal isolate exhibited a maximum biomass dry weight of 8.92 g/L after 5 days of incubation in Potato dextrose broth (PDB) under 115 rpm at 32 ^{o}C. Thereafter, marginal variations in biomass of the fungus were observed till the 9th day, after which a slight decrease in net biomass of *Aspergillus terreus* was noted.

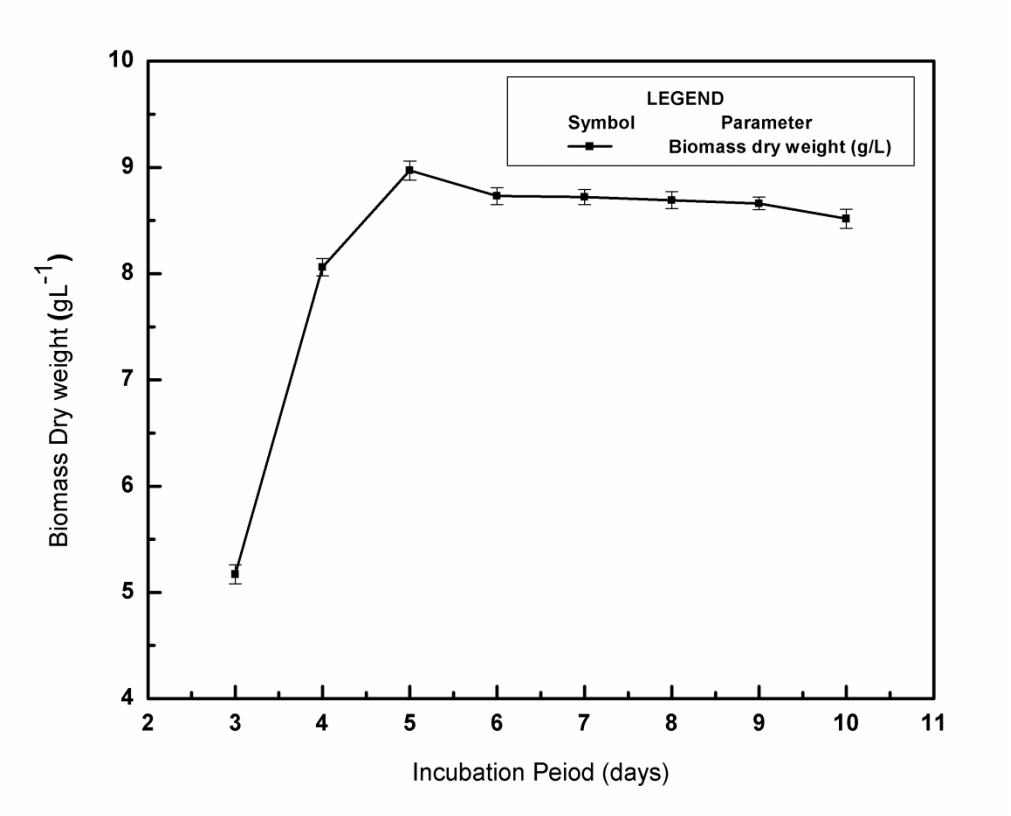

Fig.4.5 Growth curve of marine *Aspergillus terreus* used in the study

4.6 Media optimization for *Aspergillus terreus* biomass

4.6.1 Screening of Medium Component for Biomass production Using Plackett-Burman Design

Statistical methods for medium optimization have proven to be powerful and useful tools in biotechnology (Zhang et al. 2012). In the present study, the media components that influence the growth of marine *Aspergillus terreus* were screened for optimization by Plackett-Burman Design and the results were analyzed using the Design Expert software (version 8.0.7.1). The amount of biomass produced was found to vary from 13.99 g/L to 7.98 g/L due to the influence of different salts as given in Table 4.2. The medium components were screened and those with a

p – value of < 0.1 using 90% confident level were accepted as significant factors affecting the fungal biomass. According to ANOVA for the model, it was inferred that peptone, potassium di-hydrogen phosphate (KH_2PO_4) and ferrous sulphate heptahydrate ($FeSO_4.7H_2O$) were the most significant variables influencing *Aspergillus terreus* growth.

The normal plot of standardized effects of all variables and Pareto chart (Fig.4.6) were used to compare the relative magnitude and the statistical significance of the main effects i.e. peptone, potassium di-hydrogen phosphate (KH_2PO_4) and ferrous sulphate heptahydrate ($FeSO_4.7H_2O$). The half normal plot was used to select the effects to be included in the model. According to this plot the factors that lie farther away from the line indicate a significant effect (Fig.4.6). Pareto chart is an additional graphic plot used to display the t-value of the effects. In the pareto chart, the effects that are above the Bonferroni limit and t-value are considered significant and the effects are represented in the decreasing order of the absolute value of the standardized effects. The pareto chart obtained in the present study affirms the role of peptone, potassium di-hydrogen phosphate (KH_2PO_4) and ferrous sulphate heptahydrate ($FeSO_4.7H_2O$) as significant media components that influence the growth of the marine biomass, *Aspergillus terreus*. The significance of nitrogen source and trace metals like potassium and magnesium for the growth and metabolite production by *Aspergillus terreus* was earlier reported by researchers (Ghanem et al. 2000).

The results thus obtained were further analyzed using the statistical tools in Design Expert software (version 8.0.7.1). Accordingly, the "Pred R-Squared" of 0.6166 was found in reasonable agreement with the "Adj R-Squared" of 0.7535. The estimated Model Values "Prob> F" was found to be less than 0.0500, indicating that the model is significant. In this case peptone, KH_2PO_4, $FeSO_4.7H_2O$ were found to be the significant model terms.

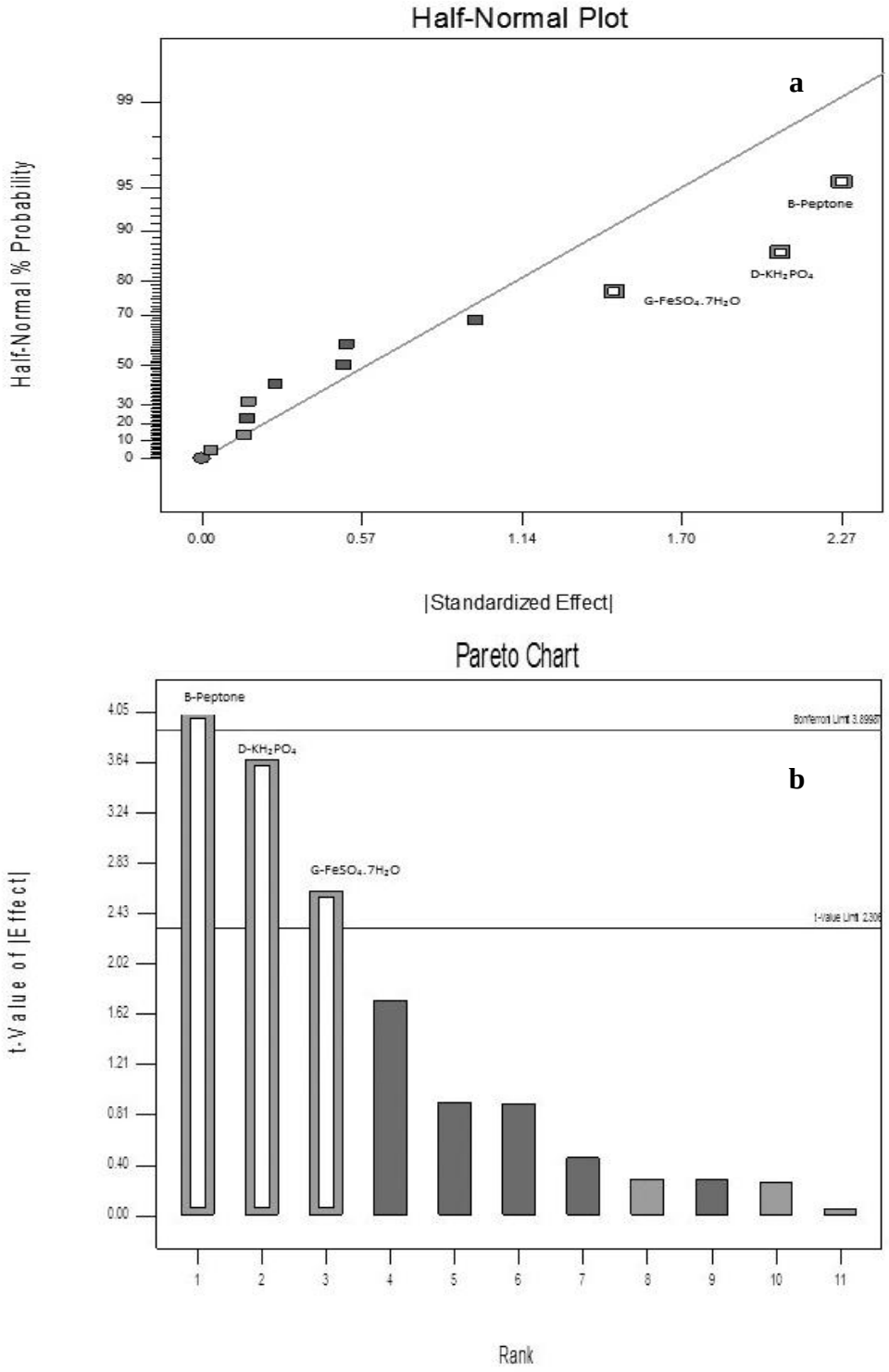

Fig.4.6 (a) Half-Normal Plot; (b) Pareto Chart for Plackett-Burmann Design

Table 4.2 Response table for PB design

Run	Factor 1	Factor 2	Factor 3	Factor 4	Factor 5	Factor 6	Factor 7	Response
	Sucrose	Peptone	$MgSO_4$	KH_2PO_4	$NaNO_3$	KCl	$FeSO_4$	(g/L)
1	40	5	0.4	05	10	0.4	0.04	10.021
2	40	5	0.8	1	5	0.8	0.04	12.263
3	40	10	0.4	0.5	5	0.8	0.01	11.535
4	30	5	0.4	1	5	0.8	0.04	12.457
5	40	10	0.4	1	10	0.8	0.01	11.632
6	30	10	0.8	1	5	0.4	0.01	13.997
7	30	5	0.4	0.5	5	0.4	0.01	7.988
8	40	5	0.8	1	10	0.4	0.01	8.960
9	30	5	0.8	0.5	10	0.8	0.01	8.235
10	30	10	0.4	1	10	0.4	0.04	13.592
11	30	10	0.8	0.5	10	0.8	0.04	11.264
12	40	10	0.8	0.5	5	0.4	0.04	11.530

4.6.2 Determination of optimal concentration of medium component using Response surface method: Box – Behnken Design (BBD)

Statistical designs are effective tools that can be used to account for the main as well as the interactive influences of fermentation parameters on the overall process performance. Among them, response surface methodology (RSM) is a collection of certain statistical techniques for designing experiments, building models, evaluating the effect of the factors and searching for optimal conditions for desirable responses (Myers and Montgomery 1995). Therefore, during the

past decades, RSM has been extensively applied in the optimization of medium composition, and other manufacturing processes (Venil and Lakshmanaperumalsamy 2009).

In this study, RSM (Box – Behnken design) was employed to investigate the interactions among the selected factors viz., Peptone, Potassium di-hydrogen phosphate (KH_2PO_4) and Ferrous sulphate heptahydrate ($FeSO_4.7H_2O$) in the culture medium and to determine their optimum levels for a maximum biomass production. The experimental observations demonstrated a marked difference ranging from 10.01 to 4.58 g/L of fungal biomass due to the variation in media composition. The highest biomass of 10.01 g/L was observed when the Peptone, Potassium dihydrogen phosphate (KH_2PO_4) and ferrous sulphate heptahydrate ($FeSO_4.7H_2O$) concentrations were 10, 1 and 0.06 g/L respectively (Run 9). The least biomass of 4.58 g/L was observed when the peptone, potassium di-hydrogen phosphate (KH_2PO_4) and ferrous sulphate heptahydrate ($FeSO_4.7H_2O$) concentrations were 5, 1 and 0.03 g/L respectively. The response of various trials in terms of the *Aspergillus terreus* biomass is represented in Table 4.3.

4.6.3 Statistical analysis

The adequacy of the model was checked using analysis of variance (ANOVA) which was tested using Fisher's statistical analysis and the results are presented in Table 4.4. The model F value of 14.03% implied that the model was significant and also showed that there was 0.11% chance that the model F value could occur due to noise. The R^2 value (multiple correlation coefficients) closer to 1 denoted better correlation between the observed and predicted responses. The coefficient of variation (CV) indicates the degree of precision with which the experiments were compared. The lower reliability of the experiment is usually indicated by high value of CV.

Table 4.3 Box-Behnken Design matrix for independent variables in uncoded units along with experimental and predicted values of biomass

Run	Factor 1	Factor 2	Factor 3	Experimental	Predicted
	Peptone	KH_2PO_4	$FeSO_4$	(g/L)	(g/L)
1	10	0.75	0.03	5.79	5.72
2	10	0.75	0.09	7.90	7.92
3	5	1.00	0.03	4.58	4.90
4	10	1.00	0.06	9.05	9.38
5	15	1.25	0.06	7.34	7.59
6	10	1.00	0.06	9.88	9.38
7	5	1.25	0.06	5.55	5.26
8	15	1.00	0.03	6.87	6.65
9	10	1.00	0.06	10.01	9.38
10	10	1.00	0.06	8.34	9.38
11	15	0.75	0.06	6.31	6.60
12	10	1.25	0.03	7.02	7.00
13	5	0.75	0.06	4.98	4.74
14	5	1.00	0.09	6.00	6.22
15	10	1.25	0.09	8.18	8.25
16	15	1.00	0.09	8.99	8.68
17	10	1.00	0.06	9.65	9.38

The results obtained from the BBD were fitted to a second order polynomial equation (Eq.6) to explain the dependence of *Aspergillus terreus* growth and biomass production on the medium components.

$$Biomass\left({}^{g}/_{L}\right) = 9.38420 + 3.75.A + 0.9235.B + 1.6312.C + 0.5123.A.B + 0.869.A.C - 0.21.B.C - 0.6911A^2 - 0.3548B^2 - 0.1167.C^2 \quad (6)$$

. The response plots of the variables under consideration are depicted in Fig. 4.7. The convex natures of the plots signify an optimized response. Further the maximum biomass obtained experimentally under the optimized conditions and the responses predicted by the model are given Table 4.5.

Table 4.4 ANOVA for Response Surface Quadratic model

Source	Sum of Squares	Degrees of freedom	Mean square	F value	P value
Model	45.52	9	5.06	14.03	0.0011 significant
A-Peptone	8.83	1	8.83	24.49	0.0017
B-KH_2PO_4	1.13	1	1.13	3.14	0.1199
C-$FeSO_4.7H_2O$	5.62	1	5.62	15.59	0.0055
AB	0.054	1	0.054	0.15	0.7113
AC	0.12	1	0.12	0.35	0.5745
BC	0.18	1	0.18	0.50	0.5010
A^2	16.64	1	16.64	46.15	0.0003
B^2	7.68	1	7.68	21.30	0.0024
C^2	2.61	1	2.61	7.23	0.0312
Residual	2.52	7	0.36		
Lack of Fit	0.61	3	0.20	0.43	0.7458 not significant
Pure Error	1.91	4	0.48		

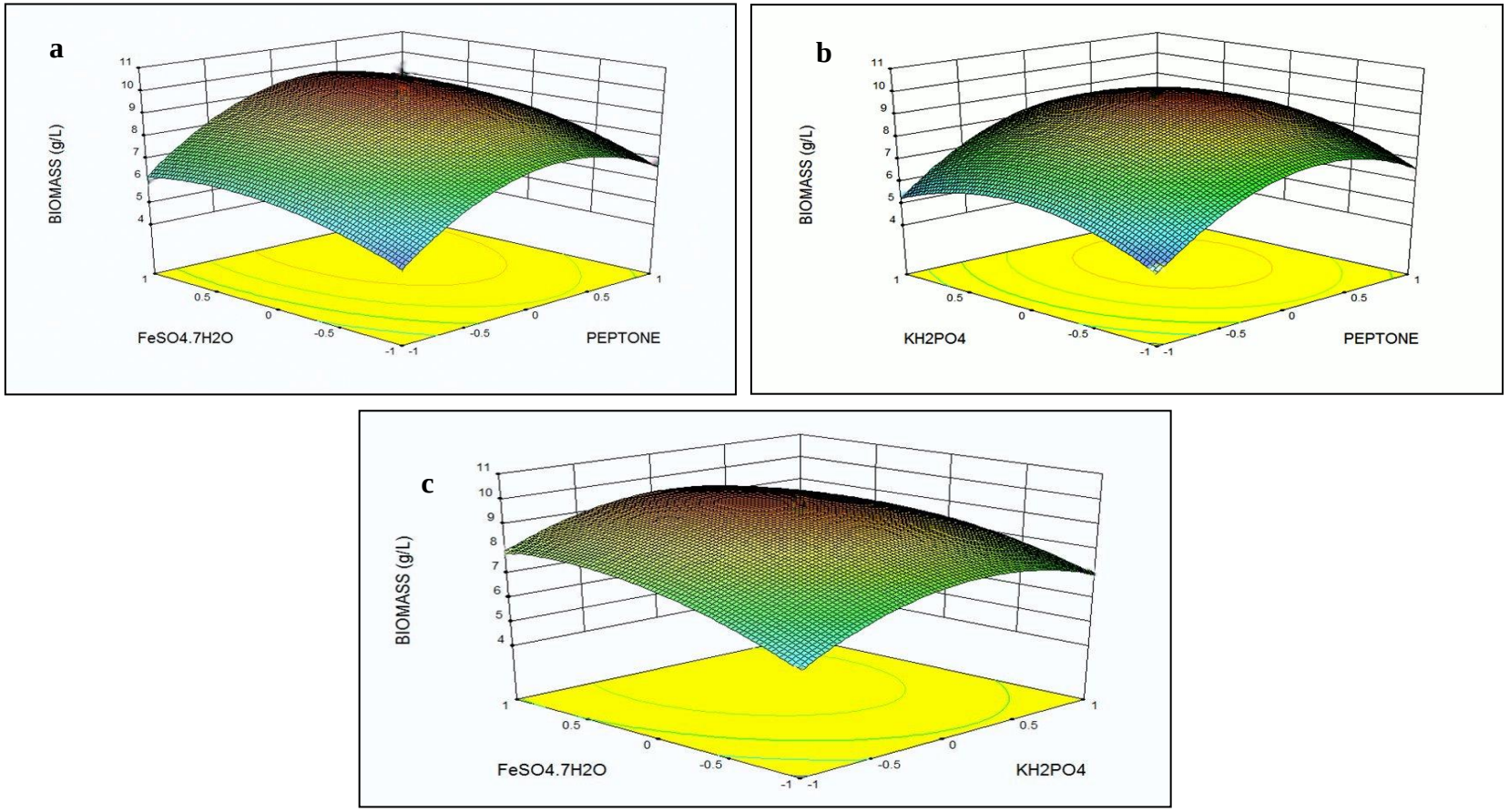

Fig. 4.7 Surface and Contour plot of Biomass (g/L) vs. (a) Peptone (g/L) and $FeSO_4.7H_2O$ (g/L); (b) Peptone (g/L) and KH_2PO_4 (g/L); (c) $FeSO_4.7H_2O$ (g/L) and KH_2PO_4 (g/L)

Table 4.5 Predicted and Experimental Biomass Yield at Optimum Values

Condition	Peptone g/L	KH_2PO_4 g/L	$FeSO_4.7H_2O$ g/L	Biomass g/L
Predicted	6.23	1.19	0.09	10.935
Experimental	6.23	1.19	0.09	10.372

4.7 Biosynthesis and characterization of Lead Selenide (PbSe) nanocrystallites in marine *Aspergillus terreus*

Biosynthesis of PbSe QPs was initiated using 5 day old fungal spores grown in the optimized media. The spores along with the precursor solution were subjected to a 60 ^{o}C heat shock followed by a temperature quenching and overnight incubation. Subsequent to the aforementioned steps, the flasks were observed with a distinct amber colored supernatant above a residue of the reacted biomass. The supernatant was filtered, centrifuged and subjected to further characterization to confirm the biosynthesis of PbSe nanocrystals. The concentration of the PbSe QPs in the colloidal solution was estimated to be 0.02 M.

4.8 Morphological Characterization

Fig.4.8a visualizes biosynthesized PbSe nano rod dispersed in acetone under a transmission electron microscope (TEM). The micrograph illustrates biosynthesized nano rods of variant lengths with an average diameter of approximately 57.94 nm and with aspect ratios between 5-10. The particle size histogram of PbSe (Fig 4.8b) was constructed by measuring the particle diameter in a grid containing 50 particles using ImageJ software. The histogram reveals broad distribution of particle sizes ranging from 20-160 nm. A marked preponderance of nano rods were found in diameter ranges between 40-80 nm. Our findings were further attested using

SEM (Fig 4.8c) analysis that confirmed the formation of PbSe QPs in typical size ranges from 50-100 nm. SEM analysis was coupled with compositional analysis using Energy Dispersive Analysis of X-ray (EDAX) method that approve a ratio of approx. 1:1 of Lead (Pb) and Selenium (Se) in the biosynthesized nano rods (Fig 4.8d). The size and surface morphology of the biosynthesized PbSe QPs are in par with their chemically synthesized counterparts reported in literature (Zhu et al. 2001; Vaidyanathan et al. 2006; Shandalov et al. 2008; Li et al. 2012).

The crystallinity of the biosynthesized PbSe QPs were confirmed using X-ray diffraction studies. Fig.4.9 shows the XRD profile of PbSe synthesized using *Aspergillus terreus*. Multiple sharp peaks indicate high level of crystallinity in the biosynthesized PbSe. Prominent Bragg reflections at 2θ values of 25.73^{o}, 29.2^{o} and 41.3^{o} can be observed. The corresponding inter-planar distances were calculated to be 3.45, 3.05 and 1.84 Å which can be attributed to the (11), (200) and (311) planes respectively (Table 4.6). Our results are well in agreement with the JCPDS data (Reference code: 00-065-1040) (Kassim et al. 2011) and confer the biosynthesized PbSe a typical Clausthalite type Rock Salt Structure having Face Centered Cubic Lattice with lattice parameter values of a = b = c = 6.128 Å .

Table 4.6 Planar spacing of the biosynthesized PbSe QPscalculated according to XRD peak data

Sl. No	2θ (deg)	hkl	d (Å)	d* (Å)
1	25.715	111	3.452	3.536
2	29.215	200	3.057	3.062
3	49.375	311	1.846	1.846

Where 2θ is the XRD peak value, hkl represent the associated peak, d signifies the calculated inter planar spacing and d is the standard inter planar distance according to JCPDS data (Reference code: 00-065-1040).

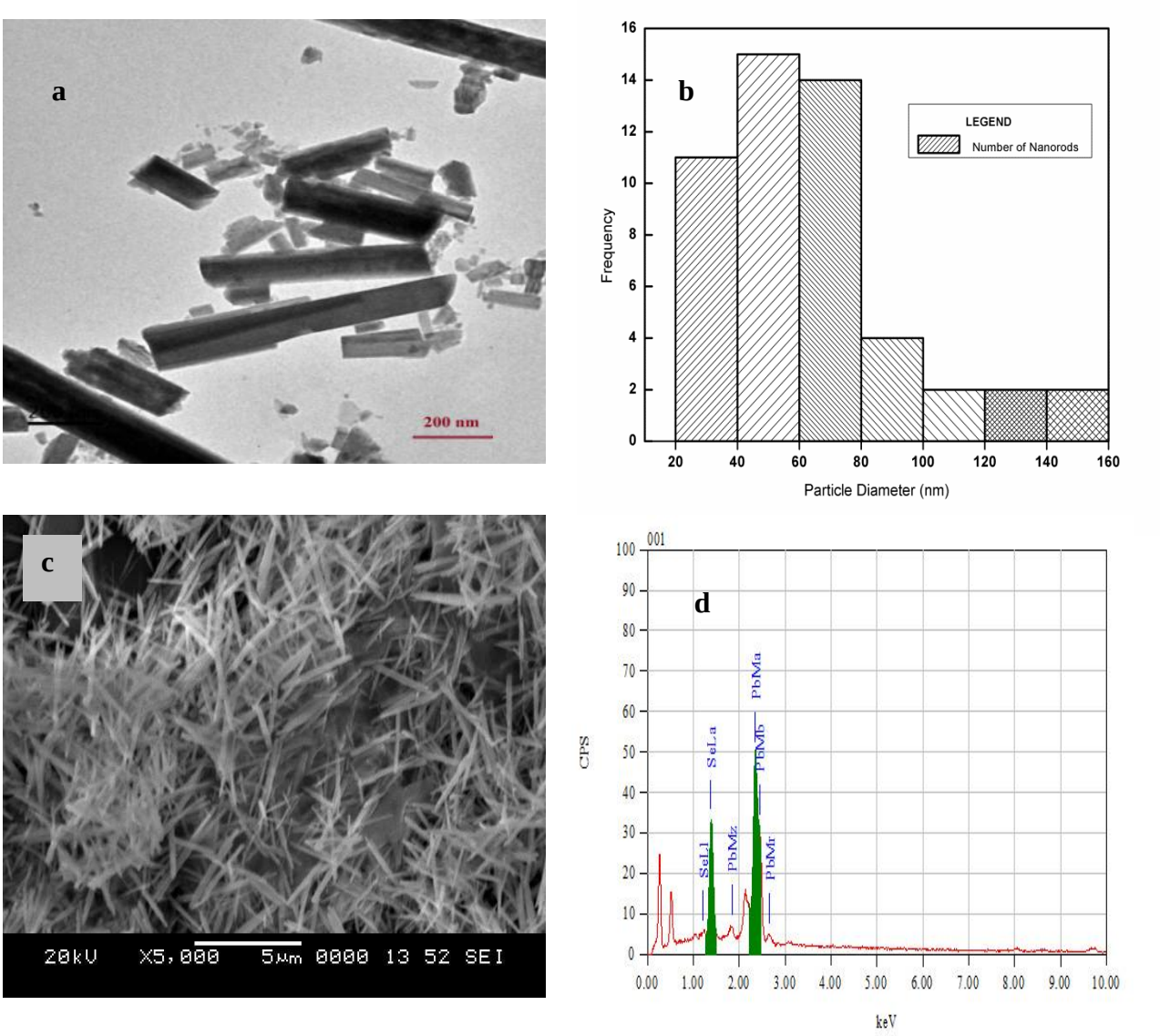

Fig. 4.8 Morphological characterization (a) TEM image; (b) Particle size distribution; (c) SEM image; (d) EDAX of biosynthesized PbSe QPs

The crystallite size was calculated using Scherrer formula (Koch et al. 2007):

$$R_{(hkl)} = \frac{0.89\lambda}{\beta cos\theta} \quad (7)$$

Where; R is the crystallite size, λ is the X-ray wavelength, β is the Full wave Half Maxima (FWHM), θ is the Bragg angle

For this calculation, the highest intensity (101) plane has been used, and it was assumed that the peak is Gaussian. The Gaussian fitting of the (101) peak is shown in Fig. 4.9. Here, in our experiment, $\lambda = 1.54^{\circ}A$, $\beta = 0.35182^{\circ}$ and $\theta = 29.215^{\circ}/2$. These results are in concordance with the standardized data (Table 1). The crystallite size was found to be ~3.057 nm, which is less than the diameter of the nano rods. This indicates a radial distribution of multiple crystallites in the nano rods (Samanta 2011).

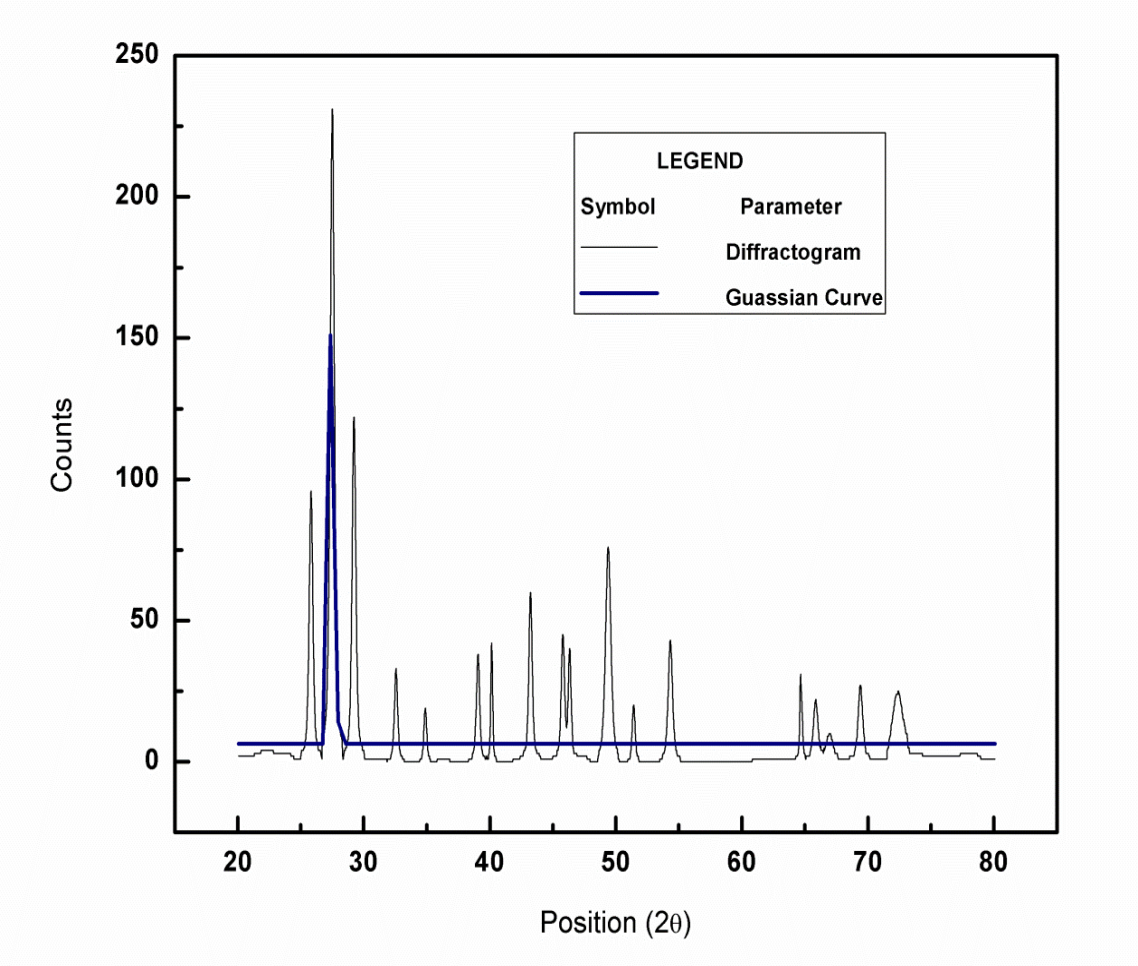

Fig. 4.9 XRD profile of PbSe QPs

4.9 Optical Characterization

UV-Vis spectra (Fig. 4.10a) of the colloidal PbSe QPs exhibit the appearance of an absorption edge at 375 nm and a weak absorption peak at 872 nm. The absorption maxima at lower wavelengths (< 300) indicate the presence of protein-capping that is reported to enhance the stability and biocompatibility of the nanoparticles and to prevent their aggregation (Bao et al. 2010b). The absorption peak at 375 nm and 872 nm is characteristic of PbSe particles in the quantum size regime (Baek et al. 2008).

FT–IR spectroscopy (Fig. 4.10b) was used to confirm the chemical composition of the ligands capping on the surface of the QDs. The biosynthesized PbSe QPs show absorption bands at wave numbers that direct the presence of amide and carboxylic groups of proteins. FTIR data also point towards absorption wave numbers that attribute to typical hydrocarbon functional groups on protein molecules (Stürzenbaum et al. 2013). The inherent biocompatibility and the remarkable band gap tailoring amenability of lead selenide (PbSe) QPs projects their potential application in effective fluorescence based biosensors.

The fluorescence of the biologically synthesized PbSe nanoparticles was checked by analyzing their fluorescence spectrum that displayed peak emissions at 425 nm and 475 nm (Fig 4.11a). While chemically synthesized PbSe QPs arrayed a fluorescence emission in the IR region of the electromagnetic spectrum, the biosynthesized PbSe QPs were found to exhibit fluorescence in the visible region (Tischler et al. 2010). Fig 4.11b depicts the fluorescence of the biosynthesized PbSe nanorods under short wavelength ultraviolet (UV) illumination.

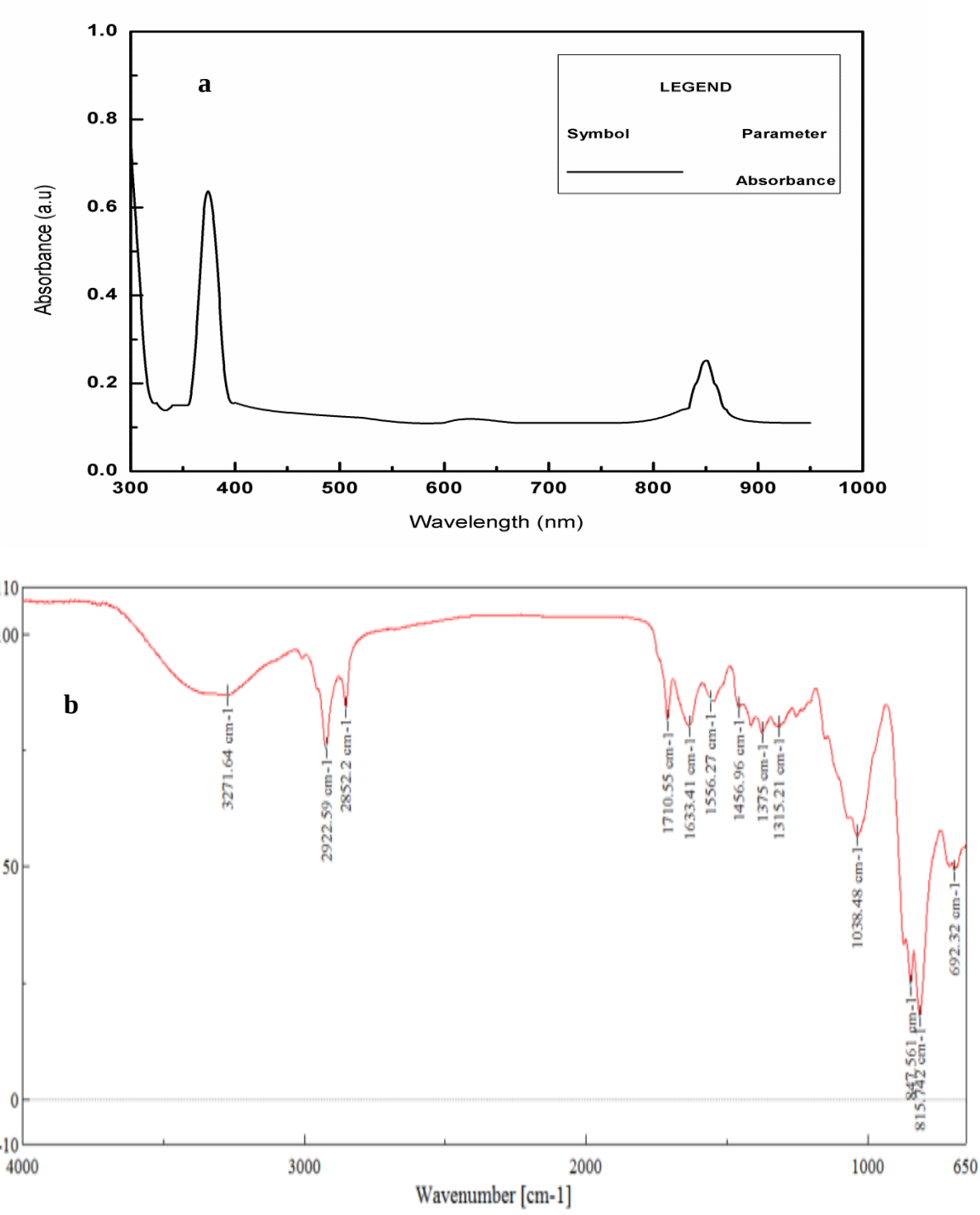

Fig. 4.10 Optical properties (a) UV-Vis spectrum ; (b) FTIR spectrum of the biosynthesized PbSe QPs

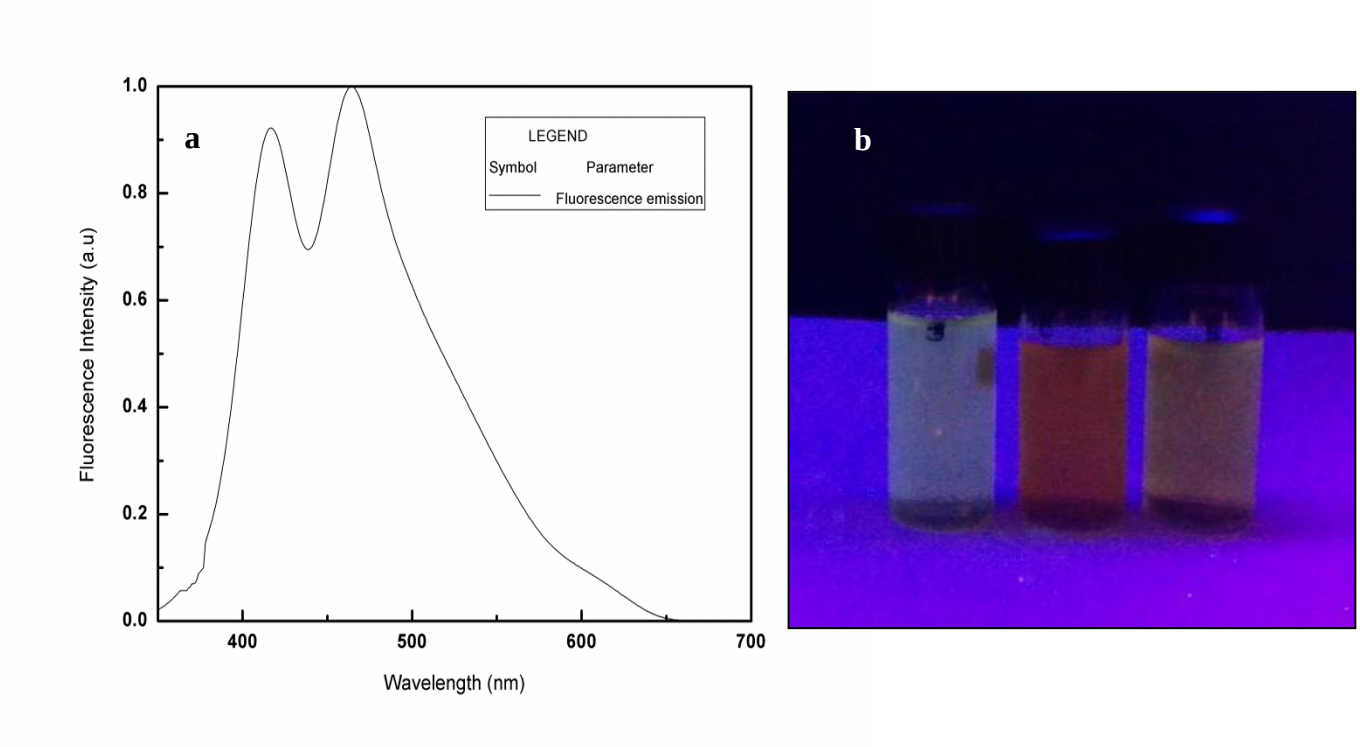

Fig.4.11 (a) Fluorescence spectra of the biosynthesized PbSe QPs; (b) Fluorescence of under UV- illumination

Further, the band gap of the material was calculated graphically using the Tauc equation (8):

$$\alpha h\nu = D(h\nu - E_g)^{n/2} \quad (8)$$

Where; hν is the energy of the photon, E_g is the band gap of the material, D is a constant and for a direct band gap material value of n=1.

Fig.4.12 shows the plot of $(\alpha h\nu)^2$ versus hν. Extrapolating the linear portion of the plot on the hν axis, the band gap was found to be 1.25eV, which is remarkably higher than that of the bulk PbSe (0.28 eV). This band gap enhancement occurs due to the size effect of the PbSe nano rods (Kassim et al. 2011).

The band gap of the nano sized PbSe was compared with the band gap of the bulk compound using the modified Brus equation (9).

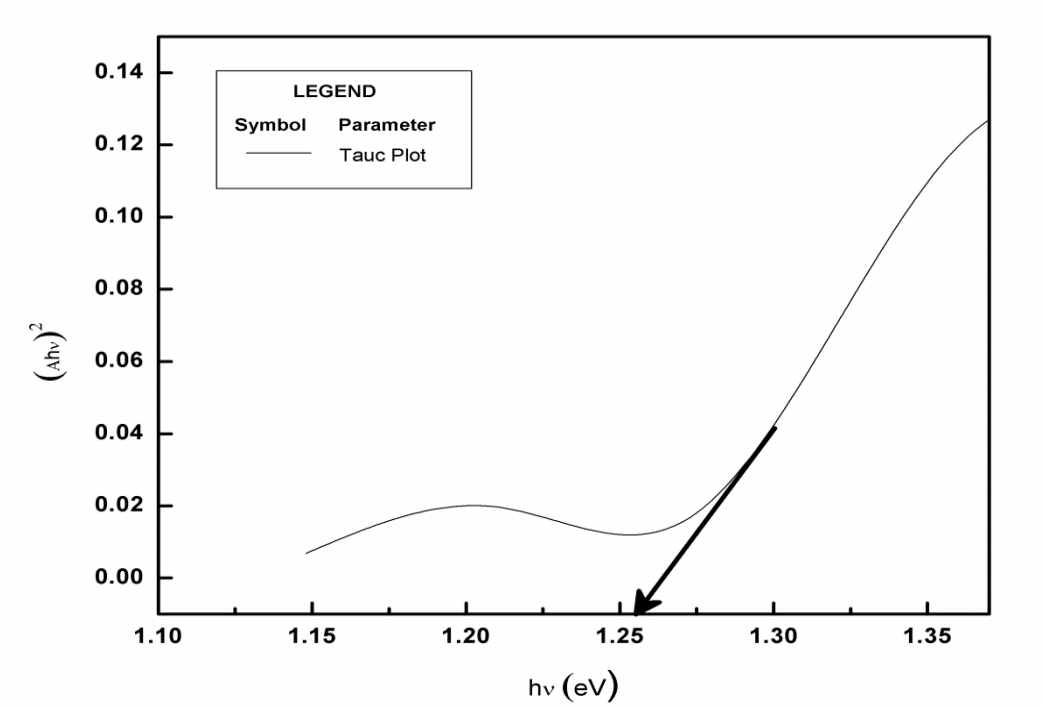

Fig.4.12 Tauc Plot of the biosynthesized PbSe QPs

$$E_{g\ nano} = E_{gbulk} + \frac{h^2\pi^2}{2\mu R^2} \quad (9)$$

Where; h is Plank`s Constant, μ is the reduced effective mass of electron and hole.

For PbSe, E_{gbulk}= 0.28eV, μ = 0.035. Substituting the values, the Bohr radius was calculated to be 1.07 nm. As the TEM images reveal larger size of nanocrystals in comparison to the calculated Bohr Radius, the confinement of the electron and hole was characterized to be in the weak quantum confinement regime (Samanta 2011). A significant increment in the band gap coupled with a weak confinement effect in comparison to the bulk PbSe, shape these nano sized counter parts as promising candidates in energy sector, bio-imaging and bio-sensing (Tischler et al. 2010).

In order to utilize the PbSe QPs for optical sensing and bio-imaging, it is important to understand the variation of their optical constants. Although literature directs attention towards

various attempts to study the optical constants of chemically synthesized PbSe QPs, the optical enumerations for biosynthesized PbSe quantum particles is scant. The absorbance data as obtained from UV-Vis spectroscopic studies were used to estimate the behavior of the absorption and extinction coefficient, reflectance and dielectric constant of the PbSe nano fabrication.

The absorption coefficient of PbSe QPs in a hypothetical medium with a QR volume fraction of one was calculated by the equation 10.

$$\alpha = {\ln 10 \times A}/{fl} \quad (10)$$

Where α is the absorption coefficient, A is the absorption, f is the QP volume fraction, l is the cuvette length. The variation of absorption coefficient with incident photon energy is depicted in Fig 4.13.

It has been observed that the absorption coefficient increase almost linearly with the increase in the incident photon energy. The linear increase in absorption coefficient with photon energy could be attributed to the higher electron-hole pair generation and subsequent recombination when excited with photons of increasing wavelengths (Okuno et al. 2000). Our results attest the findings that excitation with photons of increasing wavelengths results in bond breaking and bond rearrangement, which in turn result in a change in the local structure in the lead chalcogenides. These include subtle effects such as shifts in absorption edge and the atomic and molecular reconfiguration which is associated with changes in absorption coefficient and absorption edge shift (Alvi and Khan 2013). Further, the reflectance of the quantum rod sample was calculated in the wavelength range 200-1000 nm using the theory of reflectivity of light. From Fig.4.14, it can be inferred that the reflectance of the PbSe QPs increase in the wavelength

range 300–400 nm and 800– 1000 nm. This trend in the variation of reflectance is in concordance with prior literature (Khan et al. 2010).

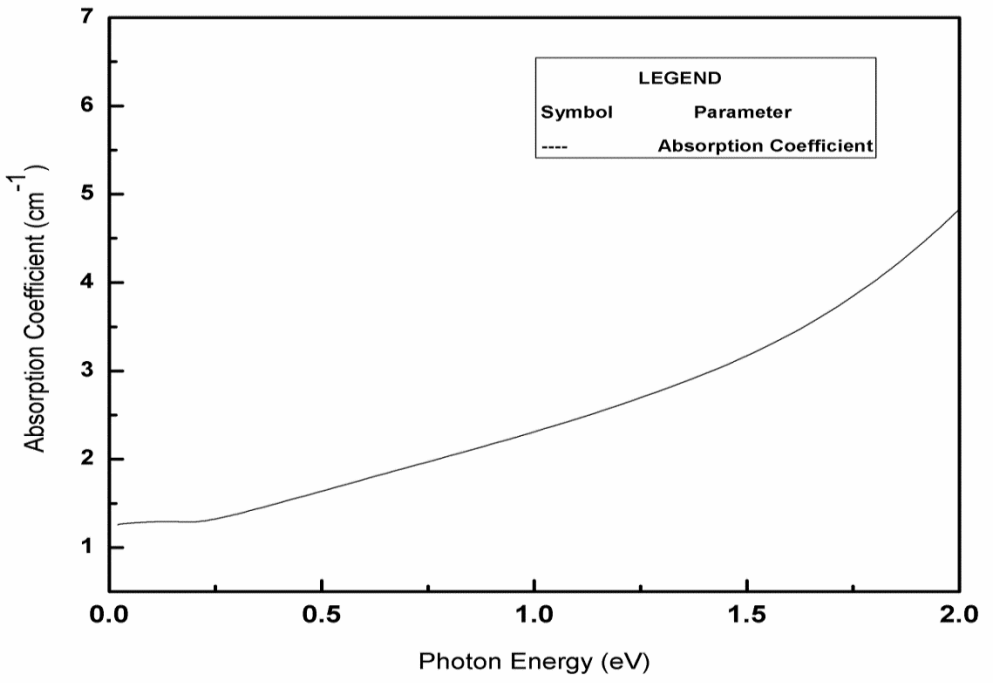

Fig.4.13 Variation of absorption coefficient of PbSe QPs with incident photon energy

The knowledge of the wavelength dependent refractive index and extinction coefficient is very important from the fundamental and technological context. Moreover, the refractive index is necessary for the design and modeling of optical components and optical coating. The wavelength dependent refractive index (n) and extinction coefficient (k) of the biosynthesized PbSe QPs was calculated using equation 11 derived from the theory of reflectivity of light.

$$n = \left[(1+R)\{(1+R)^2 - (1-R)^2(1+k^2)^{\frac{1}{2}}\}\right] \Big/ (1-R) \qquad (11)$$

Where, R is the reflectance, calculated from the absorbance and transmittance of the sample.

The molar extinction coefficient was calculated according to the equation 12:

$$k = {}^{\alpha\lambda}/_{4\pi} \quad (12)$$

Where α is the absorption coefficient, λ is the wavelength

The plot of refractive index (n) against the incident photon energy (Fig. 4.15) intuits that the refractive index (n) increase almost linearly with increase in photon energy for photons with wavelengths in the UV and NIR regions. Further, it was examined that the refractive index (n) of the material had a notable negative drift in the visible region of the electromagnetic spectrum. The extinction coefficient (k) of the PbSe QPs was found to increase linearly after the incidence of photons with energy greater than 2.5 eV (Fig. 4.16). The increase in the values of n and k could be due to the presence of large number of unsaturated defects or bonds in the biosynthesized PbSe QRs and their inherent localized states (Khan et al. 2010).

Dielectric constant, a parameter that signifies the electron storage potential of materials, was calculated using the following equations 13 &14

$$\varepsilon' = n^2 - k^2 \quad (13)$$

$$\varepsilon'' = 2nk \quad (14)$$

These parameters plotted against incident photon energy (Fig 4.17) array that the biosynthesized PbSe QPspossess elevated values for dielectric constant (> 20); pronouncing increased electron-hole mobility's at room temperature.

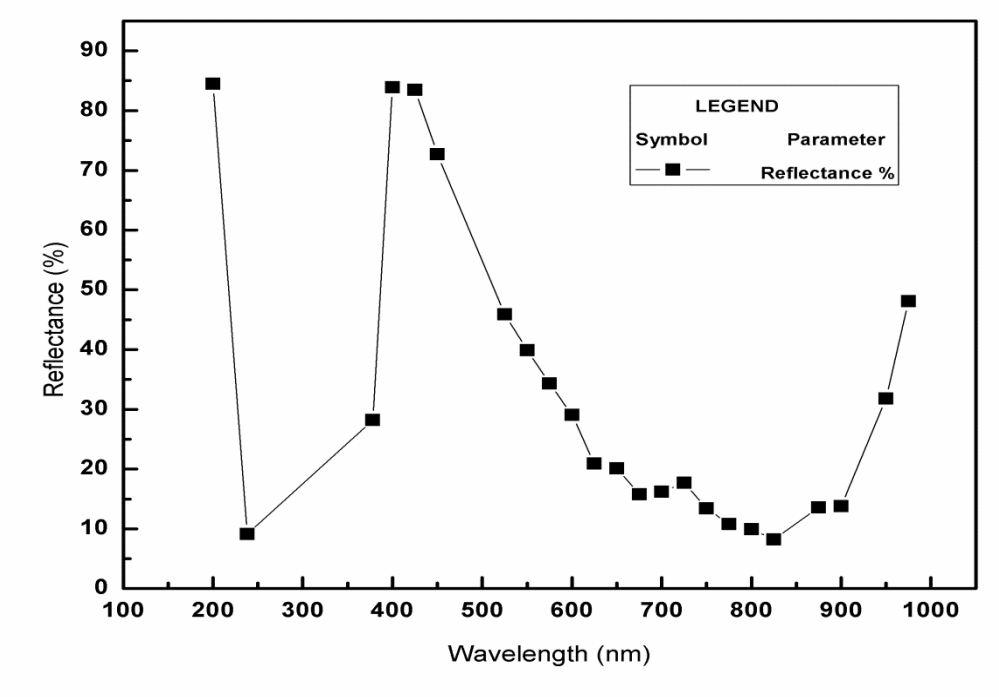

Fig.4.14 The variation in reflectance of the PbSe QPs with incident photon wavelength

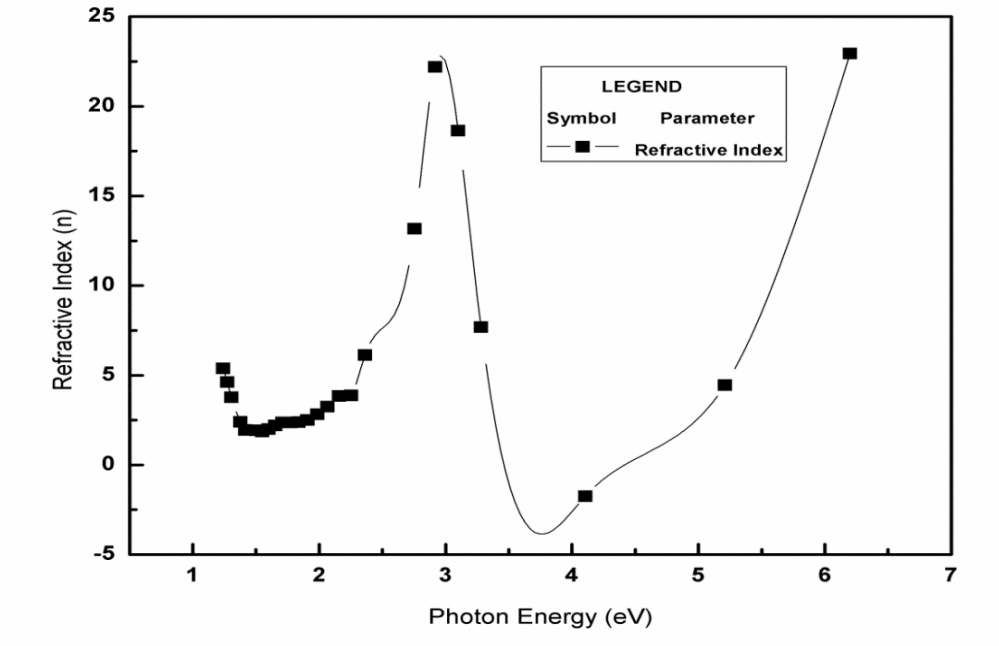

Fig.4.15 Variation of refractive index of PbSe QPs with incident photon energy

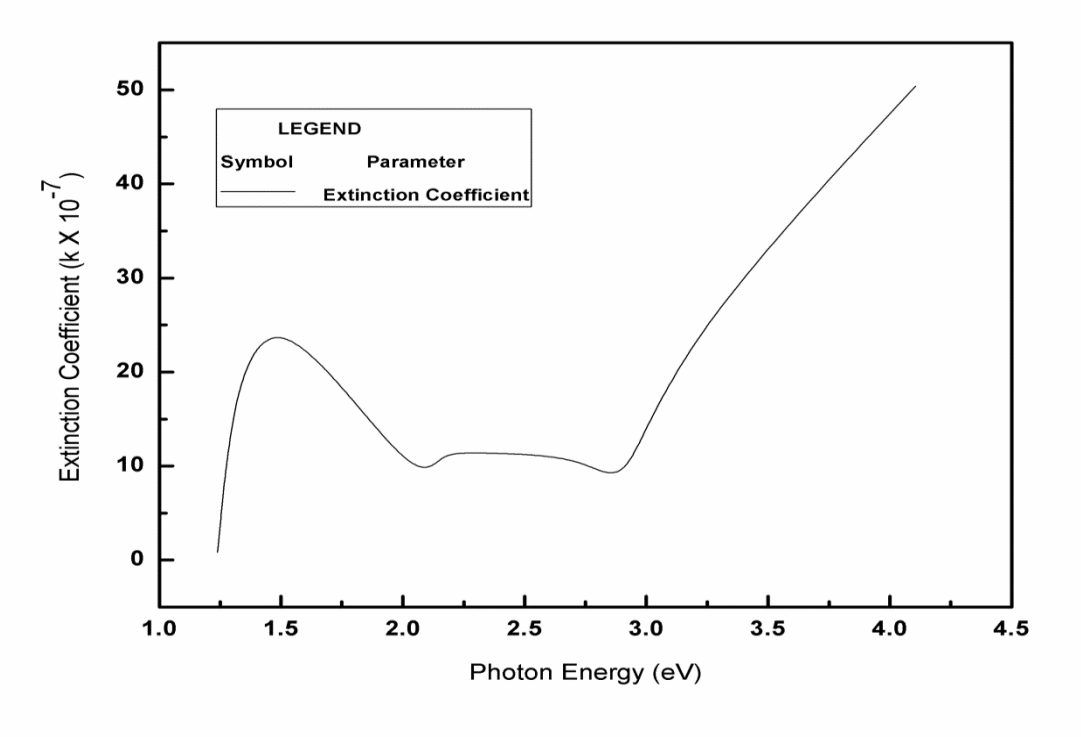

Fig.4.16 Variation of extinction coefficient of PbSe QPs with incident photon energy

The aforementioned pattern was comparable to that observed for the other optical constants and was typical for photons in the UV and NIR region of the electromagnetic spectrum. The variation in the real and imaginary part of dielectric constant with increase in photon energy could be explained by the presence of structural defects and localized states which give rise to a local potential, however, since the bonding in lead chalcogenides being covalent in nature does not result in large changes in the local potential at higher photon energies. The results appeal to previous findings (Khan et al. 2010) and also attest that the real and the imaginary part of dielectric constant are proportional to the refractive index and absorbance respectively (Hamizi and Johan 2012).

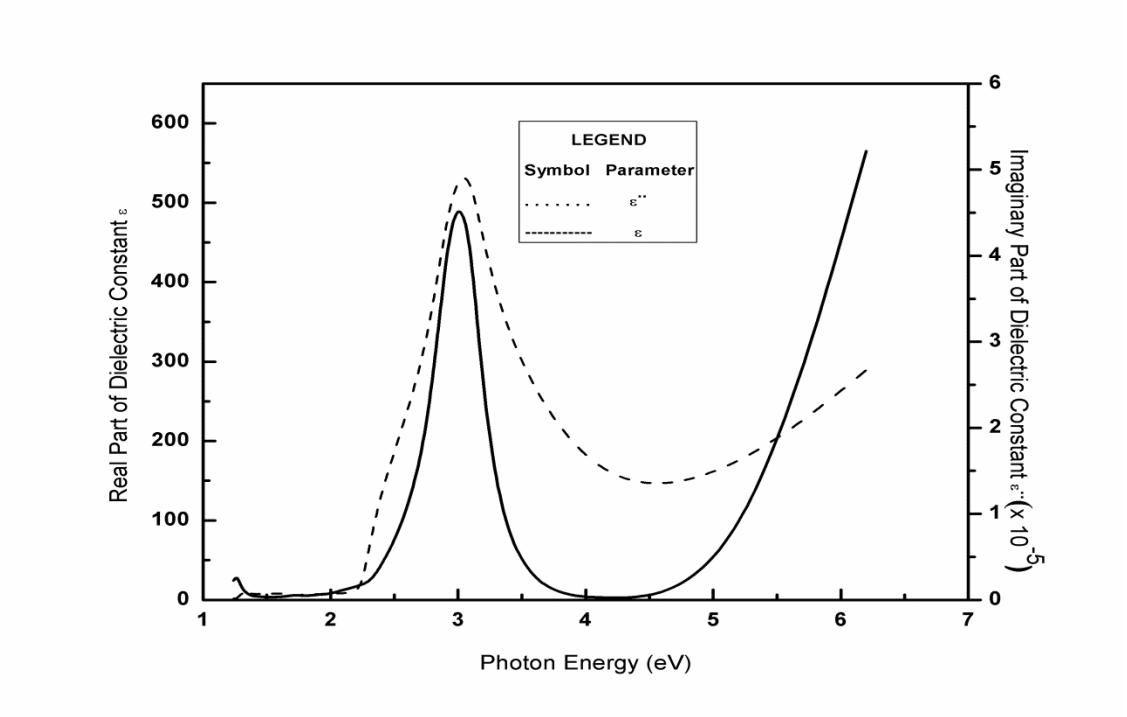

Fig.4.17 Variation of dielectric constant of PbSe QPs with incident photon energy

Further, the stability of the QPs with respect to its absorbance maxima was apprehended (Fig.4.18). It was observed that the absorbance of the PbSe QP solution remained stable at 375 nm for a period of 8 days after which it increased to higher wavelength ranges. The shift in absorbance maxima to higher wavelengths could be attributed to increase in particle size due to the formation of aggregates.

Fluorescence quantum yield is an important parameter that facilitates the utilization of the QPs for sensing applications. The quantum yield is the probability that a photon is emitted after one photon has been absorbed. Of the various studies on quantum yield measurements for nanocrystals, Bruchez et al. (1998) reported 15% and 6% quantum yields for green and red CdSe quantum dots coated in a layer of CdS. While quantum yield for quantum dots has been reported

as high as 80% (Qu and Peng 2002), dots made aqueous typically have much lower quantum yield (Cai et al. 2007). In the present study, the quantum yield was calculated using equation 15:

$$\emptyset_s = \emptyset_r . \frac{A_r}{A_s} . \frac{F_s}{F_r} . \frac{\eta_s^2}{\eta_r^2} \quad (15)$$

Where

Subscript 's' refers to the PbSe quantum rods, 'r' refers to rhodamine 6G used as reference, ∅ is the quantum yield (%), A is the absorbance in (a.u), F is the intensity of the fluorescence peak in a.u at the excitation wavelength, η is the refractive index of the solvent used for dissolving the quantum rods.

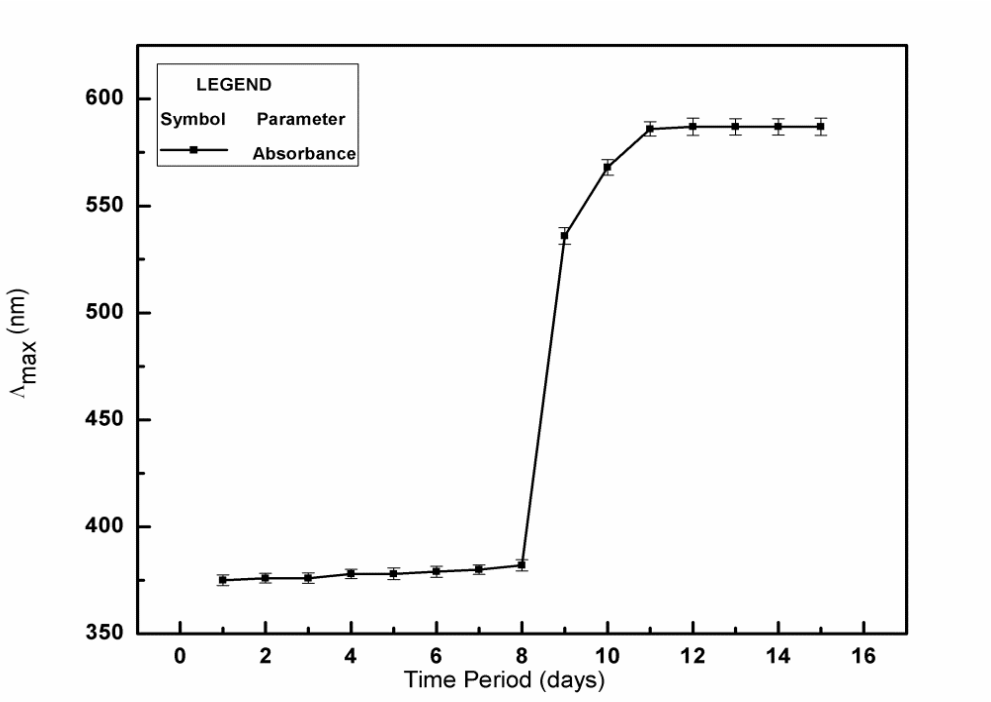

Fig.4.18 Photo stability of the biosynthesized PbSe QPs

Based on equation 15, the quantum yield of the biosynthesized PbSe QPswas calculated as 49.7%. Earlier Grabolle et al. (2008) had reported 50% quantum yield from chemically synthesized CdSe quantum dots. Also, Laverdant et al.(2011) had reported that commercially available QDs (Invitrogen QDot565 in decane) produce a fluorescence quantum yield of 38%. These data from literature further project the remarkable fluorescence quantum yield in biologically synthesized PbSe QPs thereby directing their prospective utilization in the development of highly efficient sensor systems.

4.10 Redox properties of biosynthesized PbSe quantum particles

Cyclic voltammetry is one of the most commonly used methods used for the study of electron transfer and its consequences. With the cyclic voltammetric method one can simultaneously activate molecules by electron transfer and probe subsequent chemical reactions. Further, the electrochemical properties of QPs are significant for their applications in nanoscale electronic, optoelectronic and sensing devices (Jin et al. 2014). Fig.4.19 shows the experimental results of linear scan voltammetry conducted on a glassy carbon electrode modified with PbSe quantum rods. With respect to the reported results for Se (Bouroushian 2010), Ag_2Se and PbSe nanotubes (Zhang et al. 2007; Mao et al. 2009), the peak at 1 (-0.71 V) on the anodic curve in Fig..4.19 can be attributed to the oxidation of the PbSe quantum rods ($PbSe + 2OH^- \rightarrow Pb(OH)_2 + Se^0 + 2e^-$). Further, the peak 2 (-0.36 V) and peak 3 (-0.04 V) on the anodic curve was designated to the oxidation of Se ($Se^0 + 2OH \rightarrow SeO_2 + 2e^- + 2H$) and the oxidation of $Pb(OH)_2$ ($Pb(OH)_2 + 2OH^- \rightarrow PbO_2 + 2H_2O + 2e^-$) respectively. Spanning through the cathodic curve, the peaks 4 at -0.19 V and 5 at -0.72 V corresponds to the reduction of PbO_2 ($PbO_2 + 2H_2O + 2e^- \rightarrow Pb(OH)_2 + 2OH^-$) and $Pb(OH)_2$ ($Pb(OH)_2 + 2e^- \rightarrow Pb + 2OH^-$) respectively. Similar observations were reported by Luo Jin et al. (2014) on the linear voltammograms of chemically

synthesized PbSe. According to the authors, insolubility of the PbO_2 formed during the redox reaction accounts to the formation of weak cathodic peaks.

To affirm the findings of linear scan voltammetry, successive voltammetric scans under the same conditions were carried out that revealed similar electrochemical reaction products as shown in Fig.4.20. From the cyclic voltammograms, it was inferred that the peaks 1-5 are similar and hence could be designated to the aforementioned redox reaction schemes. The marginal decrease in the peak intensity after successive electrolysis could be attributed to the gradual consumption/degradation of the PbSe QPs drop casted on the surface of the glassy carbon electrode (He et al. 2009). Clearly these results along with the voltammograms of the blank glassy carbon electrode (Fig.4.21) support the designations for the redox peaks analyzed for the biosynthesized PbSe quantum particles.

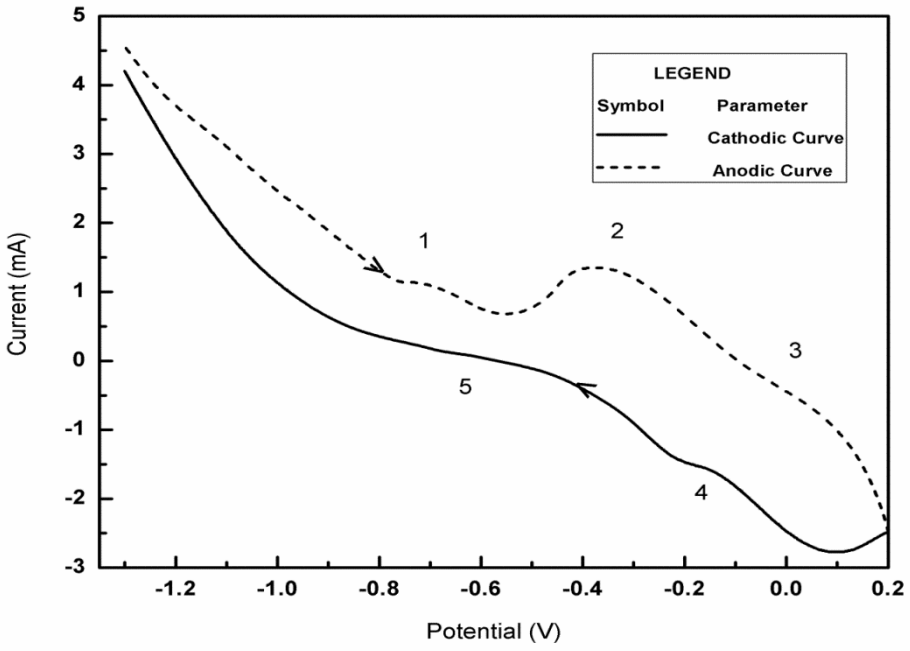

Fig.4.19 Linear voltammogram obtained by GC electrode modified with biosynthesized PbSe QPs

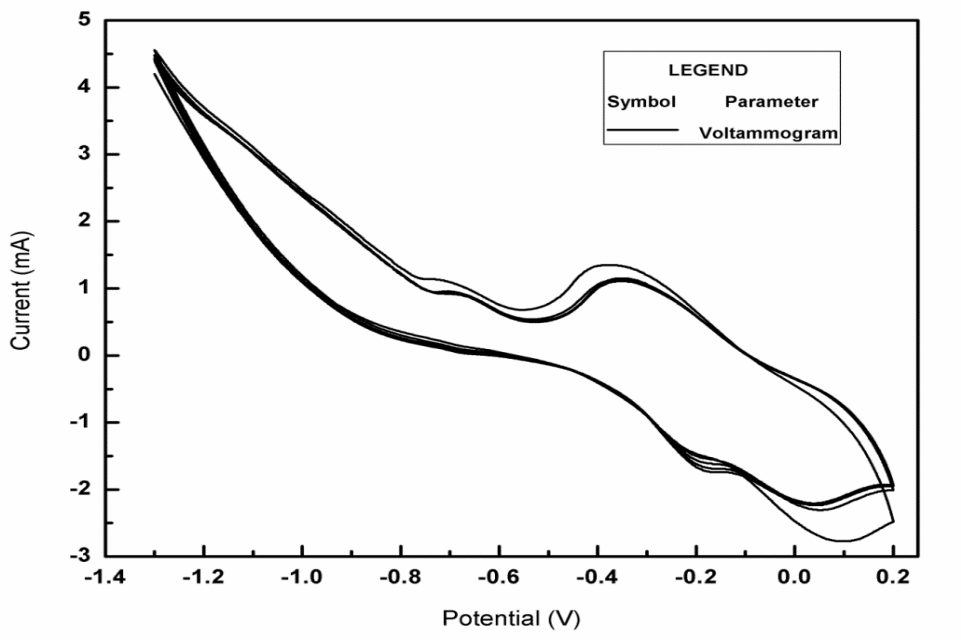

Fig.4.20 Cyclic voltammogram obtained by GC electrode modified with biosynthesized PbSe QPs

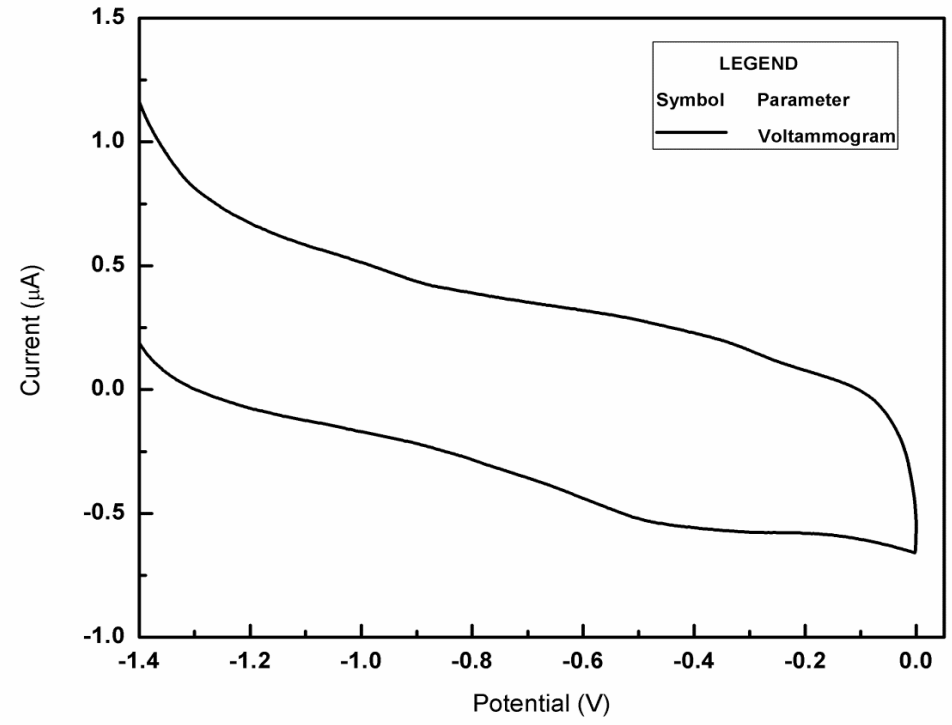

Fig.4.21 The voltammogram obtained by a blank glassy carbon electrode

4.11 Optimization of the PbSe QP fluorescence by response surface methodology

Statistical methods for process parameter optimization have proved to be a powerful and useful tool in research. RSM employs quantitative data from appropriate experiments to develop multivariate equations and solve them simultaneously for the design of experiments, constructing models, evaluating the effects of factors, and analyzing the optimum conditions of factors for desirable responses (Hormozi-Nezhad et al. 2012). Over the past decade, many researchers have applied RSM for controlling different aspects for the synthesis of nanomaterials (Ganea et al. 2008; Edrissi and Soleymani 2011; Hormozi-Nezhad et al. 2012). In the present study, a BBD was used for optimizing the process parameters for an enhanced fluorescence by the biosynthesized PbSe QDs. The BBD Matrix detailing the experimental runs along with the observed and predicted response (i.e., fluorescence intensity) for each of these runs is represented in Table 4.7.

The adequacy of the model was checked using analysis of variance (ANOVA) (Table 4.8). The model F value of 7.02% implies the significance of the model and that there is only 0.88% chance that the F value could occur due to noise. The low coefficient of variation (CV) (0.08) indicated that the experiments performed were highly reliable. The statistical p value $\leq$ 0.05 for the model and for the independant and mutual interactions between reaction time, temperature and pH denotes the significance of these terms in enhancing the fluorescence yield of the PbSe QDs. The results obtained from the BBD were fitted to a second order polynomial equation (Eq. 16) to explain the dependence of the PbSe QD fluorescnce intensityon the process parameters considered during its synthesis from marine *Aspergillus terreus*.

Table 4.7 BBD Matrix of the process parameters for the optimization of fluorescence of the PbSe QPs

Run	A	B	C	Response (* 10^6)
1	45	9	35	4.24
2	20	9	10	0.95
3	45	9	35	4.83
4	45	9	35	4.45
5	70	9	10	3.24
6	45	6	10	1.24
7	45	9	35	4.12
8	45	6	60	2.88
9	20	6	35	0.90
10	70	6	35	2.98
11	20	12	35	0.54
12	20	9	60	3.42
13	70	9	60	2.02
14	45	9	35	4.47
15	45	12	60	3.20
16	70	12	35	3.12
17	45	12	10	3.34

A= Temperature (°C) ; B= pH; C=Reaction period (min) and Response in terms of Fluorescence Intensity (X 10^6 A.U)

$$Fluorescence\ Intensity = 3.13 \times 10^6 + (6.92 \times 10^5)A + (2.76 \times 10^5)B + (3.45 \times 10^5)C + (1.25 \times 10^5)AB - (9.21 \times 10^5)AC - (4.44 \times 10^5)BC - (1.39 \times 10^6)A^2 - (1.13 \times 10^6)B^2 - (6.19 \times 10^5)C^2 \quad (16)$$

The graphical representations of the responses in terms of 3-D contour plots are depicted in Fig.4.22 (a), (b) and (c). The 3-dimensional contour plots clearly depict that the optimum point of all variables lies at the centre of the chosen range of the parameters under consideration for an enhanced fluorescence by the biosynthesized PbSe QDs.

Table 4.8 ANOVA for Response Surface Quadratic model

Source	Sum of Squares	Degrees of freedom	Mean square	F value	P value
Model	26.50	9	2.94	7.02	0.0088 significant
A-Temperature	3.82	1	3.82	9.12	0.01
B-pH	0.61	1	0.61	1.46	0.26
C-Reaction Time	0.95	1	0.95	2.26	0.17
AB	0.06	1	0.06	0.15	0.70
AC	3.39	1	3.39	8.09	0.02
BC	0.79	1	0.79	1.88	0.21
A^2	8.19	1	8.19	19.53	0.01
B^2	5.46	1	5.46	13.03	0.01
C^2	1.61	1	1.61	3.65	0.09
Residual	2.9	7	0.41		
Lack of Fit	2.64	3	0.88	11.95	0.81 not significant
Pure Error	0.29	4	0.07		

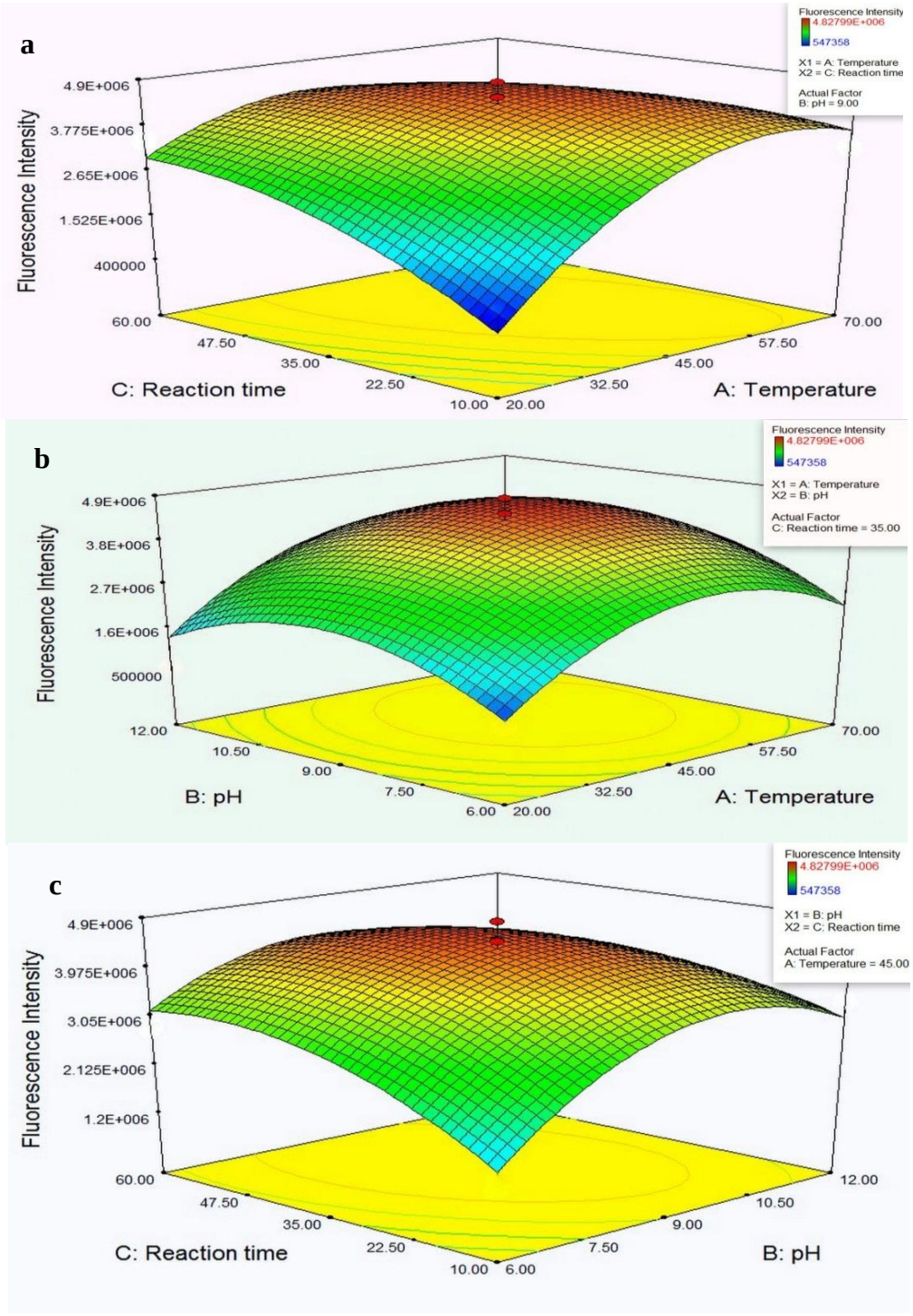

Fig. 4.22 3-Dimensional response surface plots showing the variation of fluorescence intensity with respect to:(a) reaction time and temperature; (b) temperature and pH; (c) reaction time and pH

According to experimental verifications based on the parameter values recommended by the model, maximum fluorescence intensity of 4.51×10^6 A.U was observed at 450 nm under conditions; pH = 9.97, reaction time = 28 min and reaction temperature = 58^oC (Table 4.9) . The experimental and theoretical response values under the aforementioned conditions were comparable and were notably higher (3 times) than the fluorescence intensity under synthesis conditions mentioned earlier. It was also noted that the fluorescence onset exhibited a blue shift from 475 nm to 450 nm in the PbSe QDs synthesized under optimized conditions in comparison to the protocols reported earlier.

Table 4.9 Predicted and experimental fluorescence intensity at optimum values

Condition	pH	Reaction time min	Temperature ^oC	Fluorescence Intensity $\times 10^6$ A.U
Predicted	9.97	28	58	4.85
Experimental	9.97	28	58	4.51

According to Jamieson et al.**,** the spectral signature of QDs is an assertive indicator of its size (Jamieson et al. 2007b) and that a reduction in the semiconductor dimensions to its exciton Bohr radii can result in an idealized intense fluorescence spectra in these nanofabrications (Chan et al. 2002). Hence, to verify this relation, the sizes of the QDs synthesized under the optimized conditions were visualized using a transmission electron microscope (TEM). Our observations revealed the formation of spherical nanoparticles with diameter ranges from 10-30 nm (Fig.4.23a). HRTEM images (Fig.4.23b) and the SAED pattern of the spot array (Fig.4.23c) revealed distinctive lattice fringes in the spherical nanocrystals with d-spacing that correspond to the planes 111, 200, 220, 222, 400, 420 of the typical PbSe Clausthalite type Rock Salt Structure

having Face Centered Cubic Lattice with lattice parameter values of a = b = c = 6.128 (JCPDS Reference Code: 00-065-1040). The biosynthesis of PbSe quantum rods (QRs) with diameter ranges 20-160 nm was reported in previous trials.

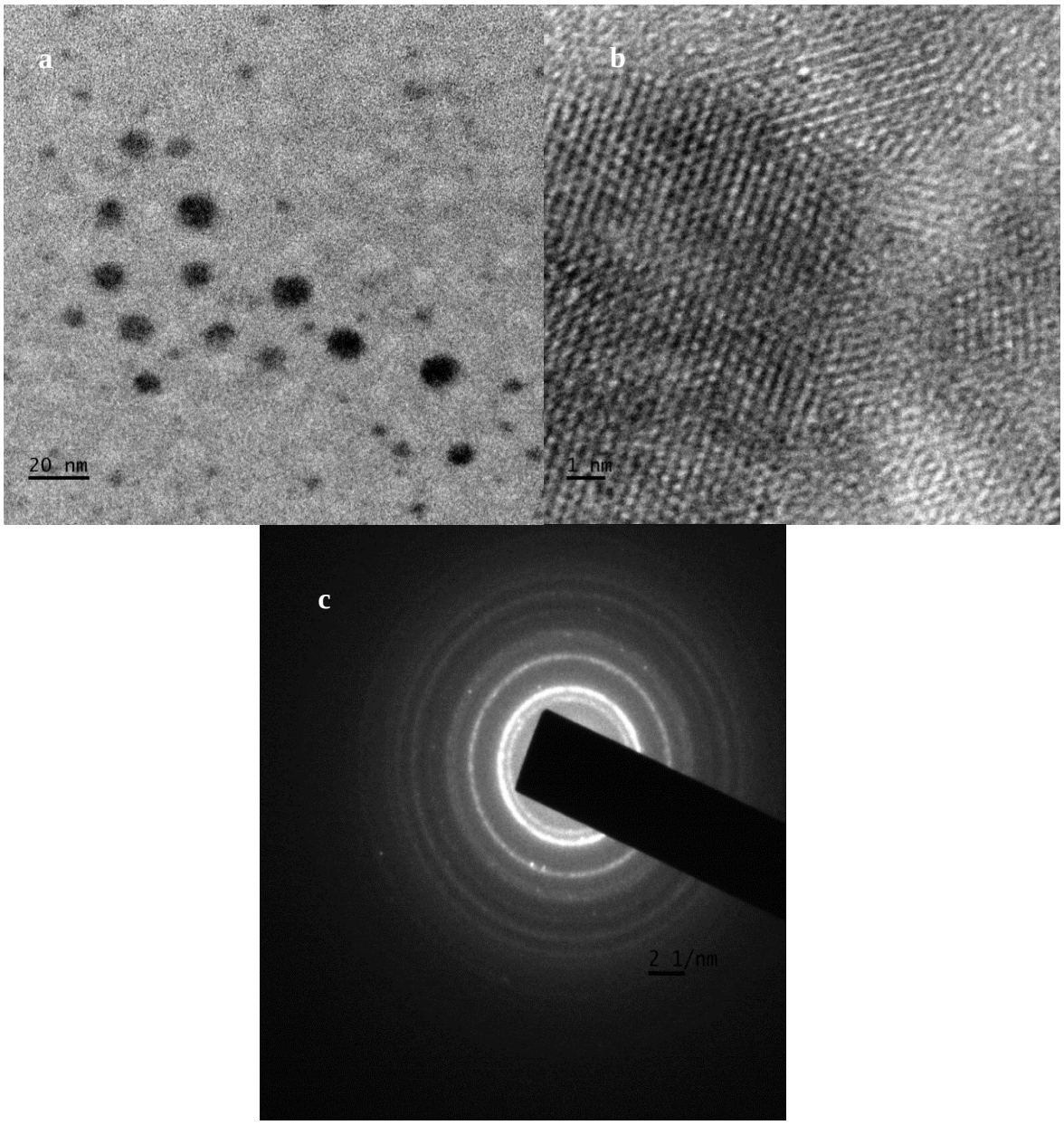

Fig. 4.23 Morphological features of the biosynthesized PbSe synthesized under optimized conditions viewed under (a) TEM; (b) HRTEM; (c) SAED diffraction pattern

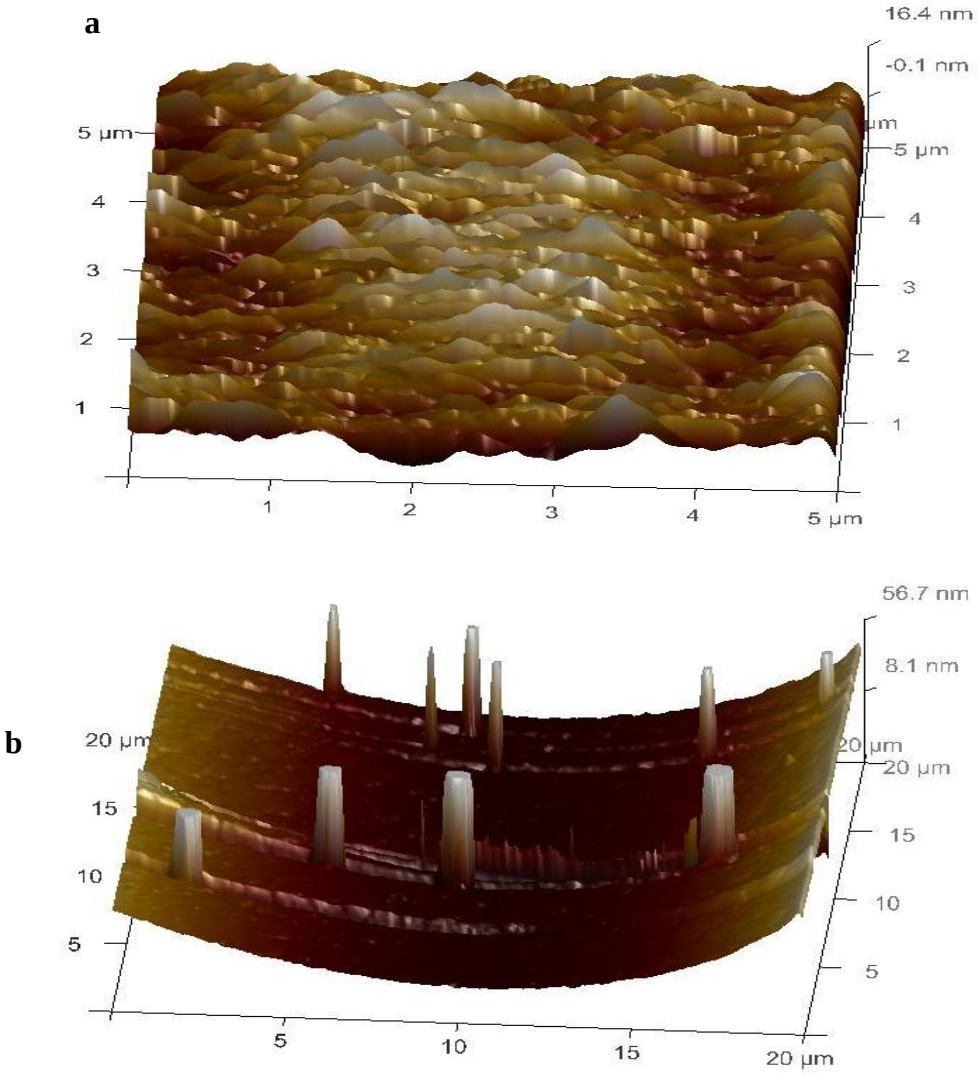

Fig. 4.24 Atomic Force Microscopic images showing surface distribution :(a) Biosynthesized PbSe on glass substrate; (b) Control (Glass substrate alone)

Further, AFM studies were conducted to study the surface distribution of PbSe quantum dots synthesized under optimized conditions. Fig. 4.24 shows the topography of the PbSe QD on the glass substrate. The average (R_a) and root mean square (rms; R_q) surface roughness were found to be 3.65 nm and 4.63 nm, respectively. The density of QDs was approximately 1.040/μm^2. Analysis of Fig. 4.24 a and b clearly indicate that the substrate surface is well covered by fine spherical or elliptical nature of the grains with varying heights. The morphological evidences from TEM and AFM images clearly indicate the size tunable fluorescence emission from the biosynthesized PbSe QDs.

4.12 Applications of biosynthesized PbSe QPs

4.12.1 Antibacterial Properties

Bacterial biofilms are one of the major disadvantages that impede the use of biosynthesized nanoparticles as thin films and in membranes for analyte detection in solution (Weir et al. 2008). The filter paper bioassay for anti-bacterial activity of the biosynthesized PbSe QPs dispensed on filter paper discs, revealed the formation of distinct zones of inhibition by common gram positive and gram negative bacterial pathogens. The results and images of the inhibition zones are presented in Table 4.10 and Fig.4.25, respectively. It can be observed that the biosynthesized PbSe QPs had an anti-bacterial activity comparable to that of standard antibiotics against pathogens like *Bacillus cereus* and *E-coli* (Table 1). Based on these findings, it can be inferred that the biosynthesized PbSe quantum rods can serve as a broad spectrum antibacterial agent.

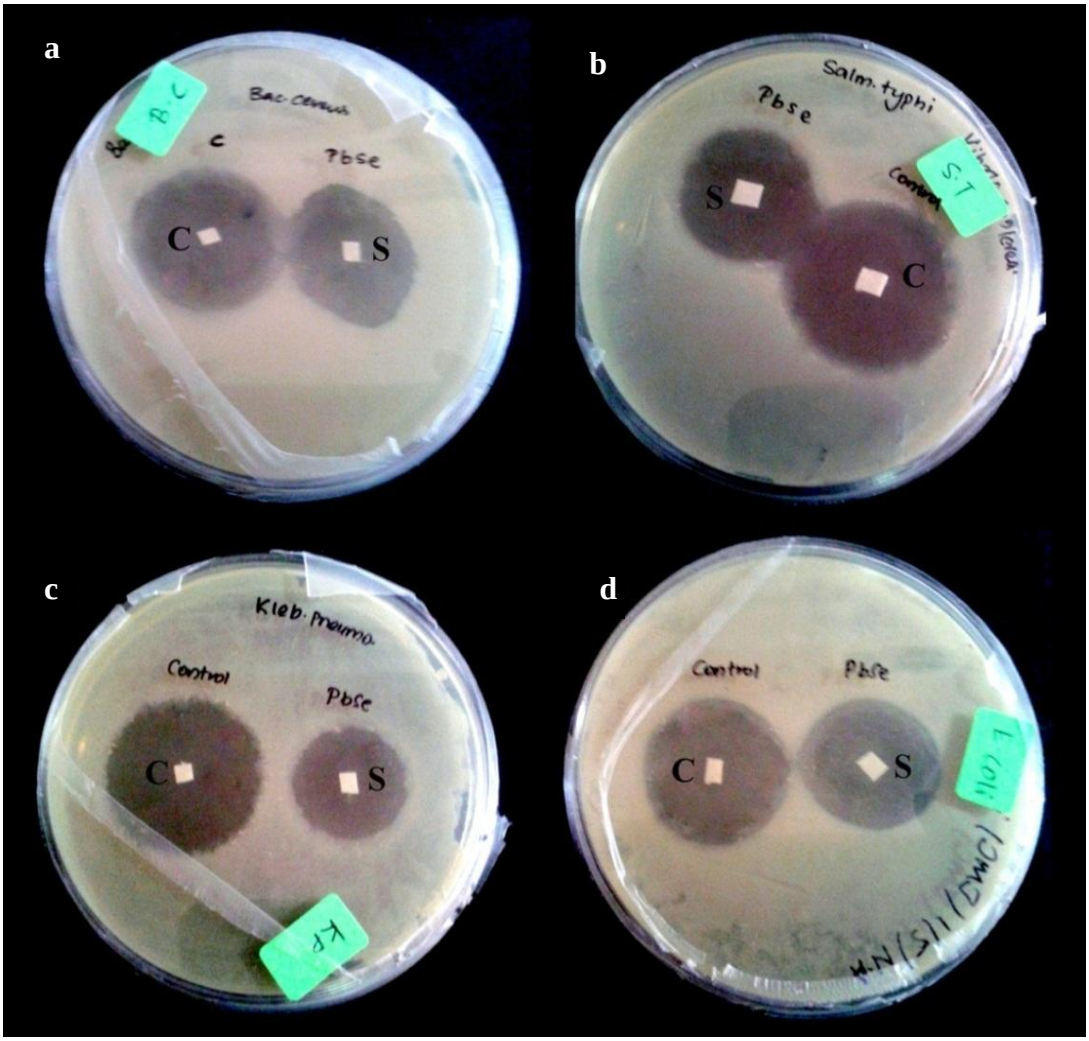

Fig. 4.25 Comparison of the zone of inhibition between (a) *Bacillus cereus* and (b) *Salmonella typhi;* (c) *Klebsiella pneumonia;* (d) *Escherichia coli* for control and biosynthesized PbSe QPs.

Table 4.10 Zone of inhibition of the PbSe QRs and standard antibiotic

Bacteria	Zone of Inhibition (mm)	
Gram (+) Bacteria	Control	PbSe QRs
Staphylococcus aureus	26 ± 0.52	10 ± 0.17
Bacillus cereus	31 ± 0.38	24 ± 0.48
Bacillus endophyticus	30 ± 0.19	12 ± 0.12
Gram (-) Bacteria		
Salmonella typhi	34 ± 0.22	21 ± 0.47
Escherichia coli	28 ± 0.51	24 ± 0.36
Klebsiellapneumoniae	32 ± 0.39	22 ± 0.26
Vibrio cholerae	33 ± 0.58	21 ± 0.29
Vibrio parahaemolyticus	32 ± 0.30	23 ± 0.02

4.12.2 Cadmium ion (Cd^{2+}) sensing in solution using PbSe

4.12.3 The quenching effect of metal ions on the fluorescence of PbSe QDs

The effect of 10 different metal ions namely Cd^{2+}, Fe^{3+}, Cu^{2+}, Hg^{2+}, Al^{3+}, Pb^{2+}, Mn^{2+}, Zn^{2+}, Mg^{2+} and Ni^{2+} on the fluorescence of the PbSe QDs was analyzed. The respective metal chlorides at 25 μM concentrations were used for the initial study and the fluorescence intensity ratio (F_0/F) of the PbSe QD solution in the absence and presence of the metal ions were observed. According to Fig.4.26, a notable fluorescence quenching can be observed in the presence of Cd^{2+} ions. While the other tested metal ions had little or no effect on the fluorescence of the PbSe QDs, ions like Fe^{3+}, Cu^{2+}, Pb^{2+} and Zn^{2+} is found to exhibit a lesser degree of fluorescence quenching. Similar observations were reported earlier for the selective detection of Cu^{2+} ions using grapheme QDs. The authors reported that Cu^{2+} ions quenched the fluorescence

intensity of the grapheme QDs by 2-3 times in comparison to other tested metal ions like Fe, Al, Co, Cd, Pb etc. (Wang et al. 2014).

Based on these results, the Cd^{2+} induced PbSe QD fluorescence quenching was studied in detail. Fig.4.27a shows that the emission intensity of the PbSe QDs exhibits a gradual decrease with the increase in concentration of Cd^{2+} ions. It is evident that the fluorescence of the PbSe QDs experienced a radical fall at Cd^{2+} concentrations around 40 μM, after which the fluorescence evinced a gradual decrease, its value attaining fixed levels after Cd^{2+} concentrations around 90 μM. The results of the present study are contrary to the observations by (Li et al. 2007a) who reported the fluorescence enhancement in CdSe/ZnS core/shell QDs capped with l-carnitine in the presence of Cd^{2+} ions in the concentration a dynamic range up to 50 μM. The luminescence increase was attributed to the formation of a cadmium–carnitine complex on the surface of the QDs. However, authors also reported a decrease in the carnithine capped QD fluorescence intensity at Cd^{2+} concentrations around 100 μM (Li et al. 2007a).

Further, the ratio of the fluorescence intensities of the aqueous QDs in the presence and absence of Cd^{2+} ions was plotted against the Cd^{2+} ions in the concentration range 0-350 μM (Fig.4.27b). A linear relationship was obtained for the fluorescence intensities of the QDs at 319 nm in the concentration range 0-20 μM. The standard additions method was applied to the quenching responses in the above mentioned concentration ranges (Shrivastava and Gupta 2011). Accordingly, under the current experimental conditions, the limit of Cd^{2+} detection was estimated to be 2.31 μM based on 3 S_b/K. Where, S_b is the standard deviation of the corrected blank signals of the PbSe QDs and K is the slope of the calibration curve.

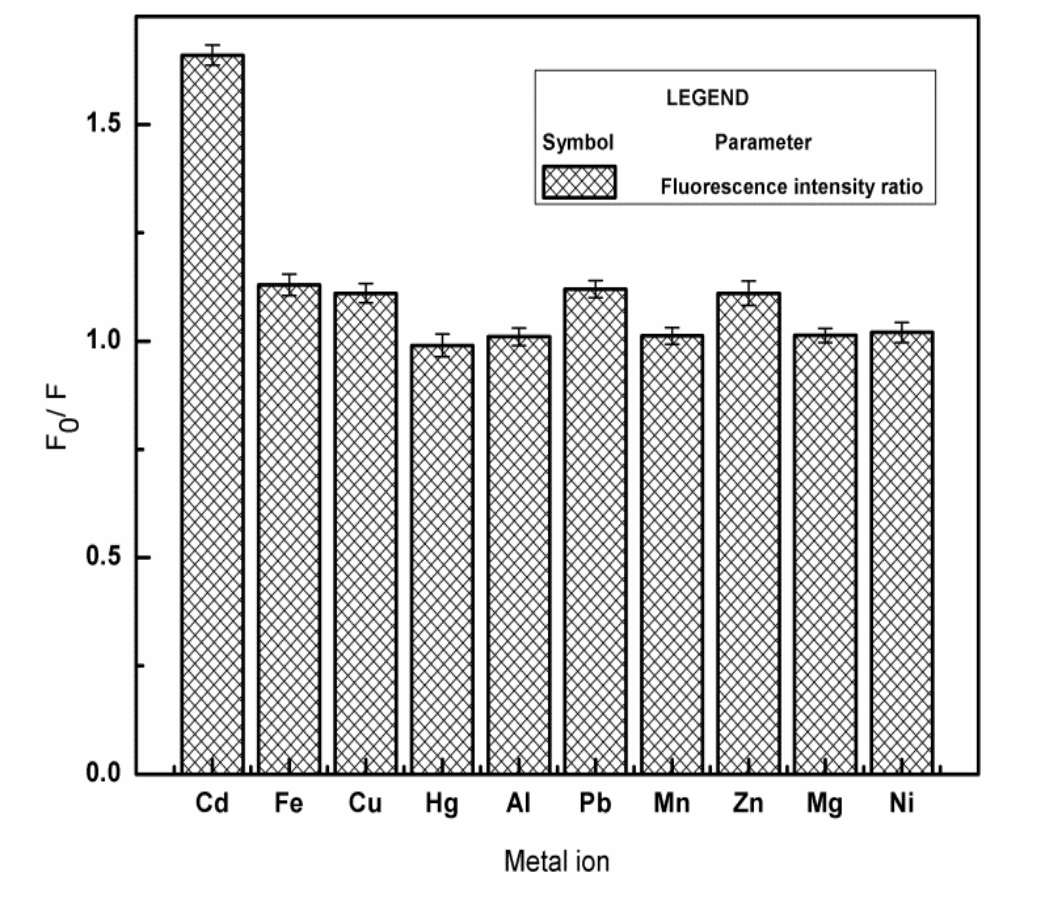

Fig. 4.26 Variation of fluorescence intensity ratio of PbSe QDs in the presence of various metal ions

Li et al. 2007a detected Cd^{2+} ion concentrations upto 0.15 μM in aqueous media using carnithine capped CdSe/ZnS core/shell QDs. Although the calculated LOD for Cd^{2+} ions using biosynthesized PbSe QDs is comparatively low, the present findings hold promise as a naïve effort to utilize the fungal protein capped biosynthesized PbSe QDs as significant sensing platforms that satisfactorily meets the Cd^{2+} ion detection limits by Environmental Protection Agency (EPA) (Rivas et al. 2009).

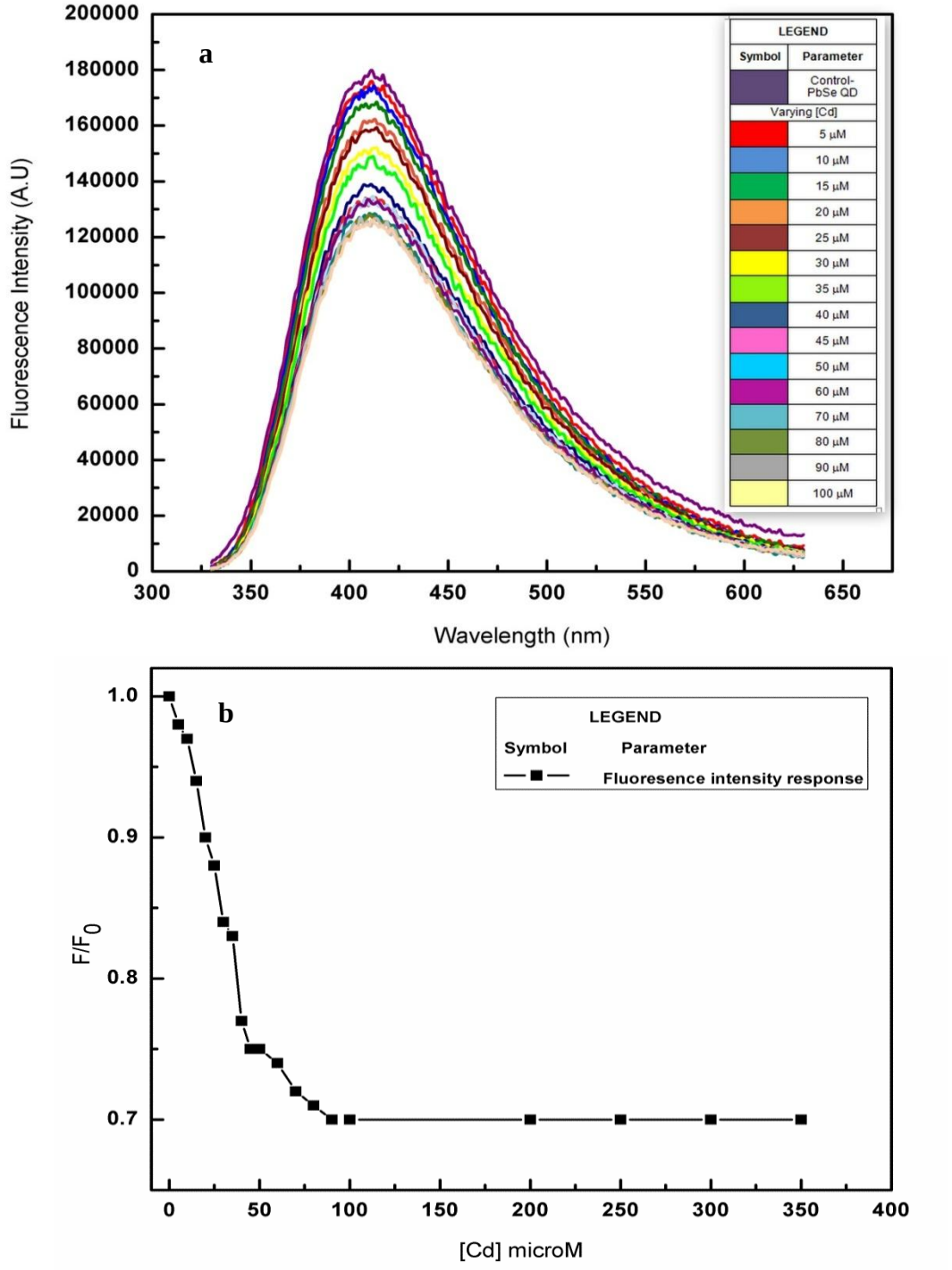

Fig. 4.27 (a) Emission spectra of PbSe QDs in the presence of Cd^{2+} (from up to down, the concentration of Cu^{2+} is 0, 5,10, 15, 20, 25, 30, 35, 40, 45, 50, 60, 70, 80, 90, 100 μM, respectively); (b) Fluorescence intensity response of PbSe QDs to the concentration Cd^{2+}

4.12.4 The possible Cd^{2+} ion Sensing Mechanism

A variety of molecular interactions between the analyte/quencher and the flurophore can result in quenching. Typically, these interactions are categorized as Collisional/Dynamic quenching and Static quenching (Chen and Rosenzweig 2002; Bo and Ping 2005). The fluorescence quenching originating from collisional interactions between the flurophore and the quencher is called collisional or dynamic quenching. But static quenching occurs as a result of the formation of a non-fluorescent complex between the flurophore and the quencher (Fan et al. 2009). Dynamic quenching can be best described by the Stern-Volmer plot that follows a linear trend for quenching based on collisional interactions (Bo and Ping 2005). However, the formation of the non-fluorescent complex in case of static quenching results in slight modifications in the Stern-Volmer equation (equation 5),; K_{SV} is now the association constant K_S and $\tau_0=\tau$, as the fluorescence lifetime of the fluorophore remains unperturbed by the static quenching. These modifications account for the non-linearity in the Stern-Volmer plot in case of static quenching (Wang et al. 2014).

In the present study, the mechanism of PbSe QDs' fluorescence quenching by Cd^{2+} ions were explored by examining the trend of the Stern –Volmer plot for Cd^{2+} concentrations ranging from 0-20 μM (Fig.4.28). The non-linear nature of the plot signifies that, for the given concentration of Cd^{2+}, the metal ions' binding on to the surface of QDs' result in triggering the recombination centers of electrons with holes, leading to the quenching of fluorescence of the QDs (Rodrigues et al. 2014). Similar observations that attest the formation of network like structure and induced aggregation of Cd^{2+} ions on the surface of carnitine capped CdSe/ZnS core/shell QDs have earlier been reported at high cadmium ion concentrations (Li et al. 2007a). However, in order to understand the fluorescence quenching mechanism more precisely, further

studies on fluorescence life time of the QDs in the presence and absence of Cd ions have to be carried out.

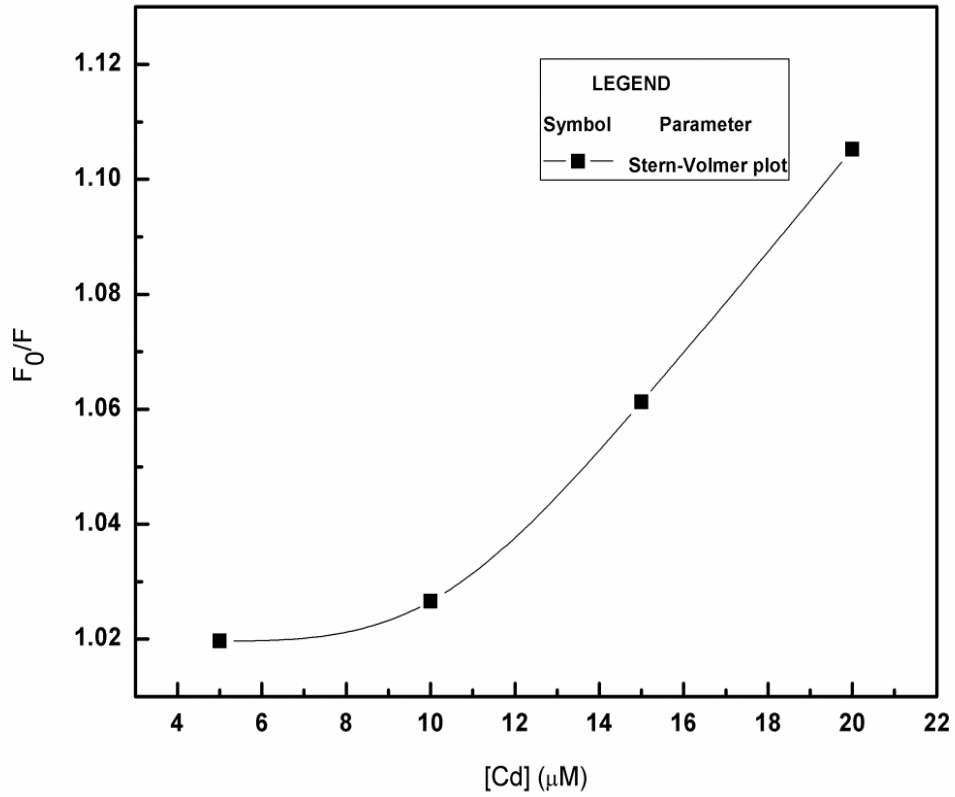

Fig. 4.28 Stern–Volmer plots describing the dependency of the fluorescence intensities on the Cd^{2+} concentration over the range of 0–20 μM.

4.13 Exploring the fungal protein cadre involved in biosynthesis of PbSe QDs

The present study employed marine *Aspergillus terreus* for the biosynthesis of PbSe QDs using a green and cost effective protocol. However, the mechanism of formation of QDs by biosynthesis is still largely unexplored (Kumar and Yadav, 2009). Understanding the cascade of nanoparticle formation is essential from the view-point of maximizing the utility of these nano factories. The following sections explicate the observations of the present study to investigate the mechanism behind the formation of PbSe QDs using marine *Aspergillus terreus*.

4.13.1 Morphological studies by scanning electron microscopy (SEM) with Energy Dispersive Analysis using X-rays (EDAX)

The remarkable ability of filamentous fungi to bind metal ions is very well documented (Ghosh et al. 2015). The binding of metal ions can be achieved by various processes ranging from physico-chemical interactions, such as absorption or adsorption of metals and their chelation by extra- or intracellular proteins; regulating metal uptake and/or efflux by intracellular sequestration and compartmentalization (Sathiyasarathi and Kumar, 2012). In particular, fungalprotein secretions play a vital role in extracellular co-precipitation of metals; a common phenomenon to tackle the high metal concentration among filamentous fungi (Jain et al. 2014). In the present study, the scanning electron micrographs of the fungal biomass before and after the biosynthesis of PbSe QDs were analyzed (Fig.4.29). Accordingly, it can be noted that the hyphae of *Aspergillus terreus* without the Pb and Se stress were cylindrical and septate, characterized by smooth hyphal filaments. However, the fungal morphology in Pb and Se stressed environment is found to have certain kind of surface roughness and agglomerations, along with hyphal rupture as given Fig.4.29.b. Such surface modifications were earlier reported for *Aspergillus*sp exposed to heavy metals (Cánovas et al. 2004). To further analyze the elemental composition on the surface in the Pb and Se treated biomass, the EDAX results were analyzed, which directed attention towards Pb and Se traces on them (Fig.4.29.c).

The marginal peaks of these metal/metalloid ions in the EDAX spectra and the surface aberrations indicated that surface adsorption and intracellular uptake, could be the initial fungal response which further accelerated the subsequent metal detoxification surge. Irrespective of surface adsorption or intracellular uptake of the metal/metalloid salts, an active microbial metabolism resulting in the production of intracellular detoxifying compounds result in an

increased cytosolic pressure leading to the outward growth of the cell wall structures (Paraszkiewicz et al. 2010). According to Courbot et al. (2004), these intracellular compounds resort to the vacuoles which in turn serve as storage compartments.

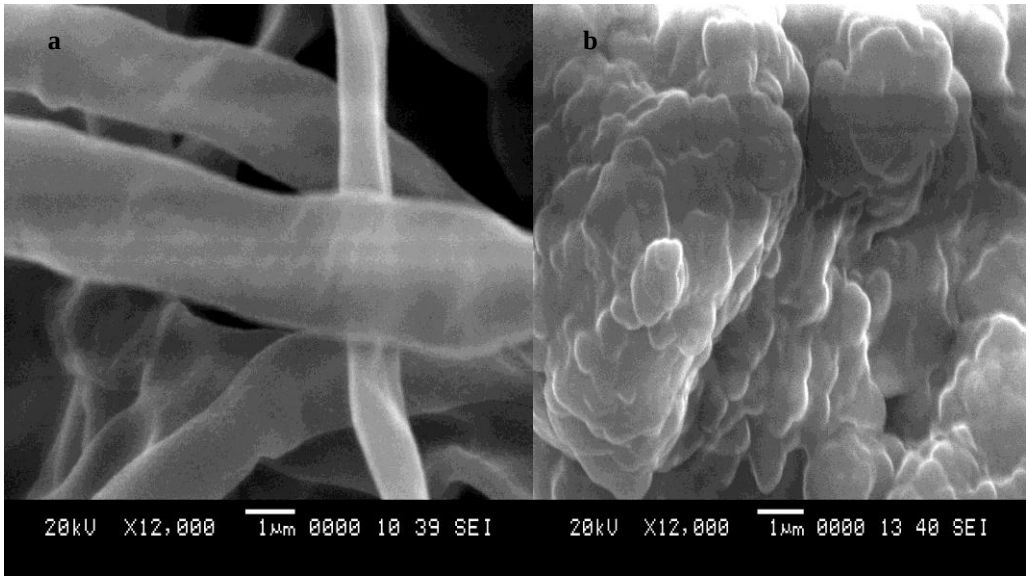

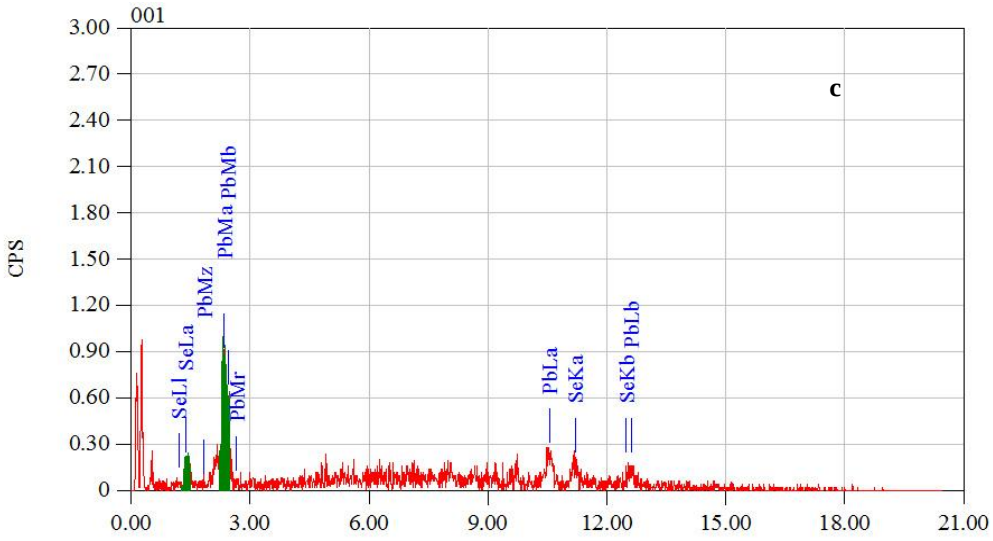

Fig. 4.29 SEM images of *Aspergillus terreus* (a) untreated (b) Pb-Se treated (c) EDAX of the Pb-Se treated biomass

4.13.2 Fourier Transform Infra-red Spectroscopic Analysis (FTIR)

The FTIR spectra of the control and the Pb-Se treated biomass were recorded at a wave number range of 1000-2500 cm^{-1} to expound the possible cell-stress (metal-metalloid) interactions that lead to the appearance of any microbial stress associated functional groups. The utility of FTIR spectrum as preliminary indicators of primary and secondary stress factors has been reported earlier (Qian and Krimm 1994). In the present study, the FTIR spectrum of the biomass exposed to the precursors for PbSe QD biosynthesis was compared to that of the control to determine the functional groups characteristic to acids, proteinitous and non proteinitous compounds (Kong and Yu 2007; Ivanova et al. 2008). The spectrum of the biomass subjected to PbSe biosynthesis revealed the involvement of oxalic acids as indicated by the absorption peaks at 2495± 5, 1700± 5, 1261± 5, 1201± 5 and 1126± 5 cm^{-1} and thiol groups at 2561± 5 cm^{-1} respectively (Fig. 2b) (Damodaran et al. 2013). The aforementioned peaks were absent/ exhibited a shift in the spectrum for the control as indicated by Fig.4.30a.

These results indicate the prominent involvement of proteins in Se biosorption and bioreduction by the fungus. Sarkar et al (2011) reported that the proteins and acidic compounds are key components for the bio-reduction of the metal/metalloid salts and the subsequent synthesis of fungal proteins that stabilize nanoparticles. Although the results discussed here are in accordance the above literature the stress factors need to be further comprehended through LC-MS analysis.

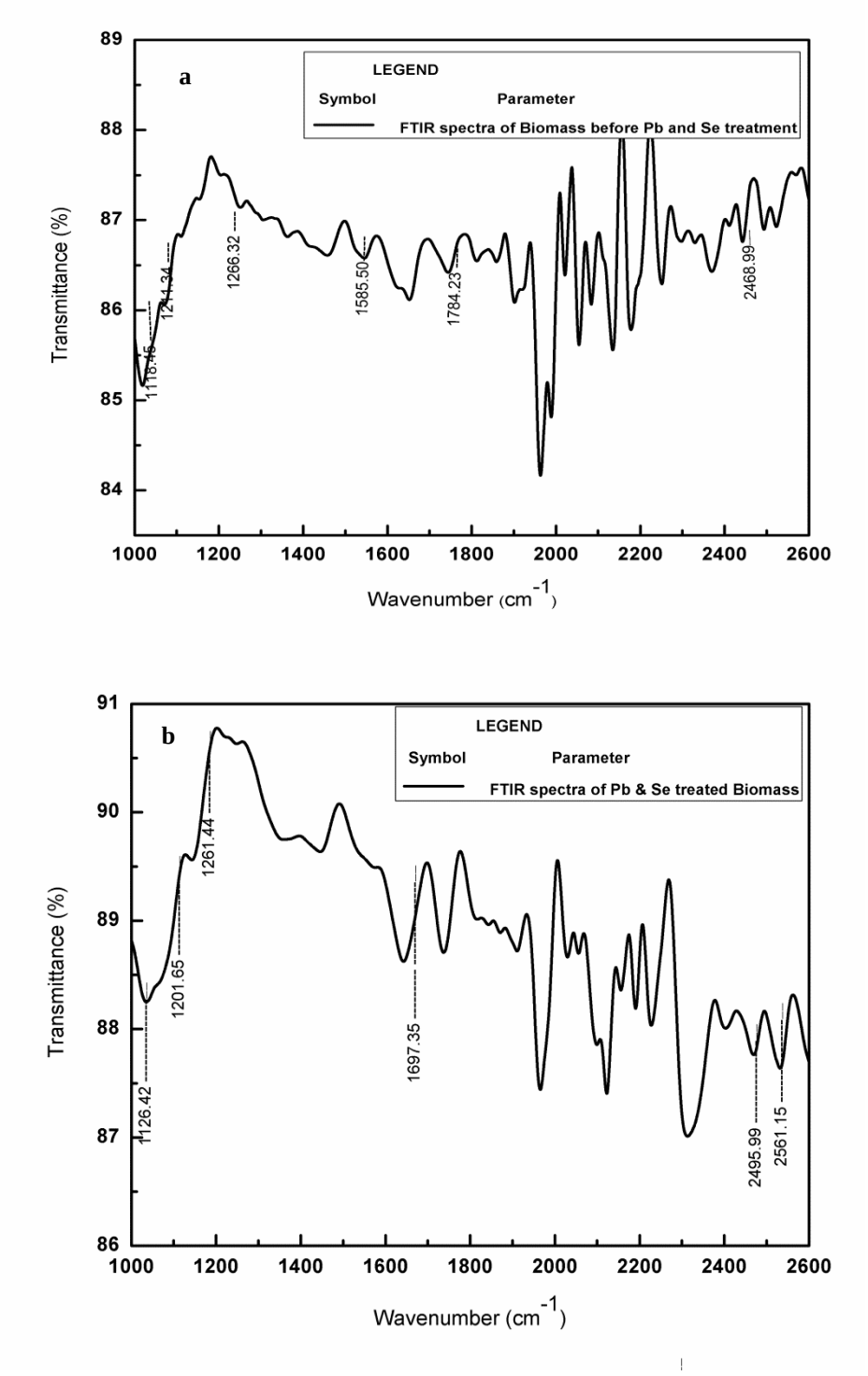

Fig. 4.30 FTIR spectra of the fungal biomass (a) before biosynthesis reaction (control) (b) after reaction with Pb-Se salts

4.13.3 Liquid Chromatography-Mass Spectrometry Analysis

The LC-MS chromatograms for the supernatant after the completion of the biosynthesis reaction are shown in Fig.4.31a and b. The supernatant of the reaction sample in HPLC is found to elute at retention times; 6.979, 10.678, 12.350 and 22.503 min (Fig. 5.4.3 a). According to literature retention times between 6-10 min correspond to the presence of cysteine (Cys) and glutamine (Glu) residues which are the subunits of phytochelatins (γ-glutamylcysteine) (Damodaran et al. 2013). Further, the peaks obtained at 12.35 min and 22.50 min can be attributed to the presence of Phytochelatins (PC_2 and PC_3 respectively). The m/z peaks of the sample (Fig. 5.4.3 b) at 308, 541 and 680 can be correlated to the m/z peaks of glutathione (GSH), PC_2, and PC_3 respectively (Robin et al. 2011). Previous studies (Grill et al. 1985, Liedschulte et al. 2010, Gekeler et al. 1988 and Gill and Tuteja 2011), attest the role of phytochelatins of the general formula $(\gamma\text{-Glu-Cys})_n$ as the principal heavy metal detoxifying component in both plant and fungal kingdom. They can be viewed as linear polymers of the γ-glutamylcysteine (γ-Glu-Cys) portion of glutathione that could be enzymatically produced by the stepwise condensation of γ-Glu-Cys moieties. The PC's have been reported to play a key role in maintaining cell homeostasis under heavymetal stress by binding to heavy metals like Cd, Pb, Zn, Cr, and so forth and directing them to vacuoles or periplasmic space for storage (Gill and Tuteja 2011).

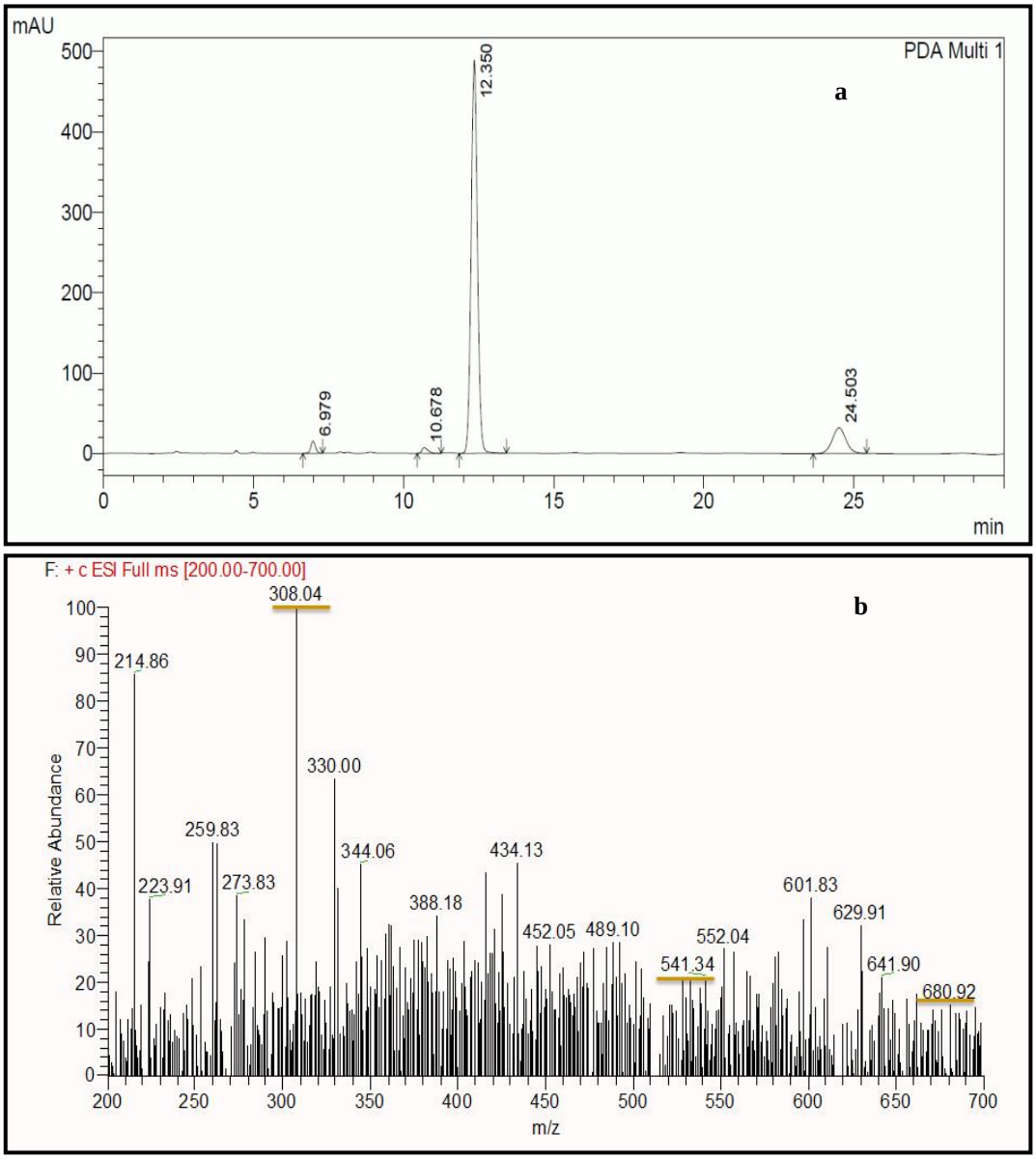

Fig. 4.31 (a) Chromatogram produced by the reaction mixture after PbSe biosynthesis at various (a) retention times (min) and (b) m/z ratios

4.13.4 Quantification of other proteins

Initially, the total protein content of the cell-free supernatant before and after biosynthesis was estimated using Bradford assay. An active protein secretion in the samples during and after the biosynthesis reaction is evident in comparison to the control (Table 4.11). The total protein

content in the supernatant before the reaction is found to be almost negligible when compared to the 10-15 folds of protein content being released during the reaction and subsequent incubation period. It is speculated that the heat shock followed by the quenching of the reaction mixture would have resulted in an outburst of the intracellular metal detoxification proteins into the supernatant. Prolonged incubation at room temperature would have further increased the vacuolar metal-protein complexes in the supernatant regulated by pH.

Several reviews have reported the ubiquitous role of metal-proteins (metallothioneins) in heavy metal detoxification (Mejáre and Bülow 2001; Hall 2002; Thirumoorthy et al. 2007). Metallothionein is a family of cysteine-rich, low molecular weight (MW ranging from 3500 to 14000 Da) protein which have the capacity to bind both physiological (such as zinc, copper, selenium) and xenobiotic (such as cadmium, lead, mercury, silver and arsenic) heavy metals through the thiol group of its cysteine residues, which represents nearly the 30% of its amino acids (Sigel et al. 2009). In the present study, the MT content in the 60 % acetone precipitated supernatant before and after the biosynthesis reaction was analyzed and tabulated (Table 5.4.4). The experimental results indicate higher levels of MT in samples after the biosynthesis reaction in comparison to the control that further affirms the activity of these metal binding proteins for effective detoxification in the fungi that plays a major role in PbSe QD synthesis.

Further, to study whether the heavy metal stress response was associated with antioxidant enzyme defense, the changes in the activities of SOD was determined. Table 4.11 shows the effect of Pb and Se on the antioxidant enzyme levels in the 60 % acetone precipitated supernatant before and after PbSe biosynthesis. These figures indicate an increased enzyme activity during the reaction compared to the SOD activity in the supernatant after the course of the reaction. It is noteworthy that the enzyme activity was absent in the control.

Table 4.11 Protein quantification before and after the biosynthesis reaction

Sl. No.	Sample	Metallothionein content		SOD Activity		
		mg/mL	µM/mL	Total MT(µM)	Enzyme activity (mUnits/mL)	Specific activity (mUnits/mgProtein)
1	Supernatant before biosynthesis	8.169×10^{-3}	3.4	340	N.D	N.D
2	Supernatant after biosynthesis	127.4×10^{-3}	68.8	6880	92.30	724.48

*ND: Non-detectable

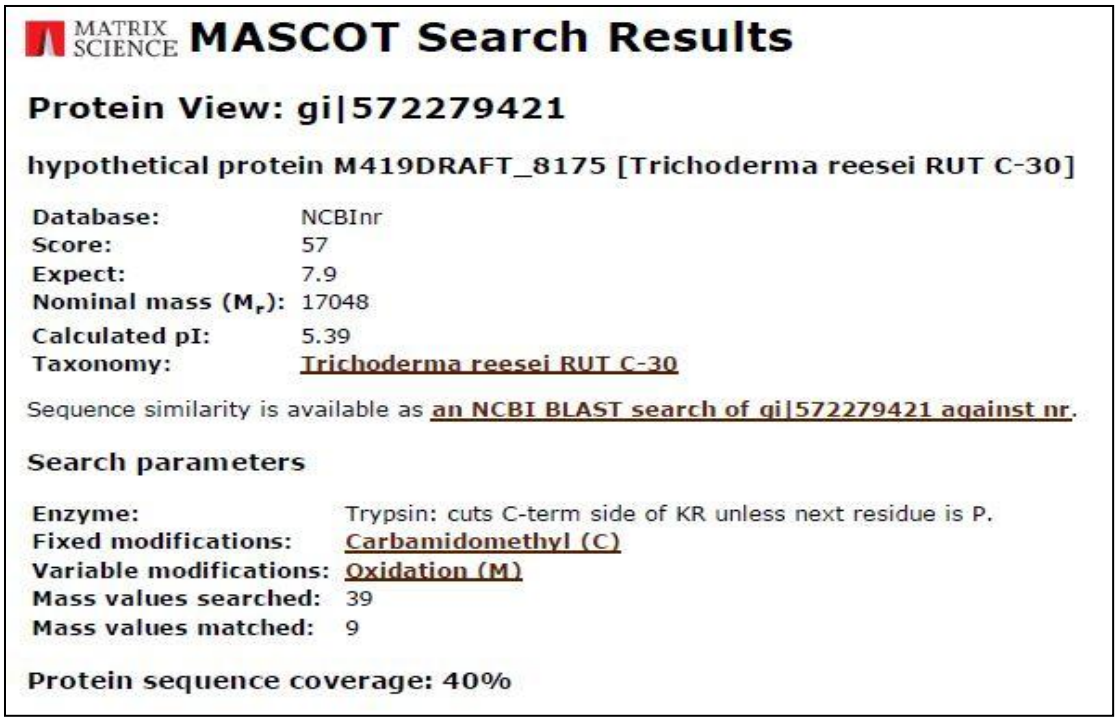

Fig.4.32 The Mascot MALDI-ToF results

MALDI-ToF mass spectrometry was used to confirm the enzyme activity in the acetone precipitated supernatant after PbSe biosynthesis reaction (Fig. 4.32). The purified enzyme exhibit a predicted molecular mass of 17.048 kDa for *Aspergillus terreus* with a predicted pI of 5.39;

both these values are comparable to those estimated for SOD by Holdom et al. (1996) and suggests that oxidative stress play a major role in *Aspergillus terreus* for the synthesis of PbSe QDs. Similar findings have been observed in *Candida intermedia* and *A. nidulans* under heavy metal stressed conditions (Fujs et al. 2005, Guelfi et al. 2003).

4.13.5 Mechanism for PbSe QD biosynthesis by *Aspergillus terreus*

Mechanisms of metal detoxification by biomolecules proceeds as cascade of events, such as induction of proteins such as metallothionein, heat-shock protein, phytochelatins, and ferritin, transferring; or by triggering antioxidant enzymes such as superoxide dismutase, catalase, glutathione, and peroxidase; or through high turnover of organic acids such as malate, citrate, oxalate, succinate, aconitate, α- ketoglutarate, etc. Primarily, the prominent metal complexation processes are the synthesis of phytochelatins and of other metal-chelating peptides (Carpenè et al. 2007). Based on the above mentioned experimental data, the mechanism for the biosynthesis of PbSe QDs by marine *Aspergillus terreus* is summarized as given in Fig.4.33.

Initially, the introduction of metal/metalloid precursors activate the cell surface functional groups such as oxalic acid and thiols compounds that reversibly bind the metals on the cell surface as a first line of cellular defense. Oxalate secretion is well-documented in other fungi, and this process has been reported to be stimulated under metal stress (Jarosz-Wilkolazka and Gadd 2003). The bulk formation of water-insoluble metal-oxalate crystals is undoubtedly an efficient way to prevent toxic metal ions entering fungal cells (Jarosz-Wilkolazka and Gadd 2003). Also, metal chelation by small molecular mass metabolites, peptides and proteins is also documented as a crucially important element of almost all metal/metalloid detoxification processes (Wysocki and Tamás 2010).

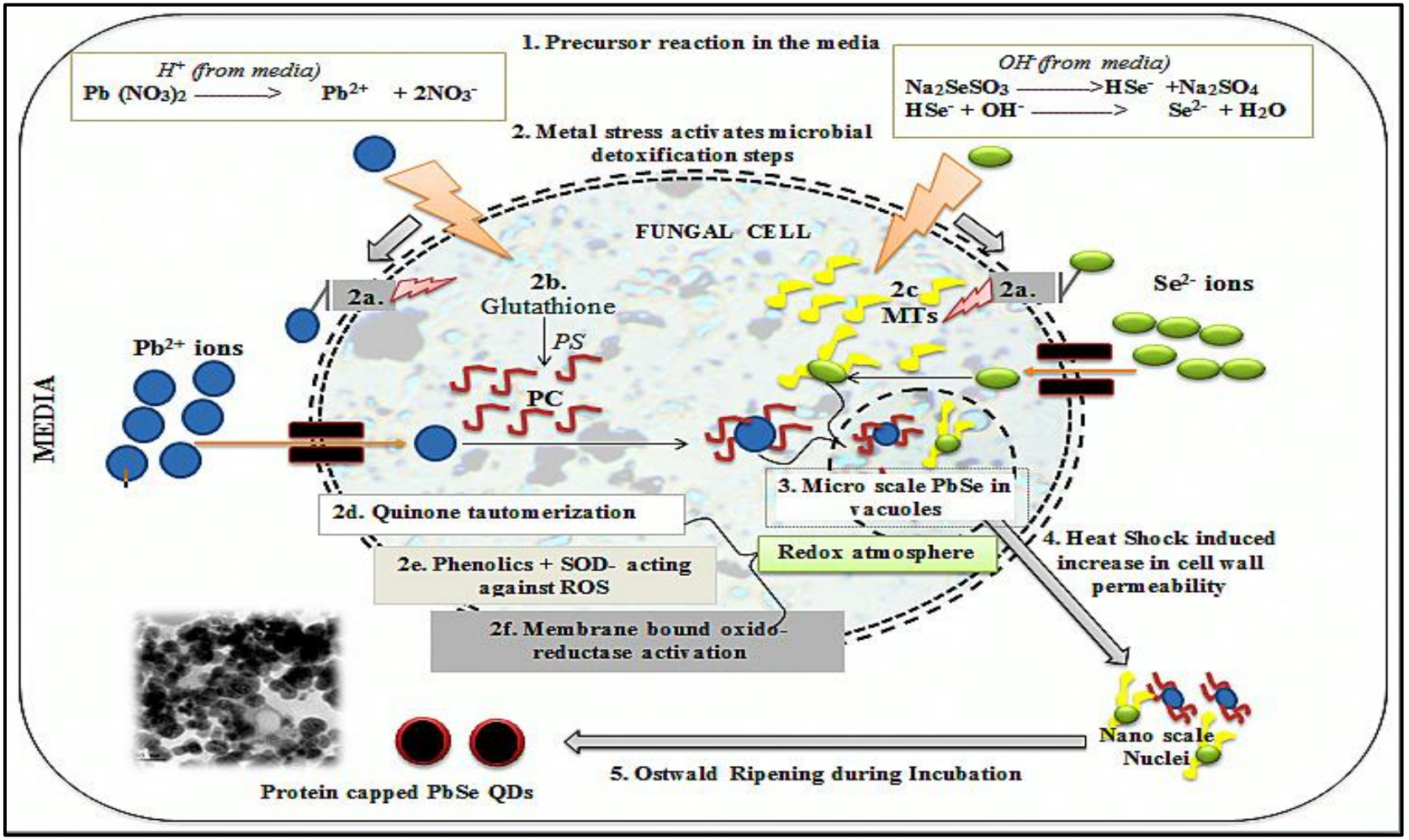

Fig. 4.33 Schematic representation of the proposed mechanism for the biosynthesis of PbSe QDs by *Aspergillus terreus*

In Fig.4.33: (1) Precursors undergo initial redox reactions in the media generating metal/metalloid ions. (2) The metal stress activates the fungal detoxification mechanisms: (a) Surface functional groups; oxalic acids, thiols etc. get activated thus reversibly binding the metal ions (b) Metal stress activate Phytochelatin synthase (PS) to convert glutathione to Phytochelatins (PC) which bind the metal ions and transport them via the ATP binding cassette; (c) Similarly, metallothioneins bind the metal/metalloid ions; (d) Quinone tautomerization (e) Super Oxide Dismutase (SOD) activity and (f) other oxido-reductases create a redox atmosphere to form (3) microscale PbSe and to further initiate transformation to nano scale PbSe in the vacuoles; (4) Heat shock increases the cell wall permeability to drain out the contents into the media where (5) Ostwald ripening of the nuclei take place to result in Protein capped QD formation.

The presence of these metal ions in the biological system activates phytochelatin synthase enzyme which utilizes glutathione from the cells to assemble phytochelatins. The metal/metalloid ions tend to bind to the thiol groups leading to the formation of low molecular weight phytochelatin-metal complexes. These complexes are more likely to be transported by ATP-binding cassette membrane transport proteins into a vacuole (Slocik et al. 2004). Subsequently, the selenide ions, in the reaction mixture (produced due to the reducing atmosphere in the growth media) (Prasad and Jha 2010b), also enter the fungal cytosol. Once within the cytosol, the selenide ions complexes with the thiol groups of the metallothioneins. Our observations are in concordance with that of Pal and Das (2005), who report that upon exposure to metal ions, fungi synthesize MT and phytochelatins (PC), and cellular resistance to heavy metal cytotoxicity due to the binding of metal ions either to MT or PC.

The metal toxicity is also believed to have induced the ROS, thus activating the enzymes to detoxify ROS, namely, SODs. These enzymes utilize the phenolics as preferential electron donors and initiate a series of redox reactions within the fungus. Along with this, a number of simple hydroxy/methoxy derivatives of benzoquinones and toluquinones are elaborated by lower fungi (especially *Penicillium* and *Aspergillus* species) (Goodwin 1965) that facilitate redox reactions due to its tautomerization (Prasad and Jha 2010b). The induced heat shock is anticipated to increase the permeability of the fungal cells, to transport the metal-peptide complexes to the extracellular environment, wherein the redox atmosphere and involvement of glutathiones/ metallothioneins assist the process of nano-fabrication (Jha and Prasad 2010) the process of nano-transformation followed by the Oswald ripening, leading to the fabrication of PbSe QDs (Bao et al. 2010a).

5. SUMMARY AND CONCLUSION

Lead selenide (PbSe) QPs have been recognized as significant sensing and imaging platforms due to their remarkable opto-electronic properties. However, chemical syntheses of these technologically relevant entities are not cost effective and eco-friendly. The present study is an endeavor towards the greener and economical synthesis of PbSe QPs in marine fungus. A heavy metal/metalloid (Pb and Se) tolerant *Aspergillus terreus*, isolated from marine sources near the industrial belt in Mangalore, Karnataka, India, was used for biosynthesis of PbSe QPs. Thereafter, the morphological, structural, optical and electrochemical features of the biosynthesized PbSe QPs were studied using advanced characterization tools. Further, the statistical optimization of the fluorescence in the biosynthesized PbSe and its application in heavy metal sensing in aqueous solutions were carried out. The antibacterial properties of the biosynthesized PbSe were also described and finally the fungal protein cadre involved in the biosynthesis of PbSe QDs was explored. The important conclusions drawn from the current study are summarized below:

- Sea water in proximity to industrial areas in Mangalore, India,found to havehigh concentrations of Pb and Sewas used for the isolation of 4 fungi namely; *Aspergillus*sp (Black), *Aspergillus*sp (Brown), *Fusarium* sp., *Penicillium* sp. Initial tolerance studies of these fungi demonstrated remarkable Pb and Se tolerance by*Aspergillus* sp. (Brown) compared to the rest.

- Molecular identification using ITS sequencing confirmed that the metal/metalloid tolerant fungus exhibited 99% similarity with *Aspergillus terreus*(NCBI Accession number AB647191.1).

- Statistical models (Plackett-Burman and Box-Benhken Design) revealed that, 6.23 g/L of peptone, 1.19 g/L of KH_2PO_4 and 0.09 g/L of $FeSO_4.7H_2O$ along with other medium components at a pH 7.5, 32^oC and 115 rpm resulted in an optimized growth (10.372 g/L) of *Aspergillus terreus* biomass after an incubation period of 5-6 days.

- Morphological characterization of the biosynthesized PbSe QPs using TEM and SEM revealed rod like structures with an average diameter of 57.94 nm and aspect ratios ranging from 5-10. The clausthalite type rock salt structure of the PbSe quantum rods were affirmed using XRD data.

- Optical characterization using UV- Vis indicated absorbance typical to PbSe QPs in the quantum regime at 375 nm and 872 nm and the characteristic peaks below 300 nm indicate biocompatible protein coatings on the QPs. FTIR analysis affirmed the presence of protein coatings on the QPs that enhance the biocompatibility.

- The Tauc plot revealed the existence of wider energy gap (1.25eV) in the nano fabrication in comparison to the bulk PbSe (0.28eV). The mass approximation method highlighted the presence of quantum confinement effects in the biosynthesized PbSe nano rods.

- The variation of optical constants like absorption coefficient, extinction coefficient, refractive index and reflectance were comparable to that of the chemically synthesized counterparts. The absorbance of the PbSe QPs was observed to remain stable at 375 nm for a period of 8 days after which it increased to higher wavelength ranges.

- The high dielectric constant and remarkable fluorescence of the biogenic PbSe quantum rods pronounce their application in opto-electronic devices in the near infra-red and ultraviolet spectral regime. The colloidal solution of PbSe QPs exhibited a fluorescence yield of 49.7% .

- The linear voltammograms of the biosynthesized PbSe QPs were characterized with five reaction peaks corresponding to the oxidation of PbSe, Se and $Pb(OH)_2$ and the reduction of PbO_2 and $Pb(OH)_2$. These observations were confirmed by successive cyclic voltammetric analyses.

- Further, in an effort to enhance the fluorescence of the biosynthesized PbSe QPs, statistical methods (BBD) were utilized. A size tunable blue shift in the PbSe QD fluorescence was observed for biosynthesis reaction at Pb:Se precursor molar concentration of 1:5 at an operational pH= 9.97, reaction time = 28 min and reaction temperature= 58 ^{o}C followed by quenching at 4^{o}C and left undisturbed for a 12 ± 2 hr under ambient condition.

- It was observed that under the optimized conditions of biosynthesis, PbSe QDs with size ranges from 10-25 nm with clausthalite type face centered cubic lattice structure were synthesized by *Aspergillus terreus*.

- The fluorescence intensity of the biosynthesized PbSe QDs was found to vary inversely with the Cd^{2+} ions present in the colloidal solution over a range of 0-100 μM with detection limits around 2.31 μM. Further, the Stern-Volmer plot of the emission intensities of PbSe QDs at different Cd^{2+} concentrations revealed that the metal ions bind on the surface of QDs inducing recombination centers for electrons and holes, resulting in a quenching of QD's fluorescence.

- The biosynthesized PbSe QPs exhibited an anti-bacterial activity comparable to that of standard antibiotics against gram positive and gram negative bacterial pathogens.

- Studies on the mechanistic aspects PbSe QD biosynthesis using marine *Aspergillus terreus* revealed that the presence of heavy metals/metalloids induces specific metal detoxification pathways in the fungus consisting of metallothioneins, super oxide dismutases and phytochelatins etc. Based on these findings a possible mechanism for the biosynthesis of PbSe QDs by marine *Aspergillus terreus* has also been elucidated.

Based on the above summarized results, it can be concluded that biosynthesis of PbSe QPs in marine *Aspergillus terreus* is an eco-friendly and cost effective alternative to the currently

employed chemical synthesis procedures. The structural and opto-electronic properties of the biosynthesized PbSe are in par with the chemically synthesized counterparts and capacitate their application in efficient cadmium ion sensing in aqueous solutions. Further, the ingenious heavy metal detoxification mechanism in the marine fungus directs their prospective utilization for the large scale biosynthesis of PbSe QPs.

5.2. Scope for Future Work

- Exploration and utilization of the heavy metal detoxification pathways in other heavy metal tolerant fungi and bacteria for the biosynthesis of QPs.
- Studies on the extracellular biosynthesis of QPs and the reaction kinetics that govern nucleation and growth of QPs in a typical biosynthesis procedure.
- Reactor studies for the large scale biosynthesis of PbSe QPs using marine *Aspergillus terreus*.
- The remarkable fluorescence in the PbSe QPs can be utilized for bio-imaging and drug delivery. The electrochemical properties can be further explored so as to apply these entities in solar energy harvesting.
- Development of nano-engineered membrane systems impregnated with PbSe QPs that can act as fluorescence based indicators of bio-burden/heavy metal threshold.
- Studies on the utilization of metal detoxification proteins as bio-indicators for aquatic heavy metal pollution.
- Improving the efficiency of QP biosynthesis by enhancing the fungal detoxification mechanisms via genetic engineering.

Ahmad, A., Mukherjee, P., Mandal, D., Senapati, S., Khan, M.I., Kumar, R., et al. (2002). "Enzyme Mediated Extracellular Synthesis of CdS Nanoparticles by the Fungus, *Fusarium oxysporum*." *J. Am. Chem. Soc.* 124, 12108–12109.

Alivisatos, A.P. (1996). "Semiconductor Clusters, Nanocrystals, and Quantum Dots." *Science* 271, 933–937.

Allan, G., and Delerue, C. (2004). "Confinement Effects in PbSe Quantum Wells and Nanocrystals." *Phys. Rev. B* 70, 245321.

Altavilla, C., and Ciliberto, E. (2010). Inorganic Nanoparticles: Synthesis, Applications, and Perspectives (CRC Press).

Alvi, M.A., and Khan, Z.H. (2013). "Synthesis and Characterization of Nanoparticle Thin Films of a-(PbSe)100-xCdx Lead Chalcogenides." *Nanoscale Res. Lett.* 8, 148.

Andreev, A.D., and Lipovskii, A.A. (1999). "Anisotropy-Induced Optical Transitions in PbSe and PbS Spherical Quantum Dots." *Phys. Rev. B* 59, 15402–15404.

Baek, I.-C., Seok, S.-I., and Chung, Y.-C. (2008). "The Synthesis of a High Yield PbSe Quantum Dots by Hot Solution Method." *Bull. Korean Chem. Soc.* 29, 1729–1731.

Bai, H.J., Zhang, Z.M., Guo, Y., and Yang, G.E. (2009). "Biosynthesis of Cadmium Sulfide Nanoparticles by Photosynthetic Bacteria *Rhodopseudomonas palustris*." *Colloids Surf. B Biointerfaces* 70, 142–146.

Bao, H., Hao, N., Yang, Y., and Zhao, D. (2010a). "Biosynthesis of Biocompatible Cadmium Telluride Quantum Dots Using Yeast Cells." *Nano Res.* 3, 481–489.

Bao, H., Lu, Z., Cui, X., Qiao, Y., Guo, J., Anderson, J.M., et al. (2010b). "Extracellular Microbial Synthesis of Biocompatible CdTe Quantum Dots." *Acta Biomater.* 6, 3534–3541.

Basabe-Desmonts, L., Reinhoudt, D.N., and Crego-Calama, M. (2007). "Design of Fluorescent Materials for Chemical Sensing." *Chem. Soc. Rev.* 36, 993–1017.

Bauer, A.W., Kirby, W.M., Sherris, J.C., and Turck, M. (1966). "Antibiotic Susceptibility Testing by a Standardized Single Disk Method." *Am. J. Clin. Pathol.* 45, 493–496.

Beauchamp, C., and Fridovich, I. (1971). "Superoxide Dismutase: Improved Assays and an Assay Applicable to Acrylamide Gels." *Anal. Biochem.* 44, 276–287.

Bick, J.A., Dennis, J.J., Zylstra, G.J., Nowack, J., and Leustek, T. (2000). "Identification of a New Class of 5′-Adenylylsulfate (APS) Reductases from Sulfate-Assimilating Bacteria." *J. Bacteriol.* 182, 135–142.

Bo, C., and Ping, Z. (2005). "A New Determining Method of copper(II) Ions at Ng Ml-1 Levels Based on Quenching of the Water-Soluble Nanocrystals Fluorescence." *Anal. Bioanal. Chem.* 381, 986–992.

Bouroushian, M. (2010). Electrochemistry of the Chalcogens. In Electrochemistry of Metal Chalcogenides, (Berlin, Heidelberg: Springer Berlin Heidelberg), pp 57–75.

Bruchez, M., Moronne, M., Gin, P., Weiss, S., and Alivisatos, A.P. (1998). "Semiconductor Nanocrystals as Fluorescent Biological Labels." *Science* 281, 2013–2016.

Cai, W., Hsu, A.R., Li, Z.-B., and Chen, X. (2007). "Are Quantum Dots Ready for in Vivo Imaging in Human Subjects?." *Nanoscale Res. Lett.* 2, 265.

Cánovas, D., Vooijs, R., Schat, H., and Lorenzo, V. De (2004). "The Role of Thiol Species in the Hypertolerance of Aspergillus Sp. P37 to Arsenic." *J. Biol. Chem.* 279, 51234–51240.

Carpenè, E., Andreani, G., and Isani, G. (2007). "Metallothionein Functions and Structural Characteristics." *J. Trace Elem. Med. Biol.* 21, 35–39.

Chan, W.C.W., Maxwell, D.J., Gao, X., Bailey, R.E., Han, M., and Nie, S. (2002). "Luminescent Quantum Dots for Multiplexed Biological Detection and Imaging." *Curr. Opin. Biotechnol.* 13, 40–46.

Chen, Y., and Rosenzweig, Z. (2002). "Luminescent CdS Quantum Dots as Selective Ion Probes." *Anal. Chem.* 74, 5132–5138.

Clapp, A.R., Medintz, I.L., and Mattoussi, H. (2006). "Förster Resonance Energy Transfer Investigations Using Quantum-Dot Fluorophores." *Chemphyschem Eur. J. Chem. Phys. Phys. Chem.* 7, 47–57.

Collins, G.P. (2005). "Cheaper Dots." *Sci. Am.* 293, 22–25.

Cui, R., Liu, H.-H., Xie, H.-Y., Zhang, Z.-L., Yang, Y.-R., Pang, D.-W., et al. (2009). "Living Yeast Cells as a Controllable Biosynthesizer for Fluorescent Quantum Dots." *Adv. Funct. Mater.* 19, 2359–2364.

Dameron, C.T., Reese, R.N., Mehra, R.K., Kortan, A.R., Carroll, P.J., Steigerwald, M.L., et al. (1989a). "Biosynthesis of Cadmium Sulphide Quantum Semiconductor Crystallites." *Nature* 338, 596–597.

Dameron, C.T., Smith, B.R., and Winge, D.R. (1989b). "Glutathione-Coated Cadmium-Sulfide Crystallites in Candida Glabrata." *J. Biol. Chem.* 264, 17355–17360.

Dameron, C.T., and Winge, D.R. (1990). "Characterization of Peptide-Coated Cadmium-Sulfide Crystallites." *Inorg. Chem.* 29, 1343–1348.

Damodaran, D., Balakrishnan, R.M., and Shetty, V.K. (2013). "The Uptake Mechanism of Cd (II), Cr (VI), Cu (II), Pb (II), and Zn (II) by Mycelia and Fruiting Bodies of *Galerina vittiformis*." *Biomed. Res. Int.*, Article ID 149120. doi:10.1155/2013/149120.

Dugan, F.M. (2006). The Identification of Fungi: An Illustrated Introduction with Keys, Glossary, and Guide to Literature (American Phytopathological Society), USA.

Edrissi, M., and Soleymani, M. (2011). "Synthesis of Nano-γ-Ferric Oxide by Thermolysis of the 2-Mercapto-5-Methylpyridine-N-Oxide-Iron(III) Complex via Factorial Design." *Chem. Eng. Technol.* 34, 991–996.

Ekimov, A.I., Hache, F., Schanne-Klein, M.C., Ricard, D., Flytzanis, C., Kudryavtsev, I.A., et al. (1993). "Absorption and Intensity-Dependent Photoluminescence Measurements on CdSe Quantum Dots: Assignment of the First Electronic Transitions." *J. Opt. Soc. Am. B* 10, 100.

Emerich, D.F., and Thanos, C.G. (2003). "Nanotechnology and Medicine." *Expert Opin. Biol. Ther.* 3, 655–663.

Fan, L.J., Zhang, Y., Murphy, C.B., Angell, S.E., Parker, M.F.L., Flynn, B.R., et al. (2009). "Fluorescent Conjugated Polymer Molecular Wire Chemosensors for Transition Metal Ion Recognition and Signaling." *Coord. Chem. Rev.* 253, 410–422.

Fernández-Argüelles, M.T., Wei, J.J., Costa-Fernández, J.M., Pereiro, R., and Sanz-Medel, A. (2005). "Surface-Modified CdSe Quantum Dots for the Sensitive and Selective Determination of Cu(II) in Aqueous Solutions by Luminescent Measurements." *Anal. Chim. Acta* 549, 20–25.

Frasco, M.F., and Chaniotakis, N. (2009). "Semiconductor Quantum Dots in Chemical Sensors and Biosensors." *Sensors* 9, 7266–7286.

Fuente, J.M. de la, and Grazu, V. (2012). Nanobiotechnology: Inorganic Nanoparticles Vs Organic Nanoparticles (Elsevier).

Fujs, S., Gazdag, Z., Poljsak, B., Stibilj, V., Milacic, R., Pesti, M., et al. (2005). "The Oxidative Stress Response of the Yeast *Candida intermedia* to Copper, Zinc, and Selenium Exposure." *J. Basic Microbiol.* 45, 125–35.

Ganea, G.M., Sabliov, C.M., Ishola, A.O., Fakayode, S.O., and Warner, I.M. (2008). "Experimental Design and Multivariate Analysis for Optimizing poly(D,L-Lactide-Co-

Glycolide) (PLGA) Nanoparticle Synthesis Using Molecular Micelles." *J. Nanosci. Nanotechnol.* 8, 280–92.

Gavrilescu, M. (2004). "Removal of Heavy Metals from the Environment by Biosorption." *Eng. Life Sci.* 4, 219–232.

Gekeler, W., Grill, E., Winnacker, E.-L., and Zenk, M.H. (1988). "Algae Sequester Heavy Metals via Synthesis of Phytochelatin Complexes." *Arch. Microbiol.* 150, 197–202.

Gericke, M., and Pinches, A. (2006). "Biological Synthesis of Metal Nanoparticles." *Hydrometallurgy* 83, 132–140.

Ghanem, N.B., Yusef, H.H., and Mahrouse, H.K. (2000). "Production of Aspergillus Terreus Xylanase in Solid-State Cultures: Application of the Plackett–Burman Experimental Design to Evaluate Nutritional Requirements." *Bioresour. Technol.* 73, 113–121.

Ghosh, A., Ghosh Dastidar, M., and Sreekrishnan, T.R. (2015). "Recent Advances in Bioremediation of Heavy Metals and Metal Complex Dyes: Review." *J. Environ. Eng.* C4015003.

Gill, S.S., and Tuteja, N. (2011). "Cadmium Stress Tolerance in Crop Plants: Probing the Role of Sulfur." *Plant Signal. Behav.* 6, 215–22.

Goodwin, T.W. (1965). "Chemistry and Biochemistry of Plant Pigments.".

Grabolle, M., Ziegler, J., Merkulov, A., Nann, T., and Resch-Genger, U. (2008). "Stability and Fluorescence Quantum Yield of CdSe–ZnS Quantum Dots—Influence of the Thickness of the ZnS Shell." *Ann. N. Y. Acad. Sci.* 1130, 235–241.

Grill, E., Winnacker, E.L., and Zenk, M.H. (1985). "Phytochelatins: The Principal Heavy-Metal Complexing Peptides of Higher Plants." *Science* 230, 674–6.

Guelfi, A., Azevedo, R.A., Lea, P.J., and Molina, S.M.G. (2003). "Growth Inhibition of the Filamentous Fungus *Aspergillus nidulans* by Cadmium: An Antioxidant Enzyme Approach." *J. Gen. Appl. Microbiol.* 49, 63–73.

Gu, P., Zhang, Y., Feng, Y., Zhang, T., Chu, H., Cui, T., et al. (2013). "Real-Time and on-Chip Surface Temperature Sensing of GaN LED Chips Using PbSe Quantum Dots." *Nanoscale* 5, 10481–10486.

Gurunathan, S., Kalishwaralal, K., Vaidyanathan, R., Venkataraman, D., Pandian, S.R.K., Muniyandi, J., et al. (2009). "Biosynthesis, Purification and Characterization of Silver Nanoparticles Using *Escherichia coli*." *Colloids Surf. B Biointerfaces* 74, 328–335.

Hall, J.L. (2002). "Cellular Mechanisms for Heavy Metal Detoxification and Tolerance." *J. Exp. Bot.* 53, 1–11.

Hamizi, N.A., and Johan, M.R. (2012). "Optical Properties of CdSe Quantum Dots via Non-TOP Based Route." *Int. J. Electrochem. Sci.* 7, 8458–8467.

He, J., Mao, S., Zhang, S., Niu, H., Jin, B., and Tian, Y. (2009). "Preparation and Electrochemical Property of PbTe Nanorods." *Mater. Sci. Semicond. Process.* 12, 217–223.

Herz, E. (2001). Colloidal semiconductor nanocrystals: A study of the syntheses of and capping structures for CdSe. Virginia Tech., USA.

Herz, L.M., Daniel, C., Silva, C., Hoeben, F.J.M., Schenning, A.P.H.J., Meijer, E.W., et al. (2003). "Fast Exciton Diffusion in Chiral Stacks of Conjugated \textit{p} -Phenylene Vinylene Oligomers." *Phys. Rev. B* 68, 045203.

Hiraki, M. (1994). "Populations of Cd-Tolerant Microorganisms in Soils Polluted with Heavy Metals." *Soil Sci. Plant Nutr.* 40, 515–524.

Holdom, M.D., Hay, R.J., and Hamilton, A.J. (1996). "The Cu,Zn Superoxide Dismutases of *Aspergillus flavus, Aspergillus niger, Aspergillus nidulans, and Aspergillus terreus*: Purification and Biochemical Comparison with the *Aspergillus fumigatus* Cu,Zn Superoxide Dismutase." *Infect. Immun.* 64, 3326–3332.

Holmes, J.D., Richardson, D.J., Saed, S., Evans-Gowing, R., Russell, D.A., and Sodeau, J.R. (1997). "Cadmium-Specific Formation of Metal Sulfide 'Q-Particles' by *Klebsiella pneumoniae*." *Microbiology* 143, 2521–2530.

Hormozi-Nezhad, M.R., Jalali-Heravi, M., Robatjazi, H., and Ebrahimi-Najafabadi, H. (2012). "Controlling Aspect Ratio of Colloidal Silver Nanorods Using Response Surface Methodology." *Colloids Surf. Physicochem. Eng. Asp.* 393, 46–52.

Huang, C., Liu, S., Chen, T., and Li, Y. (2008a). "A New Approach for Quantitative Determination of Glucose by Using CdSe/ZnS Quantum Dots." *Sens. Actuators B Chem.* 130, 338–342.

Huang, C., Liu, S., Chen, T., and Li, Y. (2008b). "A New Approach for Quantitative Determination of Glucose by Using CdSe/ZnS Quantum Dots." *Sens. Actuators B Chem.* 130, 338–342.

Iram, S., Parveen, K., Usman, J., Nasir, K., Akhtar, N., Arouj, S., et al. (2012). "Heavy Metal Tolerance of Filamentous Fungal Strains Isolated from Soil Irrigated with Industrial Wastewater." *Biologija* 58,.

Ivanova, J., Chernev, G., and Samuneva, B. (2008). "Effect of Ag, Cu AND Zn containing hybrid nanomatrixes on the green algae *Chlorella keissleri*." *Gen Appl Plant Physiol.* 3-4, 339–345.

Jain, N., Bhargava, A., Sabat, D., and Panwar, J. (2014). "Unveiling the Potential of Metal-Tolerant Fungi for Efficient Enzyme Production." *Process Biochem.* 49, 1858–1866.

Jamieson, T., Bakhshi, R., Petrova, D., Pocock, R., Imani, M., and Seifalian, A.M. (2007a). "Biological Applications of Quantum Dots." *Biomaterials* 28, 4717–4732.

Jamieson, T., Bakhshi, R., Petrova, D., Pocock, R., Imani, M., and Seifalian, A.M. (2007b). "Biological Applications of Quantum Dots." *Biomaterials* 28, 4717–4732.

Jansen, E., Michels, M., Til, M. van, and Doelman, P. (1994). "Effects of Heavy Metals in Soil on Microbial Diversity and Activity as Shown by the Sensitivity-Resistance Index, an Ecologically Relevant Parameter." *Biol. Fertil. Soils* 17, 177–184.

Jarosz-Wilkolazka, A., and Gadd, G.M. (2003). "Oxalate Production by Wood-Rotting Fungi Growing in Toxic Metal-Amended Medium." *Chemosphere* 52, 541–7.

Jha, A.K., and Prasad, K. (2010). "Leaf." *Int. J. Green Nanotechnol. Phys. Chem.* 1, P110–P117.

Jiang, X. (2012). In-Gap State of Lead Chalcogenides Quantum Dots. In Fingerprints in the Optical and Transport Properties of Quantum Dots, A. Al-Ahmadi, ed. (InTech),.

Jin, R. (2012). "The Impacts of Nanotechnology on Catalysis by Precious Metal Nanoparticles." *Nanotechnol. Rev.* 1, 31–56.

Jin, W.J., Fernández-Argüelles, M.T., Costa-Fernández, J.M., Pereiro, R., and Sanz-Medel, A. (2005). "Photoactivated Luminescent CdSe Quantum Dots as Sensitive Cyanide Probes in Aqueous Solutions." *Chem. Commun.* 883–885.

Joshi, P.K., Swarup, A., Maheshwari, S., Kumar, R., and Singh, N. (2011). "Bioremediation of Heavy Metals in Liquid Media through Fungi Isolated from Contaminated Sources." *Indian J. Microbiol.* 51, 482–487.

Jr, C.P.P., and Owens, F.J. (2003). Introduction to Nanotechnology, John Wiley & Sons, Hoboken, New Jersey.

Kairdolf, B.A., Smith, A.M., Stokes, T.H., Wang, M.D., Young, A.N., and Nie, S. (2013). "Semiconductor Quantum Dots for Bioimaging and Biodiagnostic Applications." *Annu. Rev. Anal. Chem. Palo Alto Calif* 6, 143–162.

Kamat, P.V. (2008). "Quantum Dot Solar Cells. Semiconductor Nanocrystals as Light Harvesters†." *J. Phys. Chem. C* 112, 18737–18753.

Kang, I., and Wise, F.W. (1997). "Electronic Structure and Optical Properties of PbS and PbSe Quantum Dots." *J. Opt. Soc. Am. B* 14, 1632.

Kang, S.H., Bozhilov, K.N., Myung, N.V., Mulchandani, A., and Chen, W. (2008). "Microbial Synthesis of CdS Nanocrystals in Genetically Engineered *E. coli*." *Angew. Chem. Int. Ed.* 47, 5186–5189.

Kassim, A., Min, H.S., Monohorn, S., and Nagalingam, S. (2011). "Synthesis of PbSe thin film by chemical bath deposition and its characterization using XRD, SEM and UV-Vis spectrophotometer." *Makara Sci. Ser.* 14, 117-120.

Khan, S.A., Khan, Z.H., El-Sebaii, A.A., Al-Marzouki, F.M., and Al-Ghamdi, A.A. (2010). "Structural, Optical and Electrical Properties of Cadmium-Doped Lead Chalcogenide (PbSe) Thin Films." *Phys. B Condens. Matter* 405, 3384–3390.

Kim, K.-E., Kim, T.G., and Sung, Y.-M. (2012). "Fluorescent Cholesterol Sensing Using Enzyme-Modified CdSe/ZnS Quantum Dots." *J. Nanoparticle Res.* 14, 1179-1180.

Koch, C., Ovid'ko, I., Seal, S., and Veprek, S. (2007). Structural Nanocrystalline Materials: Fundamentals and Applications, Cambridge University Press, England.

Koneswaran, M., and Narayanaswamy, R. (2009). "L-Cysteine-Capped ZnS Quantum Dots Based Fluorescence Sensor for Cu^{2+} Ion." *Sens. Actuators B Chem.* 139, 104–109.

Kong, J., and Yu, S. (2007). "Fourier Transform Infrared Spectroscopic Analysis of Protein Secondary Structures." *Acta Biochim. Biophys. Sin.* 39, 549–59.

Konstantatos, G., and Sargent, E.H. (2013). Colloidal Quantum Dot Optoelectronics and Photovoltaics, Cambridge University Press, England.

Kowshik, M., Deshmukh, N., Vogel, W., Urban, J., Kulkarni, S.K., and Paknikar, K.M. (2002a). "Microbial Synthesis of Semiconductor CdS Nanoparticles, Their Characterization, and Their Use in the Fabrication of an Ideal Diode." *Biotechnol. Bioeng.* 78, 583–588.

Kowshik, M., Vogel, W., Urban, J., Kulkarni, S.K., and Paknikar, K.M. (2002b). "Microbial Synthesis of Semiconductor PbS Nanocrystallites." *Adv. Mater.* 14, 815.

Kruger, N.J. (1994). "The Bradford Method for Protein Quantitation." *Methods Mol. Biol. Clifton NJ* 32, 9–15.

Kumar, S.A., Ansary, A.A., Ahmad, A., and Khan, M.I. (2007). "Extracellular Biosynthesis of CdSe Quantum Dots by the Fungus, *Fusarium oxysporum*." *J. Biomed. Nanotechnol.* 3, 190–194.

Kumar, V., and Yadav, S.K. (2009). "Plant-Mediated Synthesis of Silver and Gold Nanoparticles and Their Applications." *J. Chem. Technol. Biotechnol.* 84, 151–157.

Laverdant, J., Marcillac, W.D. de, Barthou, C., Chinh, V.D., Schwob, C., Coolen, L., et al. (2011). "Experimental Determination of the Fluorescence Quantum Yield of Semiconductor Nanocrystals." *Materials* 4, 1182–1193.

Leatherdale, C.A., Kagan, C.R., Morgan, N.Y., Empedocles, S.A., Kastner, M.A., and Bawendi, M.G. (2000). "Photoconductivity in CdSe Quantum Dot Solids." *Phys. Rev. B* 62, 2669–2680.

Li, C., Bai, T., Li, F., Wang, L., Wu, X., Yuan, L., et al. (2012). "Growth Orientation, Shape Evolution of Monodisperse PbSe Nanocrystals and Their Use in Optoelectronic Devices." *CrystEngComm* 15, 597–603.

Liedschulte, V., Wachter, A., Zhigang, A., and Rausch, T. (2010). "Exploiting Plants for Glutathione (GSH) Production: Uncoupling GSH Synthesis from Cellular Controls Results in Unprecedented GSH Accumulation." *Plant Biotechnol. J.* 8, 807–20.

Lifshitz, E., Bashouti, M., Kloper, V., Kigel, A., Eisen, M.S., and Berger, S. (2003). "Synthesis and Characterization of PbSe Quantum Wires, Multipods, Quantum Rods, and Cubes." *Nano Lett.* 3, 857–862.

Li, H., Zhang, Y., and Wang, X. (2007a). "L-Carnitine Capped Quantum Dots as Luminescent Probes for Cadmium Ions." *Sens. Actuators B Chem.* 127, 593–597.

Linde, A.R., and Garcia-Vazquez, E. (2006). "A Simple Assay to Quantify Metallothionein Helps to Learn about Bioindicators and Environmental Health." *Biochem. Mol. Biol. Educ. Bimon. Publ. Int. Union Biochem. Mol. Biol.* 34, 360–3.

Ling, P.A. (2005). Trends in Quantum Dots Research, Nova Publishers, New York.

Li, S., Shen, Y., Xie, A., Yu, X., Zhang, X., Yang, L., et al. (2007b). "Rapid, Room-Temperature Synthesis of Amorphous Selenium/protein Composites Using *Capsicum annuum L* Extract." *Nanotechnology* 18, 405101.

Liu, F., Kang, S.H., Lee, Y.-I., Choa, Y., Mulchandani, A., Myung, N.V., et al. (2010). "Enzyme Mediated Synthesis of Phytochelatin-Capped CdS Nanocrystals." *Appl. Phys. Lett.* 97, 123703.

Luo, Q.-Y., Lin, Y., Li, Y., Xiong, L.-H., Cui, R., Xie, Z.-X., et al. (2014). "Nanomechanical Analysis of Yeast Cells in CdSe Quantum Dot Biosynthesis." *Small Weinh. Bergstr. Ger.* 10, 699–704.

Luo Jin, Zhu, Y., Yin, D.,and He, Z.(2014). "A Simple Synthesis of PbSe Nanoparticles via Composite-Molten-Salt Method and Their Electrochemistry Properties." *Rare. Metal. Mat. Eng*. 43, 2100–2103.

Machol, J.L., Wise, F.W., Patel, R., and Tanner, D.B. (1994). "Optical Studies of IV–VI Quantum Dots." *Phys. Stat. Mech. Its Appl.* 207, 427–434.

Maclurcan, D., and Radywyl, N. (2011). Nanotechnology and Global Sustainability, CRC Press, USA.

Malarkodi, C., Rajeshkumar, S., Paulkumar, K., Vanaja, M., Gnanajobitha, G., and Annadurai, G. (2014). "Biosynthesis and Antimicrobial Activity of Semiconductor Nanoparticles against Oral Pathogens." *Bioinorg. Chem. Appl.* 2014, 1–10.

Malik, P., Singh, J., and Kakkar, R. (2014). "A Review on CdSe Quantum Dots in Sensing." 5, 612–628.

Mao, S., Zhao, J., Zhang, S., Niu, H., Jin, B., and Tian, Y. (2009). "Synthesis and Electrochemical Properties of PbSe Nanotubes." *J. Phys. Chem. C* 113, 18091–18096.

Marc Achermann, M.A.P. (2004). "Energy-Transfer Pumping of Semiconductor Nanocrystals Using an Epitaxial Quantum Well." *Nature* 429, 642–646.

Mathan, S., Subramanian, V., and Nagamony, S. (2013). "Optimization and Antimicrobial Metabolite Production from Endophytic Fungi *Aspergillus terreus* KC 582297." *Eur. J. Exp. Biol.* 3, 138–144.

Mathieu, H., Lefebvre, P., and Christol, P. (1992). "Simple Analytical Method for Calculating Exciton Binding Energies in Semiconductor Quantum Wells." *Phys. Rev. B* 46, 4092–4101.

Medintz, I.L., Mattoussi, H., and Clapp, A.R. (2008). "Potential Clinical Applications of Quantum Dots." *Int. J. Nanomedicine* 3, 151–167.

Mejáre, M., and Bülow, L. (2001). "Metal-Binding Proteins and Peptides in Bioremediation and Phytoremediation of Heavy Metals." *Trends Biotechnol.* 19, 67–73.

Mekis, I., Talapin, D.V., Kornowski, A., Haase, M., and Weller, H. (2003). "One-Pot Synthesis of Highly Luminescent CdSe/CdS Core−Shell Nanocrystals via Organometallic and "Greener" Chemical Approaches†." *J. Phys. Chem. B* 107, 7454–7462.

M G Bawendi, M L Steigerwald, and Brus, L.E. (1990). "The Quantum Mechanics of Larger Semiconductor Clusters ('Quantum Dots')." *Annu. Rev. Phys. Chem.* 41, 477–496.

Micic, O.I., Sprague, J.R., Curtis, C.J., Jones, K.M., Machol, J.L., Nozik, A.J., et al. (1995). "Synthesis and Characterization of InP, GaP, and $GaInP_2$ Quantum Dots." *J. Phys. Chem.* 99, 7754–7759.

Mi, C., Wang, Y., Zhang, J., Huang, H., Xu, L., Wang, S., et al. (2011). "Biosynthesis and Characterization of CdS Quantum Dots in Genetically Engineered *Escherichia coli*." *J. Biotechnol.* 153, 125–132.

Mihranyan, A., Ferraz, N., and Strømme, M. (2012). "Current Status and Future Prospects of Nanotechnology in Cosmetics." *Prog. Mater. Sci.* 57, 875–910.

Mohan, S.K., Viruthagiri, T., and Arunkumar, C. (2014). "Statistical Optimization of Process Parameters for the Production of Tannase by *Aspergillus flavus* under Submerged Fermentation." *3 Biotech* 4, 159–166.

Mousavi, R.A., Sepahy, A.A., and Fazeli, M.R. (2012). "Biosynthesis, Purification and Characterization of Cadmium Sulfide Nanoparticles Using *Enterobacteriaceae* and Their Application." *Proc., Int. Conf. Nanomaterials : Applications and Properties*, Sumy State University, Ukraine,1(1)01PCN30-01PCN30.

Murray, C.B., Norris, D.J., and Bawendi, M.G. (1993). "Synthesis and Characterization of Nearly Monodisperse CdE (E = Sulfur, Selenium, Tellurium) Semiconductor Nanocrystallites." *J. Am. Chem. Soc.* 115, 8706–8715.

Murray, C.B., Sun, S., Gaschler, W., Doyle, H., Betley, T.A., and Kagan, C.R. (2001). "Colloidal Synthesis of Nanocrystals and Nanocrystal Superlattices." *IBM J. Res. Dev.* 45, 47–56.

Murthy (2011). "Effect of Lead on Metallothionein Concentration in Lead-Resistant Bacteria *Bacillus cereus* Isolated from Industrial Effluent." *Afr. J. Biotechnol.* 10, 15966–15972.

Myers, R.H., and Montgomery, D.C. (1995). Response Surface Methodology: Process and Product in Optimization Using Designed Experiments, John Wiley & Sons, Inc, USA..

Narayanan, K.B., and Sakthivel, N. (2011). "Green Synthesis of Biogenic Metal Nanoparticles by Terrestrial and Aquatic Phototrophic and Heterotrophic Eukaryotes and Biocompatible Agents." *Adv. Colloid Interface Sci.* 169, 59–79.

Nyongesa, B.W., Okoth, S., and Ayugi, V. (2015). "Identification Key for *Aspergillus* Species Isolated from Maize and Soil of Nandi County, Kenya." *Adv. Microbiol.* 05, 205–229.

Okuno, T., Lipovskii, A.A., Ogawa, T., Amagai, I., and Masumoto, Y. (2000). "Strong Confinement of PbSe and PbS Quantum Dots." *J. Lumin.* 87–89, 491–493.

Overney, R.M., and Sills, S.E. (2001). Constrained systems: caught between dimensions. In ACS Symposium Series, American Chemical Society, Washington, 2–23.

Pal, S.K., and Das, T.K. (2005). "Biochemical Characterization of N-Methyl N'-Nitro-N-Nitrosoguanidine-Induced Cadmium Resistant Mutants of *Aspergillus niger*." *J. Biosci.* 30, 639–46.

Pandian, S.R.K., Deepak, V., Kalishwaralal, K., and Gurunathan, S. (2011). "Biologically Synthesized Fluorescent CdS NPs Encapsulated by PHB." *Enzyme Microb. Technol.* 48, 319–325.

Parak, W.J., Manna, L., Simmel, F.C., Gerion, D., and Alivisatos, P. (2003). Quantum Dots. In Nanoparticles, G. Schmid, ed. Wiley-VCH Verlag GmbH & Co. KGaA,Germany, 4–49.

Paraszkiewicz, K., Bernat, P., Naliwajski, M., and Długoński, J. (2010). "Lipid Peroxidation in the Fungus *Curvularia lunata* Exposed to Nickel." *Arch. Microbiol.* 192, 135–41.

Parikh, R.Y., Ramanathan, R., Coloe, P.J., Bhargava, S.K., Patole, M.S., Shouche, Y.S., et al. (2011). "Genus-Wide Physicochemical Evidence of Extracellular Crystalline Silver Nanoparticles Biosynthesis by Morganella Spp." *PloS One* 6, e21401.

Pelucchi, E., Watanabe, S., Leifer, K., Zhu, Q., Dwir, B., De Los Rios, P., et al. (2007). "Mechanisms of Quantum Dot Energy Engineering by Metalorganic Vapor Phase Epitaxy on Patterned Nonplanar Substrates." *Nano Lett.* 7, 1282–1285.

Pendyala, N.B., and Koteswara Rao, K.S.R. (2008). "Identification of Surface States in PbS Quantum Dots by Temperature Dependent Photoluminescence." *J. Lumin.* 128, 1826–1830.

Pendyala, N.B., and Koteswara Rao, K.S.R. (2009). "Efficient Hg and Ag Ion Detection with Luminescent PbS Quantum Dots Grown in Poly Vinyl Alcohol and Capped with Mercaptoethanol." *Colloids Surf. Physicochem. Eng. Asp.* 339, 43–47.

Peng, X., Schlamp, M.C., Kadavanich, A.V., and Alivisatos, A.P. (1997). "Epitaxial Growth of Highly Luminescent CdSe/CdS Core/Shell Nanocrystals with Photostability and Electronic Accessibility." *J. Am. Chem. Soc.* 119, 7019–7029.

Peng, Z.A., and Peng, X. (2001). "Formation of High-Quality CdTe, CdSe, and CdS Nanocrystals Using CdO as Precursor." *J. Am. Chem. Soc.* 123, 183–184.

Prasad, K., and Jha, A.K. (2010a). "Biosynthesis of CdS Nanoparticles: An Improved Green and Rapid Procedure." *J. Colloid Interface Sci.* 342, 68–72.

Prasad, K., and Jha, A.K. (2010b). "Biosynthesis of CdS Nanoparticles: An Improved Green and Rapid Procedure." *J. Colloid Interface Sci.* 342, 68–72.

Prokopovich, P. (2015). Biological and Pharmaceutical Applications of Nanomaterials, CRC Press, USA.

Qian, W., and Krimm, S. (1994). "Vibrational Analysis of Glutathione." *Biopolymers* 34, 1377–94.

Qu, L., and Peng, X. (2002). "Control of Photoluminescence Properties of CdSe Nanocrystals in Growth." *J. Am. Chem. Soc.* 124, 2049–2055.

Raffa, V., Vittorio, O., Riggio, C., and Cuschieri, A. (2010). "Progress in Nanotechnology for Healthcare." *Minim. Invasive Ther. Allied Technol.* 19, 127–135.

Ramanathan, R., O'Mullane, A.P., Parikh, R.Y., Smooker, P.M., Bhargava, S.K., and Bansal, V. (2011). "Bacterial Kinetics-Controlled Shape-Directed Biosynthesis of Silver Nanoplates Using Morganella Psychrotolerans." *Langmuir ACS J. Surf. Colloids* 27, 714–719.

Ramezani, F., Ramezani, M., and Talebi, S. (2010). "Mechanistic Aspects of Biosynthesis of Nanoparticles by Several Microbes." *Nanocon* 10, 1–7.

Rivas, R.E., López-García, I., and Hernández-Córdoba, M. (2009). "Determination of Traces of Lead and Cadmium Using Dispersive Liquid-Liquid Microextraction Followed by Electrothermal Atomic Absorption Spectrometry." *Microchim. Acta* 166, 355–361.

Robin, S., Leveque, N., Courderot-Masuyer, C., and Humbert, P. (2011). "LC-MS Determination of Oxidized and Reduced Glutathione in Human Dermis: A Microdialysis Study." *J. Chromatogr. B Analyt. Technol. Biomed. Life. Sci.* 879, 3599–606.

Rodrigues, S.S.M., Lima, A.S., Teixeira, L.S.G., Korn, M.D.G. a, and Santos, J.L.M. (2014). "Determination of Iron in Biodiesel Based on Fluorescence Quenching of CdTe Quantum Dots." *Fuel* 117, 520–527.

Rogach, A. (2008). Semiconductor Nanocrystal Quantum Dots: Synthesis, Assembly, Spectroscopy and Applications, Springer, USA.

Rosenthal, S., Mcbride, J., Pennycook, S., and Feldman, L. (2007). "Synthesis, Surface Studies, Composition and Structural Characterization of CdSe, Core/shell and Biologically Active Nanocrystals." *Surf. Sci. Rep.* 62, 111–157.

Rotello, V. (2012). Nanoparticles: Building Blocks for Nanotechnology, Springer Science & Business Media, USA.

Samanta, P.K. (2011). "Weak quantum confinement in zno nanorods: a one dimensional potential well approach." *Opt. Photonics Lett.* 04, 35–45.

Sanghi, R., and Verma, P. (2009). "A Facile Green Extracellular Biosynthesis of CdS Nanoparticles by Immobilized Fungus." *Chem. Eng. J.* 155, 886–891.

Sanvicens, N., and Marco, M.P. (2008). "Multifunctional Nanoparticles – Properties and Prospects for Their Use in Human Medicine." *Trends Biotechnol.* 26, 425–433.

Sarkar, J., Dey, P., Saha, S., and Acharya, K. (2011). "Mycosynthesis of Selenium Nanoparticles." *Micro Nano Lett.* 6, 599.

Sastry, M., Ahmad, A., Islam Khan, M., and Kumar, R. (2003). "Biosynthesis of Metal Nanoparticles Using Fungi and Actinomycete." *Curr. Sci.* 85, 162–170.

Sathiyasarathi, V.G., and Kumar, G.G. (2012). "Bio—Resources Mediated Nanosynthesis." *Rev. Adv. Sci. Eng.* 1, 148–161.

Schaller, R.D., and Klimov, V.I. (2004). "High Efficiency Carrier Multiplication in PbSe Nanocrystals: Implications for Solar Energy Conversion." *Phys. Rev. Lett.* 92, 186601.

Sengül, H., and Theis, T.L. (2009). "Life Cycle Inventory of Semiconductor Cadmium Selenide Quantum Dots for Environmental Applications."Nanotechnology Applications for Clean Water, William Andrew Inc, Norwhich., 561-581.

Serrano, E., Rus, G., and García-Martínez, J. (2009). "Nanotechnology for Sustainable Energy." *Renew. Sustain. Energy Rev.* 13, 2373–2384.

Shandalov, M., Rozenblat, A., Kedem, N., Popovitz-Biro, R., and Golan, Y. (2008). "Interfacial Characterization of Chemical Solution-Deposited Thin Films of PbSe on GaAs(100)." *Surf. Interface Anal.* 40, 939–943.

Shankar Congeevaram, S.D. (2007). "Biosorption of Chromium and Nickel by Heavy Metal Resistant Fungal and Bacterial Isolates." *J. Hazard. Mater.* 146, 270–7.

Shrivastava, A., and Gupta, V. (2011). "Methods for the Determination of Limit of Detection and Limit of Quantitation of the Analytical Methods." *Chron. Young Sci.* 2, 21.

Sigel, A., Sigel, H., and Sigel, R.K.O. (2009). Metallothioneins and Related Chelators, Royal Society of Chemistry, Cambridge.

Singh, A., Jain, D., Upadhyay, M.K., Khandelwal, N., and Verma, H.N. (2010). "Green Synthesis of Silver Nanoparticles Using Argemone Mexicana Leaf Extract and Evaluation of Their Antimicrobial Activities." *Dig J Nanomater Bios* 5, 483–489.

Sintuprapa, W., Thiravetyan, P., and Tanticharoen, M. (2000). "A Possible Mechanism of Zn2+ Uptake by Living Cells of Penicillium Sp." *Biotechnol. Lett.* 22, 1709–1712.

Slocik, J.M., Knecht, M.R., and Wright, D.W. (2004). "Biogenic Nanoparticles." *Encycl. Nanosci. Nanotechnol.* 1, 293–308.

Smith, A.M., and Nie, S. (2010). "Semiconductor Nanocrystals: Structure, Properties, and Band Gap Engineering." *Acc. Chem. Res.* 43, 190–200.

Street, A., Sustich, R., Duncan, J., and Savage, N. (2014). Nanotechnology Applications for Clean Water: Solutions for Improving Water Quality, William Andrew Inc, Norwhich.

Stürzenbaum, S.R., Höckner, M., Panneerselvam, A., Levitt, J., Bouillard, J.-S., Taniguchi, S., et al. (2012). "Biosynthesis of Luminescent Quantum Dots in an Earthworm." *Nat. Nanotechnol.* 8, 57–60.

Stürzenbaum, S.R., Höckner, M., Panneerselvam, a, Levitt, J., Bouillard, J.-S., Taniguchi, S., et al. (2013). "Biosynthesis of Luminescent Quantum Dots in an Earthworm." *Nat. Nanotechnol.* 8, 57–60.

Sweeney, R.Y., Mao, C., Gao, X., Burt, J.L., Belcher, A.M., Georgiou, G., et al. (2004). "Bacterial Biosynthesis of Cadmium Sulfide Nanocrystals." *Chem. Biol.* 11, 1553–1559.

Syed, A., and Ahmad, A. (2013). "Extracellular Biosynthesis of CdTe Quantum Dots by the Fungus Fusarium Oxysporum and Their Anti-Bacterial Activity." *Spectrochim. Acta. A. Mol. Biomol. Spectrosc.* 106, 41–47.

Sze, S.M., and Ng, K.K. (2006). Physics of Semiconductor Devices, John Wiley & Sons, UK.

Thirumoorthy, N., Manisenthil Kumar, K.-T., Shyam Sundar, A., Panayappan, L., and Chatterjee, M. (2007). "Metallothionein: An Overview." *World J. Gastroenterol. WJG* 13, 993–6.

Tischler, J.G., Kennedy, T.A., Glaser, E.R., Efros, A.L., Foos, E.E., Boercker, J.E., et al. (2010). "Band-Edge Excitons in PbSe Nanocrystals and Nanorods." *Phys. Rev. B* 82, 245303.

Torchynska, T., and Vorobiev, Y. (2011). Semiconductor II-VI Quantum Dots with Interface States and Their Biomedical Applications. In Advanced Biomedical Engineering, G. Gargiulo, ed., InTech Publishers, Croatia, EU.

Tsekova, K., and Todorova, D. (2002). "Copper (II) Accumulation and Superoxide Dismutase Activity during Growth of Aspergillus Niger B-77." *Z. Naturforschung Teil C Biochem. Biophys. Biol. Virol.* 57, 319–322.

Uldrich, J., and Newberry, D. (2003). The Next Big Thing is Really Small: How Nanotechnology Will Change the Future of Your Business, Crown Business, USA.

Vaidyanathan, R., Cox, S.M., Happek, U., Banga, D., Mathe, M.K., and Stickney, J.L. (2006). "Preliminary Studies in the Electrodeposition of PbSe/PbTe Superlattice Thin Films via Electrochemical Atomic Layer Deposition (ALD)." *Langmuir ACS J. Surf. Colloids* 22, 10590–10595.

Vayssieres, L. (2010). On Solar Hydrogen and Nanotechnology, John Wiley & Sons, UK.

Venil, C.K., and Lakshmanaperumalsamy, P. (2009). "Application of Statistical Design to the Optimization of Culture Medium for Prodigiosin Production by Serratia Marcescens SWML08." *Malays J Microbiol* 1, 55–61.

Ventra, M.D., Evoy, S., and Heflin, J.R. (2004). Introduction to Nanoscale Science and Technology, Springer Science & Business Media, New York.

Wang, F., Gu, Z., Lei, W., Wang, W., Xia, X., and Hao, Q. (2014). "Graphene Quantum Dots as a Fluorescent Sensing Platform for Highly Efficient Detection of copper(II) Ions." *Sens. Actuators B Chem.* 190, 516–522.

Weir, E., Lawlor, A., Whelan, A., and Regan, F. (2008). "The Use of Nanoparticles in Anti-Microbial Materials and Their Characterization." *Analyst* 133, 835–845.

Willard, D.M., Mutschler, T., Yu, M., Jung, J., and Van Orden, A. (2006). "Directing Energy Flow through Quantum Dots: Towards Nanoscale Sensing." *Anal. Bioanal. Chem.* 384, 564–571.

Wise, F.W. (2000). "Lead Salt Quantum Dots: The Limit of Strong Quantum Confinement." *Acc. Chem. Res.* 33, 773–780.

Wujcik, E., Aceto, S., Heskett, D., and Bose, A. (2015). "Synthesis of Co-Electrospun Lead Selenide Nanostructures within Anatase Titania Nanotubes for Advanced Photovoltaics." *Fibers* 3, 173–183.

Wu, W., Zhou, T., Aiello, M., and Zhou, S. (2010). "Construction of Optical Glucose Nanobiosensor with High Sensitivity and Selectivity at Physiological pH on the Basis of Organic–inorganic Hybrid Microgels." *Biosens. Bioelectron.* 25, 2603–2610.

Wysocki, R., and Tamás, M.J. (2010). "How Saccharomyces Cerevisiae Copes with Toxic Metals and Metalloids." *FEMS Microbiol. Rev.* 34, 925–51.

Xie, H.Y., Liang, J.G., Zhang, Z.L., Liu, Y., He, Z.K., and Pang, D.W. (2004). "Luminescent CdSe-ZnS Quantum Dots as Selective Cu2+ Probe." *Spectrochim. Acta - Part Mol. Biomol. Spectrosc.* 60, 2527–2530.

Yong, K.-T., Sahoo, Y., Choudhury, K.R., Swihart, M.T., Minter, J.R., and Prasad, P.N. (2006a). "Shape Control of PbSe Nanocrystals Using Noble Metal Seed Particles." *Nano Lett.* 6, 709–714.

Yong, K.-T., Sahoo, Y., Choudhury, K.R., Swihart, M.T., Minter, J.R., and Prasad, P.N. (2006b). "Shape Control of PbSe Nanocrystals Using Noble Metal Seed Particles." *Nano Lett.* 6, 709–714.

Zafar, S., Aqil, F., and Ahmad, I. (2007). "Metal Tolerance and Biosorption Potential of Filamentous Fungi Isolated from Metal Contaminated Agricultural Soil." *Bioresour. Technol.* 98, 2557–2561.

Zhang, L., Zheng, X., Jin, Z., Hu, S., and He, M.-R. (2012). "Optimization of Fermentation Conditions for Pristinamycin Production by Immobilized Streptomyces Pristinaespiralis Using Response Surface Methodology." *Electron. J. Biotechnol.* 15,.

Zhang, S.-Y., Fang, C.-X., Wei, Jin, B.-K., Tian, Y.-P., Shen, Y.-H., et al. (2007). "Synthesis and Electrochemical Behavior of Crystalline Ag_2Se Nanotubes." *J. Phys. Chem. C* 111, 4168–4174.

Zhang, X., Zhu, S., Xiong, Y., Deng, C., and Zhang, X. (2013). "Development of a MALDI-TOF MS Strategy for the High-Throughput Analysis of Biomarkers: On-Target Aptamer Immobilization and Laser-Accelerated Proteolysis." *Angew. Chem. Int. Ed.* 52, 6055–6058.

Zhang, Y.H., Zhang, H.S., Guo, X.F., and Wang, H. (2008). "L-Cysteine-Coated CdSe/CdS Core-Shell Quantum Dots as Selective Fluorescence Probe for copper(II) Determination." *Microchem. J.* 89, 142–147.

Zheng, J., Nicovich, P.R., and Dickson, R.M. (2007). "Highly Fluorescent Noble Metal Quantum Dots." *Annu. Rev. Phys. Chem.* 58, 409–431.

Zhu, J., Liao, X., Wang, J., and Chen, H.-Y. (2001). "Photochemical Synthesis and Characterization of PbSe Nanoparticles." *Mater. Res. Bull.* 36, 1169–1176.

Zouboulis, A.I., Loukidou, M.X., and Matis, K.A. (2004). "Biosorption of Toxic Metals from Aqueous Solutions by Bacteria Strains Isolated from Metal-Polluted Soils." *Process Biochem.* 39, 909–916.

SIGMA-ALDRICH®

sigma-aldrich.com

3050 Spruce Street, Saint Louis, MO 63103, USA
Website: www.sigmaaldrich.com
Email USA: techserv@sial.com
Outside USA: eurtechserv@sial.com

Product Specification

Product Name:
Albumin from bovine serum

Product Number: **A8531**
CAS Number: 9048-46-8

Storage Temperature: -20 ℃

TEST	Specification
Appearance (Color)	White to Tan
Appearance (Form)	Powder
Solubility (color)	Colorless to Tan
Solubility (tubidity)	Clear
Suitability	Suitable
Suitable for use as a gel filtration marker per Sigma Technical Bulletin GF-3 (MW approx. 66,000 Da)	
VSV and BT Virus	None Detected
Miscellaneous Supplier Data	Conforms
Inactivation Process	
pH not more than 5.0 for at least 2 hours; temperature not less than 65 deg C for at least 3 hours	
Chapter 4(C) - Untreated	----------
Product meets European Union requirements for production of technical blood products.	

Specification: PRD.1.ZQ5.10000010109

SIGMA-ALDRICH®

sigma-aldrich.com

3050 Spruce Street, Saint Louis, MO 63103, USA
Website: www.sigmaaldrich.com
Email USA: techserv@sial.com
Outside USA: eurtechserv@sial.com

Product Specification

Product Name:
L-Glutathione reduced - ≥98.0%

Product Number:	**G4251**
CAS Number:	70-18-8
MDL:	MFCD00065939
Formula:	C10H17N3O6S
Formula Weight:	307.32 g/mol
Storage Temperature:	2 - 8 ℃

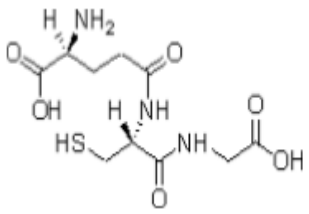

TEST	Specification
Appearance (Color)	White
Appearance (Form)	Powder
Solubility (Color)	Colorless
Solubility (Turbidity) 50 mg/mL, H2O	Clear
Infrared spectrum	Conforms to Structure
Titration with Iodine	≥ 99 %
Purity (HPLC)	≥ 98.0 %
Recommended Retest Period 5 years	----------

Specification: PRD.1.ZQ5.10000014977

SIGMA-ALDRICH

3050 Spruce Street
Saint Louis, Missouri 63103 USA
Telephone 800-325-5832 • (314) 771-5765
Fax (314) 286-7828
email: techserv@sial.com
sigma-aldrich.com

ProductInformation

Magnesium sulfate heptahydrate
ACS Reagent

Product Number **M 9397**
Store at Room Temperature
23,039-1 is an exact replacement for M 9397

Product Description

Molecular Formula: $MgSO_4 \cdot 7H_2O$
Molecular Weight: 246.5
CAS Number: 10034-99-8

This product is designated as ACS Reagent grade and meets the specifications of the American Chemical Society (ACS) for reagent chemicals.

Magnesium sulfate is used in chemistry and molecular biology as a source of magnesium ions. Magnesium has a variety of biological roles in enzymology, cell membrane and wall structural integrity, muscle cell physiology, and nucleic acid structure.[1,2] Magnesium is an essential co-factor in many enzymes, including deoxyribonuclease (DNase), the restriction enzymes *Eco*R I and *Eco*R V, and Ribonuclease H.[3,4] Magnesium also stabilizes polymeric nucleic acids such as transfer RNA and ribozymes.[5]

A protocol for chromosome and nuclei isolation that incorporates $MgSO_4$ has been published.[6] The use of $MgSO_4$ for leukotoxin production from cultured *Pasteurella haemolytica* has been reported.[7]

Precautions and Disclaimer

For Laboratory Use Only. Not for drug, household or other uses.

Preparation Instructions

This product is soluble in water (100 mg/ml), yielding a clear, colorless solution.

References

1. Cowan, J. A., in The Biological Chemistry of Magnesium, Cowan, J. A., ed., VCH Publishers (New York: 1995), pp. 1-23.
2. The Biological Chemistry of the Elements, Frausto da Silva, J. J. R., and Williams, R. J. P., Clarendon Press (Oxford, UK: 1991), pp. 243-267.
3. Brooks, J. E., Properties and uses of restriction endonucleases. Methods Enzymol., **152**, 113-129 (1987).
4. Black, C. B., and Cowan, J. A., in The Biological Chemistry of Magnesium, Cowan, J. A., ed., VCH Publishers (New York: 1995), pp. 137-157.
5. Principles of Bioinorganic Chemistry, Lippard, S. J., and Berg, J. M., University Science Books (Mill Valley, CA: 1994), pp. 192-196.
6. Trask, B., and van den Engh, G., Chromosome and nuclei isolation with the $MgSO_4$ procedure. Methods Cell. Biol., **33**, 363-367 (1990).
7. Sun, Y., and Clinkenbeard, K.D., Serum-free culture of *Pasteurella haemolytica* optimized for leukotoxin production. Am. J. Vet. Res., **59(7)**, 851-855 (1998).

GCY/NSB 3/03

SIGMA-ALDRICH

3050 Spruce Street
Saint Louis, Missouri 63103 USA
Telephone 800-325-5832 • (314) 771-5765
Fax (314) 286-7828
email: techserv@sial.com
sigma-aldrich.com

ProductInformation

NITRO BLUE TETRAZOLIUM (NBT) TABLETS

Product No. **N5514**

Product Description

Nitro Blue Tetrazolium (NBT) is used in conjunction with the alkaline phosphatase substrate 5-Bromo-4-Chloro-3-Indolyl Phosphate (BCIP) (Product No. B0274) in immunoblotting and immunohistological staining procedures. This substrate system produces an insoluble end product that is blue in color and can be observed visually.

Substrate Content	10 mg
Appearance	Yellow, round tablet, 5/32" in diameter.
Tablet Weight	25 mg (range 22.5 - 27.5 mg)
Solubility*	Clear, yellow solution
Dissolution Time*	Not more than 5 minutes
pH*	5.0 (range 4.5 - 5.5)
Activity	Comparable to the untableted powder in the BCIP/NBT substrate system.
Packaging	10 or 25 tablets per bottle. Custom packaging and bulk purchase information available upon request.

*One tablet dissolved in 1 ml of deionized water

Uses

NBT Stock Solution
Prepare NBT stock solution by dissolving one NBT tablet in 1 ml of deionized water.

BCIP Stock Solution
Prepare BCIP stock solution by dissolving one BCIP tablet (25 mg substrate content, Product No. B0274) in 0.5 ml 100% dimethylformamide (DMF, Product No. D4254).

Substrate Buffer
0.1 M Tris, 100 mM sodium chloride, 5 mM $MgCl_2$, pH 9.5, adjust pH with HCl.

Substrate Solution
Prepare substrate solution by adding 330 µl of NBT stock solution to 10 ml of substrate buffer, mix, then add 33 µl of BCIP stock solution, mix.

Storage

Store tablets at 2-8EC.

References

1. Blake, M.S., Anal. Biochem., **136**, 175 (1984).
2. Horowitz, J.P., et al., J. Med. Chem., **9**, 447 (1966).

Pcs2/99/1/96

SIGMA-ALDRICH®

sigma-aldrich.com

3050 Spruce Street, Saint Louis, MO 63103, USA
Website: www.sigmaaldrich.com
Email USA: techserv@sial.com
Outside USA: eurtechserv@sial.com

Product Specification

Product Name:
Lead(II) nitrate – ACS reagent, ≥99.0%

Product Number:	**228621**
CAS Number:	10099-74-8
MDL:	MFCD00011153
Formula:	N2O6Pb
Formula Weight:	331.21 g/mol

$Pb(NO_3)_2$

TEST	Specification
Appearance (Color)	White
Appearance (Form)	Powder or Solid or Crystals
ICP Major Analysis	Confirmed
Confirms Lead Component	
Complexiometric EDTA	≥ 99.0 %
Insoluble matter	≤ 0.005 %
c = 10%; Dilute HNO3	
Chloride Content	≤ 0.001 %
Copper (Cu)	≤ 0.002 %
Iron (Fe)	≤ 0.001 %
Sodium (Na)	≤ 0.02 %
Potassium (K)	≤ 0.005 %
Calcium (Ca)	≤ 0.005 %
Meets ACS Requirement	Meets Requirements
10th Edition	

HIMEDIA

Technical Data

Potato Dextrose Agar

M096

Potato Dextrose agar is recommended for the isolation and enumeration of yeasts and moulds from dairy and other food products.

Composition**

Ingredients	Gms / Litre
Potatoes, infusion from	200.000
Dextrose	20.000
Agar	15.000
Final pH (at 25°C)	5.6±0.2

**Formula adjusted, standardized to suit performance parameters

Directions

Suspend 39 grams in 1000 ml distilled water. Heat to boiling to dissolve the medium completely. Sterilize by autoclaving at 15 lbs pressure (121°C) for 15 minutes. Mix well before dispensing. In specific work, when pH 3.5 is required, acidify the medium with sterile 10% tartaric acid. The amount of acid required for 100 ml. of sterile, cooled medium is approximately 1 ml. Do not heat the medium after addition of the acid.

Principle And Interpretation

Potato Dextrose Agar is recommended by APHA (1) and F.D.A. (2) for plate counts of yeasts and moulds in the examination of foods and dairy products (3). Potato Dextrose Agar is also used for stimulating sporulation, for maintaining stock cultures of certain dermatophytes and for differentiation of typical varieties of dermatophytes on the basis of pigment production (4). It is also recommended by USP (5), BP (6) ,EP (7) and JP (8) for growth of fungi.

Potato infusion and dextrose promote luxuriant fungal growth. Adjusting the pH of the medium by tartaric acid to 3.5, inhibits the bacterial growth. Heating the medium after acidification should be avoided as it may hydrolyse the agar which can render the agar unable to solidify.

Quality Control

Appearance

Cream to yellow homogeneous free flowing powder

Gelling

Firm, comparable with 1.5% Agar gel

Colour and Clarity of prepared medium

Light amber coloured clear to slightly opalescent gel forms in Petri plates

**Aspergillus brasiliensis ATCC 16404*	50 -100	luxuriant	25 -100	>=70 %	20 -25 °C	5 -7 d
Saccharomyces cerevisiae ATCC 9763	50 -100	luxuriant	35 -100	>=70 %	30 -35 °C	2 -5 d
Rhodotorula mucilaginosa DSM 70403		luxuriant			20 -25 °C	3 -5 d
Geotrichum candidum DSM 1240		good- luxuriant			25 -30 °C	3 -5 d
Penicillium communae ATCC 10248		fair -good			25 -30 °C	3 -5 d
Trichophyton ajelloi ATCC 28454		fair-good			25 -30 °C	3 -7 d

*Key:-Formerly known as *Aspergillus niger*

Storage and Shelf Life

Store below 30°C in tightly closed container and the prepared medium at 2 - 8°C. Use before expiry date on the label.

Reference

1.Downes F. P. and Ito K., (Eds.), 2001, Compendium of Methods for the Microbiological Examination of Foods, 4th Ed., APHA, Washington, D.C.
2.FDA Bacteriological Analytical Manual, 2005, 18th Ed., AOAC, Washington, DC.
3.Wehr H. M. and Frank J. H., 2004, Standard Methods for the Microbiological Examination of Dairy Products, 17th Ed., APHA Inc., Washington, D.C.
4.MacFaddin J. F., 1985, Media for the Isolation-Cultivation-Identification-Maintenance of Medical Bacteria, Vol.1, Williams and Wilkins, Baltimore
5.The United States Pharmacopoeia, 2009, The United States Pharmacopoeial Convention. Rockville, MD.
6.British Pharmacopoeia, 2009, The Stationery office British Pharmacopoeia
7.European Pharmacopoeia, 2009, European Dept. for the quality of Medicines.
8.Japanese Pharmacopoeia, 2008.

Revision : 2 / 2015

Technical Data

Potato Dextrose Broth

M403

Potato Dextrose Broth is recommended for the isolation and enumeration of yeasts and moulds .

Composition**

Ingredients	Gms / Litre
Potatoes, infusion from	200.000
Dextrose	20.000
Final pH (at 25°C)	5.1±0.2

**Formula adjusted, standardized to suit performance parameters

Directions

Suspend 24 grams in 1000 ml distilled water. Heat if necessary to dissolve the medium completely. Sterilize by autoclaving at 15 lbs pressure (121°C) for 15 minutes. Mix well before dispensing. In specific work, when pH 3.5 is required, acidify the medium with sterile 10% tartaric acid. The amount of acid required for 100 ml. of sterile, cooled medium is approximately 1 ml. Do not heat the medium after addition of the acid.

Principle And Interpretation

Potato Dextrose Broth is recommended by APHA (1) and F.D.A. (2) for plate counts of yeasts and moulds in the examination of foods and dairy products (3). Potato Dextrose Broth is also used for stimulating sporulation, for maintaining stock cultures of certain dermatophytes and for differentiation of typical varieties of dermatophytes on the basis of pigment production (4).

Potato infusion and dextrose promote luxuriant fungal growth. Adjusting the pH of the medium by tartaric acid to 3.5, inhibits the bacterial growth. Heating the medium after acidification should be avoided.

Quality Control

Appearance
Off-white to yellow homogeneous free flowing powder

Colour and Clarity of prepared medium
Light amber coloured clear to slightly opalescent solution in tubes

Reaction
Reaction of 2.4% w/v aqueous solution at 25°C. pH : 5.1±0.2

pH
4.90-5.30

SIGMA-ALDRICH®

sigma-aldrich.com

3050 Spruce Street, Saint Louis, MO 63103, USA
Website: www.sigmaaldrich.com
Email USA: techserv@sial.com
Outside USA: eurtechserv@sial.com

Product Specification

Product Name:
Selenium powder, −100 mesh, ≥99.5% trace metals basis

Product Number:	**209651**
CAS Number:	7782-49-2
MDL:	MFCD00134090
Formula:	Se
Formula Weight:	78.96 g/mol

Se

TEST	Specification
Appearance (Color)	Dark Grey to Black
Appearance (Form)	Powder
X-Ray Diffraction	Conforms to Structure
Trace Metal Analysis	≤5,000.0 ppm
Purity 99.50% Purity Based On Trace Metals Analysis	Meets Requirements
Average Particle Size	≤150.0 micron

Remarks:
Specification Date : 06/21/2010

SIGMA-ALDRICH®

sigma-aldrich.com

3050 Spruce Street, Saint Louis, MO 63103, USA
Website: www.sigmaaldrich.com
Email USA: techserv@sial.com
Outside USA: eurtechserv@sial.com

Product Specification

Product Name:
Sucrose - ≥99.5%

Product Number:	**S8501**
CAS Number:	57-50-1
MDL:	MFCD00006626
Formula:	C12H22O11
Formula Weight:	342.30 g/mol

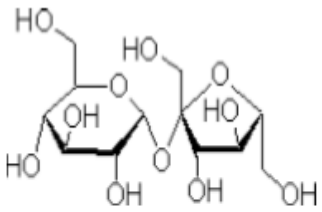

TEST	Specification
Appearance (Color)	White to Off-White
Appearance (Form)	Powder
Solubility (Color)	Colorless to Faint Yellow
Solubility (Turbidity)	Clear
5 g plus 10 ml H2O	
Infrared spectrum	Conforms to Structure
Purity (GC)	≥ 99.5 %
Recommended Retest Period	----------
5 years	

Specification: PRD.2.ZQ5.10000010853

LIST OF PUBLICATIONS BASED ON THIS RESEARCH WORK

1. **Jaya, M.J.,** Lens, P.N.L. and Raj Mohan, B. (2015). "Microbial synthesis of chalcogenide semiconductor nanoparticle: a review." Microb. biotechnol., doi:10.1111/1751-7915.12297.- Wiley (I.F: 3.2)

2. **Jaya, M.J.,** Sumit, S. and Raj Mohan, B. (2015). "Exploring the fungal protein cadre in the biosynthesis of PbSe quantum dots" Haz. Mat., - doi: 10.1016/j.jhazmat.2015.12.056. Elsevier (IF: 5.27)

3. **Jaya, M. J.,** Raj Mohan, B. and Udaya, B.K. (2014). "Biosynthesis of lead selenide quantum rods in marine *Aspergillus terreus*." Mater.Lett., 124, 279-281.- Elsevier (IF: 2.3)

4. **Jaya, M .J.,** Raj Mohan, B. and Akshay, G.K.M. (2014). "Insights into the optical and anti-bacterial properties of biogenic PbSe quantum rods." J. Saudi. Chem. Soc., doi.org/10.1016/ j.jscs.10.10 008.- Elsevier (IF: 1.3)

5. **Jaya, M. J.,** Raj Mohan, B.(2016). "Electrochemical properties of PbSe Quantum Dots biosynthesized using marine *Aspergillus terreus*" Rare Metal Materials Engineering- Elsevier (I.F: 0.198)- Accepted.

6. Raja, C.P., **Jaya, M.J.,** Raj Mohan, B. (2015). "Selenium Biosorption and Recovery by Marine *Aspergillus terreus* in an Upflow Bioreactor." J. Env. Eng., doi: 10.1061/(ASCE)EE.1943-7870.0000999.- ASCE (I.F: 1.14)

7. **Jaya, M. J.,** Raj Mohan, B. and Soubhik, K.B. (2014). "Selenium and lead tolerance in marine *Aspergillus terreus* for biosynthesis of nano particles – quantum dots/ rods." Int'l Journal of Advances in Chemical Engg.,& Biological Sciences., 1, 6-11.

8. **Jaya, M. J.,** Raj Mohan, B. and Soubhik, K.B. (2013). "Selenium and lead tolerance in marine fungus isolated from sea water." Int. J. Inno. Res. Sc. Eng. Tech., 2, 2975-2982.

Papers published in Conference Proceedings

9. **Jaya, M.J.**and Raj Mohan, B. (2015). "Optimizing the fluorescence of biogenic PbSe quantum particles for the efficient Cadmium (Cd^{2+}) ion sensing in solution" Proceedings of the ***4th International Conference on Research Frontiers in Chalcogen Cycle Science and Technology***by **UNESCO-IHE**, Institute of Water Education, Delft, Netherlands.

Papers under Review

10. **Jaya, M. J.,** Raj Mohan, B.(2016). "Optimizing the fluorescence of biogenic PbSe quantum particles for the efficient Cadmium (Cd^{2+}) ion sensing in solution" International Biodeterioration & Biodegradation- Ms. Ref. No.: IBB-D-16-00227.- Elsevier (I.F: 2.377)

Presentation at International Conferences

1. **Jaya, M.J.,** Sumit, S. and Raj Mohan, B. (2015). "Exploring the fungal protein Cadre involved in the biosynthesis of PbSe QDs by marine *Aspergillus terreus*- at the ***4thInternational Conference on Research Frontiers in Chalcogen Cycle Science and Technology*** by **UNESCO-IHE**, Institute of Water Education, Delft, Netherlands from **May 28-29 2015** at Delft, Netherlands.

2. **Jaya, M.J.** and Raj Mohan, B. (2015). "Optimizing the fluorescence of biogenic PbSe quantum particles for the efficient Cadmium (Cd^{2+}) ion sensing in solution" at the ***4thInternational Conference on Research Frontiers in Chalcogen Cycle Science and Technology*** by **UNESCO-IHE**, Institute of Water Education, Delft, Netherlands from **May 28-29 2015** at Delft, Netherlands.

Other achievements

- Recipient of the prestigious **Technion International Fellowship** to attend the **Summer School on Sensors and Nanotechnology in Technion Israel Institute of Technology**, Haifa, Israel from July- August 2015.

BIODATA

Ms. Jaya Mary Jacob

Edavomvellil House
Manian Road, Mavicherry
Payyanur P.O, Kannur, Kerala- 670 307
Contact No. +91 9916153371
E- mail: jacob.jaya@gmail.com

Academic Profile

- PhD (Chemical Engineering)- Ongoing
  Department of Chemical Engineering
  National Institute of Technology Karnataka, Surathkal
  Marks %: 84 [2012-2016]

- Summer School on Sensors and Nanotechnology
  The Russell Berrie Nanotechnology Institute and the Faculty of Mechanical Engineering
  Technion Israel Institute of Technology, Haifa, Israel
  Marks %: 91.9 [Spring 2014- 2015]

- Master of Technology (Biotechnology)
  Karunya University,Coimbatore
  Marks %: 83 (First class with Distinction) [2010-2012]

- Bachelor of Technology (Biotechnology)
  Jeppiaar Engineering College (Affiliated to Anna university), Chennai
  Marks %: 85 (First Class with Distinction) [2006-2010]

- CBSE XIIth
  KendriyaVidyalaya Payyanur
  Marks %: 82 (First Class with Distinction) [2005-2006]

Professional Profile

- Assistant Lecturer, Department of Chemical Engineering, National Institute of Technology, Karnataka, India. (December 2012- May, 2016)

- Research Scholar, Department of Chemical Engineering, National Institute of Technology, Karnataka, India. (December 2012- December 2015)

- Assistant Professor, Department of Civil Engineering, North Malabar Institute of Technology, Kerala, India. (September 2012 – December 2012)

- Agronomist, Universidad de Ciencias Applicadas Y Ambientales, Bogota, Colombia. (July - November 2011)

Publications

1. **Jaya, M.J.,** Lens, P.N.L. and Raj Mohan, B. (2015). "Microbial synthesis of chalcogenide semiconductor nanoparticle: a review." Microb. biotechnol., doi:10.1111/1751-7915.12297.- Wiley (I.F: 3.2)

2. **Jaya, M.J.,** Sumit, S. and Raj Mohan, B. (2015). "Exploring the fungal protein cadre in the biosynthesis of PbSe quantum dots" Haz. Mat., - Manuscript ID. HAZMAT-D-15-04308, Elsevier (IF: 5.27)- Under revision.

3. **Jaya, M. J.,** Raj Mohan, B. and Udaya, B.K. (2014). "Biosynthesis of lead selenide quantum rods in marine *Aspergillus terreus*." Mater.Lett., 124, 279-281.- Elsevier (IF: 2.3)

4. **Jaya, M .J.,** Raj Mohan, B. and Akshay, G.K.M. (2014). "Insights into the optical and anti-bacterial properties of biogenic PbSe quantum rods." J. Saudi. Chem. Soc., doi.org/10.1016/ j.jscs.10.10 008.- Elsevier (IF: 2.523)

5. Raja, C.P**., Jaya, M.J.,** Raj Mohan, B. (2015). "Selenium Biosorption and Recovery by Marine *Aspergillus terreus* in an Upflow Bioreactor." J. Env. Eng., doi: 10.1061/(ASCE)EE.1943-7870.0000999.- ASCE (I.F: 1.14)

6. Roopesh, G., Jason, J., Geedhika, K., Anadhan, S., Udaya, B.K., **Jaya, M.J.,**Sogra, F., Raj Mohan, B. (2015) " Microwave assisted extraction of antioxidants from a medicinal plant *Nothapodytes foetida* for the biosynthesis of Ag Nanoparticles." J. Exp.Nano.Sci.,- Taylor and Francis (IF: 0.98)- Under revision.

7. **Jaya, M. J.,** Raj Mohan, B. and Soubhik, K.B. (2014). "Selenium and lead tolerance in marine *Aspergillus terreus* for biosynthesis of nano particles – quantum dots/ rods." Int'l Journal of Advances in Chemical Engg.,& Biological Sciences., 1, 6-11.

8. **Jaya, M. J.,** Raj Mohan, B. and Soubhik, K.B. (2013). "Selenium and lead tolerance in marine fungus isolated from sea water." Int. J. Inno. Res. Sc. Eng. Tech., 2, 2975-2982.

9. **Jaya, M. J.,** Raj Mohan, B.(2016). "Electrochemical properties of PbSe Quantum Dots biosynthesized using marine *Aspergillus terreus*" Rare Metal Materials Engineering-Elsevier (I.F: 0.198)- Accepted.

Papers published in Conference Proceedings

10. **Jaya, M.J.** and Raj Mohan, B. (2015). "Optimizing the fluorescence of biogenic PbSe quantum particles for the efficient Cadmium (Cd^{2+}) ion sensing in solution" Proceedings of the ***4th International Conference on Research Frontiers in Chalcogen Cycle Science and Technology*** by **UNESCO-IHE**, Institute of Water Education, Delft, Netherlands.

Presentation at International Conferences

- **Jaya, M.J.,**Sumit, S. and Raj Mohan, B. (2015). "Exploring the fungal protein Cadre involved in the biosynthesis of PbSe QDs by marine *Aspergillus terreus*- at the ***4thInternational Conference on Research Frontiers in Chalcogen Cycle Science and Technology*** by **UNESCO-IHE**, Institute of Water Education, Delft, Netherlands from **May 28-29 2015** at Delft, Netherlands.

- **Jaya, M.J.**and Raj Mohan, B. (2015). "Optimizing the fluorescence of biogenic PbSe quantum particles for the efficient Cadmium (Cd^{2+}) ion sensing in solution" at the ***4thInternational Conference on Research Frontiers in Chalcogen Cycle Science and Technology*** by **UNESCO-IHE**, Institute of Water Education, Delft, Netherlands from **May 28-29 2015** at Delft, Netherlands.

Achievements

- Recipient of the prestigious Technion International Fellowship to attend the Summer School on Sensors and Nanotechnology in Technion Israel Institute of Technology, Haifa, Israel from July- August 2015.

- Received Young Scientist`s Grant (ITS/0724/2015-2016) from Department of Science and Technology-Science & Engineering Research Board, Govt. of India in May 2015.

- Participated and presented research paper at the *4th International Conference on Research Frontiers in Chalcogen Cycle Science and Technology* held at *UNESCO-IHE, Delft, Netherlands* from 28-29th May 2015.

- Represented India in India International week at Universidad de Ciencias Applicadas y Ambientales (UDCA), Bogota, Colombia organized by UDCA and the Indian Embassy in Colombia in 2011.

- Member of college orchestra: Participated in several inter collegiate cultural competitions at State level.

- Appreciation award from Lions Clubs International for service activities.

Declaration

I hereby declare that all the details furnished above are true to the best of my knowledge

16/12/2015 Jaya Mary Jacob